

**A STUDY OF FRETTING FATIGUE IN POST-TENSIONED  
CONCRETE BEAMS**

**APPROVED :**

\_\_\_\_\_  
**Michael E. Kreger**

\_\_\_\_\_  
**John E. Breen**

\_\_\_\_\_  
**William Spelman**

To my family and the late friend Marlan Blissett

A STUDY OF FRETTING FATIGUE IN POST-TENSIONED  
CONCRETE BEAMS

by

TASOS PANTELI GEORGIU, B.S., H.N.D.

THESIS

Presented to the Faculty of the Graduate School of

The University of Texas at Austin

in Partial Fulfillment

of the requirements

for the Degree of

MASTER OF SCIENCE IN ENGINEERING

THE UNIVERSITY OF TEXAS AT AUSTIN

August , 1989

## ACKNOWLEDGEMENTS

The author gratefully acknowledges the advice and friendship of Professor Michael E. Kreger and Professor John E. Breen throughout the research and preparation of this report. Professor William Spelman is also thanked for helping out by accepting the role of the third reader the last moment.

This research was conducted at the Phil M. Ferguson Structural Engineering Laboratory at the Balcones Research Center of The University of Texas at Austin, Austin, Texas. The help of the technical staff - Richard Marshall, Blake Stasney, Pat Ball, Robert Garcia and Wayne Little - is greatly appreciated. Irene Moore, Maxine DeButts, Lorie Golding, Sharon Cunningham and Jean Gerhke are also thanked for helping in their own way throughout the research and preparation of this manuscript.

Special thanks are extended to the Graduate Research Assistant Andreas Kotziapashis for being so creative and helpful throughout the research. Thanks are also extended to the Graduate Students David Yates, Gregor Wollmann, Joseph Diab and Tetsuya Tsujimoto for their special contributions.

Finally, the author would like to extend his special thanks to his parents, sister and brother in law for their love and encouragement, and for being so close although being thousands of miles away.

Austin, Texas

Tasos Georgiou

August, 1989

## ABSTRACT

This report is devoted to acquiring a better understanding of the effects of fretting fatigue on the fatigue life of post-tensioned tendons. Five large-scale post-tensioned concrete beams were fabricated and fatigue tested at the Ferguson Structural Engineering Laboratory of the Balcones Research Center of The University of Texas at Austin. The results of these tests are presented and analyzed along with results of previous studies on fretting fatigue of post-tensioned tendons. Mean fatigue-life models were developed for different types of tendons and post-tensioning duct. Design criteria were also developed for some types of tendons.

# TABLE OF CONTENTS

<b><u>Chapter</u></b>	<b><u>Page</u></b>
1 INTRODUCTION .....	1
1.1 General .....	1
1.2 Objectives .....	3
1.3 Scope .....	4
2 BACKGROUND INFORMATION .....	5
2.1 General .....	5
2.2 Fatigue of Prestress Concrete .....	5
2.2.1 General .....	5
2.2.2 Fatigue of Prestressing Tendons .....	10
2.2.3 Fatigue of Pretensioned Concrete Beams .....	12
2.2.4 Fatigue of Post-Tensioned Concrete .....	12
2.3 Fretting Fatigue .....	15
2.3.1 Factors Affecting Fretting Fatigue .....	18
2.3.1.1 Stress Range .....	21
2.3.1.2 Slip Amplitude .....	21
2.3.1.3 Lateral Pressure .....	23
2.3.1.4 Material Properties .....	24
2.3.1.5 Enviroment .....	24
2.4 Fretting Fatigue of Post-Tensioned Beams .....	26
2.5 Previous Studies .....	26
2.5.1 Magura and Hognestad .....	28

## TABLE OF CONTENTS (cont.)

<b><u>Chapter</u></b>	<b><u>Page</u></b>
2.5.2 Rigon and Thurlimann .....	28
2.5.3 Oertle, Thurlimann and Esslinger .....	32
2.5.4 Cordes, Lapp-Emden and Trost .....	34
2.5.5 Muller .....	34
2.5.6 Shahawi and Batchelor .....	37
2.5.7 Brondum - Nielson .....	39
2.5.8 Yates.....	40
2.5.9 Wollmann.....	43
2.5.10 Diab.....	45
<b>3 EXPERIMENTAL PROGRAM .....</b>	<b>48</b>
3.1 Introduction .....	48
3.2 Strand in Air Tests.....	48
3.2.1 Fatigue Tests.....	49
3.2.2 Static Tests .....	53
3.3 Large-Scale Beam Tests .....	53
3.3.1 Specimen Description.....	54
3.3.2 Test Variables .....	59
3.3.3 Materials .....	59
3.3.3.1 Concrete .....	59
3.3.3.2 Passive Reinforcement .....	60
3.3.3.3 Shear and Confining Reinforcement .....	63

## TABLE OF CONTENTS (cont.)

<u>Chapter</u>	<u>Page</u>
3.3.3.4 Prestressing Steel .....	63
3.3.3.5 Post-Tensioning Duct .....	64
3.3.3.6 Grout.....	64
3.3.3.7 Prestresing Hardware .....	66
3.3.4 Fabrication.....	70
3.3.4.1 Formwork.....	70
3.3.4.2 Reinforcing Cage.....	71
3.3.4.3 Concrete Placement .....	72
3.3.4.4 Post-Tensioning .....	73
3.3.4.5 Grouting .....	75
3.3.5 Test Set-Up.....	77
3.3.5.1 Loading System .....	77
3.3.5.2 Instrumentation .....	85
3.3.5.2.1 Displacements.....	85
3.3.5.2.2 Strain Gages .....	86
3.3.5.2.3 Other Instrumentation.....	88
3.3.6 Test Procedure .....	90
3.3.6.1 Initial Static Cycles - Cracking of Specimen .....	90
3.3.6.2 Determination of Effective Prestress Force.....	92
3.3.6.3 Determination of Ram Load Vs. Tendon Stress Relations .....	93
3.3.6.4 Cyclic Loading .....	93



## T A B L E O F C O N T E N T S (cont.)

<b><u>Chapter</u></b>	<b><u>Page</u></b>
3.3.6.5 Periodic Static Cycles .....	96
3.3.6.6 Static Flexural Strength Test .....	97
3.3.6.7 Post-Mortem Investigation .....	98
<b>4 LARGE - SCALE BEAM TEST RESULTS .....</b>	<b>100</b>
4.1 Introduction .....	100
4.2 Static Behavior .....	101
4.2.1 Initial Static Load Cycles .....	101
4.2.2 General Characteristics of the Static Behavior .....	103
4.2.2.1 Hysteretic Behavior .....	103
4.2.2.2 Time Dependence of Displacements .....	106
4.3 Determination of Cyclic Test Loads .....	106
4.4 Fatigue Behavior .....	108
4.5 Static Flexural Strength Test .....	113
4.6 Crack Patterns .....	116
4.7 Post-Mortem Investigation .....	119
4.8 Specimens of Group PM .....	129
4.8.1 General .....	129
4.8.2 Post-Mortem Investigation .....	133
4.9 Specimens of Group DM .....	135
4.9.1 General .....	135
4.9.2 Post-Mortem Investigation .....	138

## T A B L E O F C O N T E N T S (cont.)

<b><u>Chapter</u></b>	<b><u>Page</u></b>
4.10 Specimens of Group DP .....	140
4.10.1 General .....	140
4.10.2 Post-Mortem Investigation .....	141
5 EVALUATION AND COMPARISON OF TEST RESULTS .....	144
5.1 Introduction .....	144
5.2 Statistical Method .....	153
5.3 Paulson's Strand in Air Failure Zone .....	154
5.4 Strand in Air Fatigue Tests .....	155
5.4.1 Statistical Analysis and Comparison of Results .....	158
5.5 Previous Studies .....	158
5.5.1 Introduction .....	158
5.5.2 26.5 mm Diameter Threaded Bar Tests .....	160
5.5.3 12.2 mm Diameter Parallel Wire Tests .....	162
5.5.4 7 mm Diameter Parallel Wire Tests .....	162
5.5.5 0.6 in. Diameter, 7 Wire Strand Tests .....	165
5.5.6 0.5 in. Diameter, 7 Wire Strand Tests .....	167
5.5.7 Tests for Strand-Type Tendon with Metal Duct .....	171
5.5.8 Tests for Strand-Type Tendon with Plastic Duct .....	174
5.5.9 Tests of Beams with Parallel Wire Tendons .....	178
5.6 Two Variable Fretting Fatigue Model .....	181
5.6.1 Introduction .....	181

## T A B L E O F C O N T E N T S (cont.)

<b><u>Chapter</u></b>	<b><u>Page</u></b>
5.6.2 Estimation of Contact Load .....	181
5.6.2.1 General Characteristics of K Factors .....	184
5.6.3 Evaluation of the Beam Test Data Using Multiple Linear Regression Analysis .....	187
5.6.4 Results of the Regression Analysis .....	192
5.6.4.1 Tests of Beams with Strand-Type Tendon .....	193
5.6.4.2 Tests of Beams with Parallel Wires Tendon .....	198
5.6.4.3 Tests of Beams with Single or Multiple-Strand Tendon .....	202
6 SUMMARY, CONCLUSIONS AND RECOMMENDATIONS .....	207
6.1 Summary .....	207
6.2 Conclusions .....	208
6.3 Recommendations .....	210
6.3.1 Design Recommendations .....	210
6.3.2 Research Recommendations .....	215
References .....	216

## LIST OF TABLES

<u>Tables</u>	<u>Page</u>
2.1 Factors Affecting Fretting Fatigue (from Yates [27]) .....	20
3.1 Strand In Air Fatigue Test Results .....	51
3.2 Concrete Compressive Strengths .....	61
3.3 Grout Compressive Strengths .....	67
3.4 Cyclic Load Tests and Tendon Stresses .....	95
4.1 Information From Initial Static Load Cycles .....	104
4.2 Calculated Effective Tendon Prestress Force and Stress .....	109
4.3 Cyclic Test Loads and Tendon Stresses .....	112
4.4 Ultimate Loads for Large-Scale Beams .....	117
4.5 Fatigue Lives of Specimens .....	132
5.1 Summary of Fretting Fatigue Tests of Post-Tensioning Tendons .....	146
5.2 Linear Regression Analysis Results .....	156
5.3 Summary of Strand In Air Test Results .....	157
5.4 Data for Strand-Type Tendons .....	172
5.5 Data for Strand-Type Tendons with Plastic Duct .....	190
5.6 Data for Parallel Wire Tendons .....	191
5.7 Initial Multivariable Linear Regression Analysis Results .....	195
5.8 Multivariable Linear Regression Analysis Results for Tests with Strand Tendon and $3 \text{ kips} < q < 6 \text{ kips/ft}$ .....	197
5.9 Multivariable Linear Regression Analysis Results for Tests with Parallel Wires and $3 \text{ kips} < q < 6 \text{ kips/ft}$ .....	201
5.10 Final Multivariable Linear Regression Analysis Results .....	203

## LIST OF FIGURES

<b><u>Figures</u></b>	<b><u>Page</u></b>
2.1 Variation of Tendon Stress in Prestressed Concrete Beam Sections. . . . .	7
2.2 Typical Fatigue Strength Plot . . . . .	8
2.3 Typical Stiffness History. . . . .	9
2.4 Strand In Air Failure Zone (from Paulson [17]) . . . . .	13
2.5 Fatigue Crack Characteristics (from Waterhouse [24]) . . . . .	17
2.6 Effect of Fretting on Fatigue Life (from Waterhouse [24]) . . . . .	19
2.7 Effect of Slip Amplitude on Fretting Fatigue (from Yates [27]) . . . . .	22
2.8 Influence of Humidity on Fretting Wear for Several Steels (from Bill [2]). . . . .	25
2.9 Interaction of Local Variables Affecting Fretting Fatigue of a Post-Tensioned Tendon (from Yates [27]) . . . . .	27
2.10 Beams Tested by Magura and Hognestad [10]. . . . .	29
2.11 Beams Tested by Rigon and Thurlimann [20]. . . . .	31
2.12 Reduced-Beams Tested by Oertle, Thurlimann and Esslinger [14] . . . . .	33
2.13 Fretting Simulation Apparatus Used by Cordes, Lapp-Emden and Trost [4] . . . . .	35
2.14 Beams Tested by Muller [12] . . . . .	36
2.15 Beams Tested by Shahawi and Batchelor [21] . . . . .	38
2.16 Reduced-Beams Tested by Yates [27] . . . . .	41
2.17 Beams Tested by Diab [6]. . . . .	46
3.1 Schematic Representation of the Strand Fatigue Test Set-Up (from Paulson [17]). . . . .	50

3.2	Comparison of Strand In Air Fatigue Test Results, Paulson's Strand In Air Failure Zone and AASHTO Fatigue Model . . . . .	52
3.3	Actual Dimensions and Details of Large-Scale Beam . . . . .	56
3.4	Large-Scale Beam with Draped Tendon (Non-Prestressed Reinforcement Not Shown). . . . .	57
3.5	Large-Scale Beam with Parabolic Tendon (Non-Prestressed Reinforcement Not Shown) . . . . .	58
3.6	Passive, Longitudinal, Transverse, and Confining Reinforcement in Large-Scale Beams . . . . .	62
3.7	Measured Dimensions of Duct . . . . .	65
3.8	Embedded Anchorage Plate and Spiral Reinforcement in Place Before Casting . . . . .	68
3.9	Photographs of Post-Tensioning Procedure . . . . .	69
3.10	Photograph of the Grout Pump . . . . .	76
3.11	Photographs of the Loading Frame . . . . .	78
3.12	Photographs of Steel Pedestal, Neoprene Pads, and End Restraints . . . . .	79
3.13	Cup and Dish Assembly Between the Ram and Spreader Beam . . . . .	80
3.14	Cup and Dish Assembly, Neoprene Pad, and Hydrastone Layer Between Spreader Beam and Specimen . . . . .	81
3.15	Schematic Representation of Closed Loop Servo Control System (from Yates [27]) . . . . .	83
3.16	Some of the Equipment Used During Testing . . . . .	84
	a) Pegasus Hydraulic Servo Controller . . . . .	84

b) Equipment Used for Deformation Measurements .....	84
3.17 Locations of Strain Gages on the Strands .....	87
3.18 Location of Strain Gages on Bottom Passive Reinforcing Bars .....	89
3.19 Typical Ram Load Vs. Midspan Deflection Curve .....	91
3.20 Typical Ram Load Vs. Crack-Width Curve .....	91
4.1 Typical Specimen Response to Initial Static Load Cycles .....	102
4.2 Typical Hysteretic Behavior during Static Load Cycles.....	105
4.3 Typical Plot of Time Dependence of Displacements .....	107
4.4 Typical Ram Load Vs. Tendon Stress Relationship .....	110
4.5 Typical Ram Load Vs. Passive Reinforcement Stress Relationship.....	111
4.6 Typical Ram Load Vs. Midspan Deflection History .....	114
4.7 Typical Stiffness History .....	115
4.8 Typical Crack Patterns (before Static Flexural Strength Test) .....	118
4.9 Horizontal Crack at Bottom of Web .....	120
4.10 Photographs of Fractured Metal Duct .....	122
4.11 Condition of Metal Duct .....	124
4.12 Condition of Plastic Duct .....	124
4.13 Photograph of a Fretting Fatigue Fracture .....	126
4.14 Typical Wire Fractures .....	127
a) Typical Fretting Fatigue Fracture of Wire .....	127
b) Typical Ordinary Fatigue Fracture of Wire .....	127
c) Typical Ultimate-Strength Fracture of Wire .....	127
4.15 Photograph of an Ordinary Fatigue Fracture .....	128
4.16 Photograph of an Ultimate-Strength Fracture .....	128

4.17	Stiffness History of Specimen P-M-1-25 .....	131
4.18	Fretting Signs on Metal Duct of Specimen P-M-1-25 .....	134
4.19	Fretting Fractures of Wires of Specimen P-M-1-25 .....	134
4.20	Fractured Metal Duct of Specimen P-M-1-25 .....	134
4.21	Stiffness History of Specimen D-M-2-40 .....	137
4.22	Stiffness History of Specimen D-M-3-30 .....	137
4.23	Fretting Signs on Metal Duct of a Group DM Specimen .....	139
4.24	Fretting Fractures of Wires of a Group DM Specimen .....	139
4.25	Fractured Metal Duct of a Group DM Specimen .....	139
4.26	Stiffness History of Specimen D-P-4-30 .....	142
4.27	Stiffness History of Specimen D-P-5-30 .....	142
4.28	Condition of Plastic Duct of a Group DP Specimen .....	143
5.1	Comparison Strand In Air Fatigue Data and Strand In Air Failure Zone .....	159
5.2	Comparison of 1-26.5 mm dia. Threaded Bar Tests with AASHTO Fatigue Model .....	161
5.3	Comparison of 12.2 mm dia., Wire Tests with AASHTO Fatigue Model .....	163
5.4	Comparison of 7 mm dia., Wire Tests with AASHTO Fatigue Model .....	164
5.5	Comparison of 0.6 in. dia., 7 Wire Strand Tests with AASHTO Fatigue Model .....	166
5.6	Results of 0.5 in. dia., 7 Wire Strand Tests .....	168
5.7	Comparison of 0.5 in. dia., 7 Wire Strand Tests with Strand In Air Failure Zone and AASHTO Fatigue Model .....	170
5.8	Comparison of Tests of Strand-Type Tendon With Metal Duct with Strand In Air Failure Zone and AASHTO Fatigue Model .....	173



5.9	Comparison of Tests of Strand-Type Tendon With Plastic Duct with Strand In Air Failure Zone and AASHTO Fatigue Model .....	175
5.10	a. Comparison Between Multiple-Strand Tendon Tests for Metal Duct and Plastic Duct .....	176
5.10	b. Comparison Between Single-Strand Tendon Tests for Metal Duct and Plastic Duct .....	177
5.11	Comparison of Test Results from Beams with Wire Tendons and Metal Duct with AASHTO Fatigue Model .....	179
5.12	Comparison of Test Results from Beams with Wire Tendons and Plastic Duct with AASHTO Fatigue Model .....	180
5.13	Estimation of Lateral Load and K Factors (from Yates [27]) .....	183
	a) Estimation of Lateral Load, Q .....	183
	b) Estimation of K Factors .....	183
5.14	Variation of K Factors With Tendon Arrangement .....	185
5.15	Variation of K Factors With Number of Strands .....	185
5.16	Variation of K Factors With Ratio of Strand to Duct Size .....	186
5.17	K Factors Used for Beams with Strand-Type Tendons .....	188
5.18	K Factors Used for Beams with Wire Tendons .....	189
5.19	Fatigue Life as a Function of Stress Range and Contact Load for Beams with Strand-Type Tendon and Metal Duct .....	194
5.20	Fatigue Life as a Function of Stress Range and Contact Load for Beams with Wire Tendons and Metal Duct .....	200
5.21	Fatigue Life as a Function of Stress Range and Contact Load for Beams with Single-Strand Tendon and Metal Duct .....	204

5.22	Fatigue Life as a Function of Stress Range and Contact Load for Beams with Multiple-Strand Tendon and Metal Duct .....	205
6.1	Comparison of Model S-3-6 with AASHTO Category B and AASHTO Category C Fatigue Models .....	212
6.2	Comparison of Model S-6-9 with AASHTO Category C Fatigue Model .....	213
6.3	Comparison of Models W-0-3, W-3-6 and W-ALL with AASHTO Category B and AASHTO Category C Fatigue Models .....	214

**CHAPTER 1**  
**INTRODUCTION**

**1.1 General**

Until recently the use of prestressed concrete in the United States was very limited. During the past 30 years there has been a rapid increase in both research and usage of prestressed concrete in all types of structures. However, more emphasis has been placed on researching the behavior of pretensioned concrete as opposed to post-tensioned concrete. The reason behind this was linked to the assumption that pretensioned and post-tensioned concrete behavior are very similar. One area in which it has been realized that behavior of pretensioned and post-tensioned concrete members or structures differ dramatically is fatigue. It is now evident that the fatigue resistance of a post-tensioned concrete member can be substantially less than that of the equivalent pretensioned concrete member [14,26,27].

Many investigations have shown that failure of prestressed concrete members subjected to repeated loadings results from the fatigue failure of the prestressing tendons in the members [6,7,10,16,20,26,27].

In the case of a pretensioned concrete member, the fatigue life of the prestressing strands alone, approximately reflects the fatigue life of the member in which they are a part. For a post-tensioned concrete member the fatigue life of the prestressing tendons can be considerably less.

The reduction in fatigue life of a post-tensioned tendon can be attributed to many factors or actions such as materials used, slip between individual tendon elements (strand-to-strand), slip between the tendon and adjacent metallic components (strand-to-metal duct) and contact pressure between tendons and adjacent metallic components. The slip and contact pressure actions result in a process involving a complex state of stress in the tendon. This process is usually called "fretting".

The fretting process, or fretting fatigue, is more severe in the vicinity of cracks where the slip amplitude is higher. It is also more severe in regions of curved tendons (draped regions) where the contact pressure is high.

The effects of fretting fatigue were only recently documented for post-tensioned concrete. A research program was initiated in 1985 at the Ferguson Structural

Engineering Laboratory (FSEL) of The University of Texas at Austin in order to gain a better understanding of fretting fatigue. The present study is part of the overall research program.

The research program involved four major series of tests:

- 1) Strand in air fatigue tests [27].
- 2) Fatigue tests of reduced-beam specimens with single-strand tendons [27].
- 3) Fatigue tests of reduced-beam specimens with multiple-strand tendons [26].
- 4) Fatigue tests of large-scale post-tensioned concrete beams [6 and present study].

## **1.2 Objectives**

The overall objectives of the project are:

- 1) To investigate the fatigue resistance of typical post-tensioned concrete beams.
- 2) To investigate the influence of important variables such as tendon stress range, prestress level, lateral pressure, duct material, and type of tendon on the fatigue resistance of post-tensioned concrete members.
- 3) To develop fatigue design recommendations applicable

to post-tensioned concrete members.

### **1.3 Scope**

This report focuses on the fourth test series which deals with fatigue tests of large-scale post-tensioned concrete beams.

A literature review related to fretting fatigue, in general, and previous studies on fatigue is given in Chapter 2. The experimental program, including the design, fabrication and testing of the specimens is described in detail in Chapter 3. Chapter 4 includes a presentation of the results of the large-scale beam tests. The results of this and previous studies are evaluated and compared in Chapter 5. Finally, a summary of findings, conclusions, and recommendations for design and further research are given in Chapter 6.

## CHAPTER 2

### BACKGROUND INFORMATION

#### **2.1 General**

This chapter contains a literature review on fretting fatigue, fatigue of prestressed concrete, and related research. An extensive literature review on the above topics can be found in the thesis by Yates [27].

#### **2.2 Fatigue of Prestressed Concrete**

##### **2.2.1 General**

Fatigue is the gradual loss of strength of an element when it is subjected to repeated loading at a constant stress level. Static loading of the element to the same stress level will not result in failure.

The cause of fatigue is the growth of a crack under the influence of fluctuating tensile stress. The crack eventually reaches a critical size and a brittle failure of the element occurs. The crack can result from a defect in the microstructure of the element, or from damage sustained on the surface of the material.

In bonded prestressed concrete beams subjected to cyclic loading, fatigue is not a concern, as long as the

concrete in the beam remains uncracked [10]. Once the beam is cracked, localized tendon stress concentrations occur at the crack locations as shown in Fig. 2.1. In general, the increased stress range results in faster growth of cracks in the prestressing steel, and reduced life of the specimen. This is shown schematically in Fig. 2.2. The Endurance Limit, which is the maximum stress range for which fatigue does not occur, is also shown in the above figure.

The life of the specimen corresponds with the number of load cycles that the specimen experiences before a tendon wire fracture occurs. Wire fracture is typically accompanied by a reduction in flexural stiffness. Midspan deflection of the specimen at a given load level is used as a measure of the stiffness.

The stiffness history of a prestressed concrete beam that was initially cracked before cyclic loading is shown in Fig. 2.3. The graph is characterized by three distinct regions. The first region corresponds to the initial cracking cycles. Specimen deflections increase due to the formation and propagation of flexural crack, and the bond deterioration between prestressing steel and concrete. The second region corresponds to the load cycles between the initial



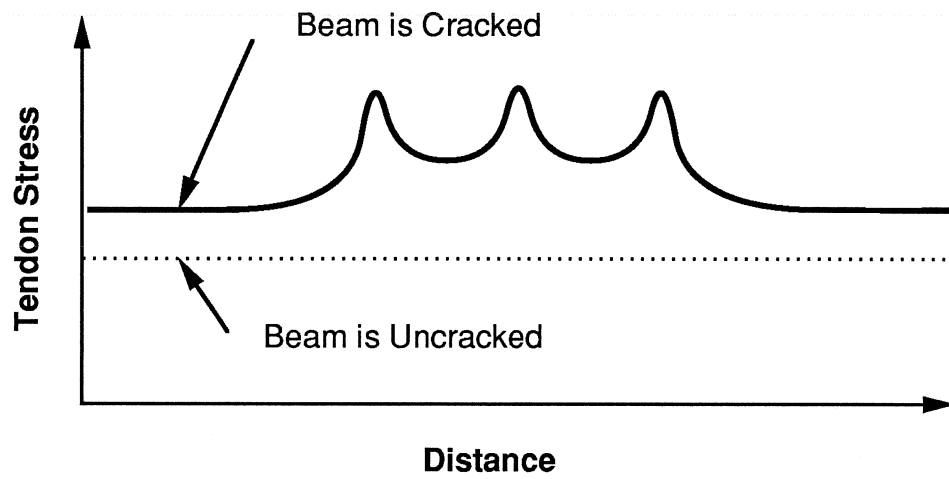
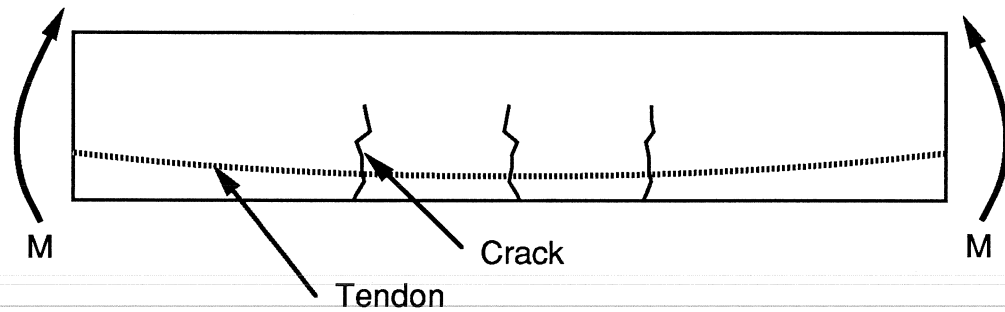


Figure 2.1 Variation of Tendon Stress in Prestressed Concrete Beam Sections  
(from Yates [27])

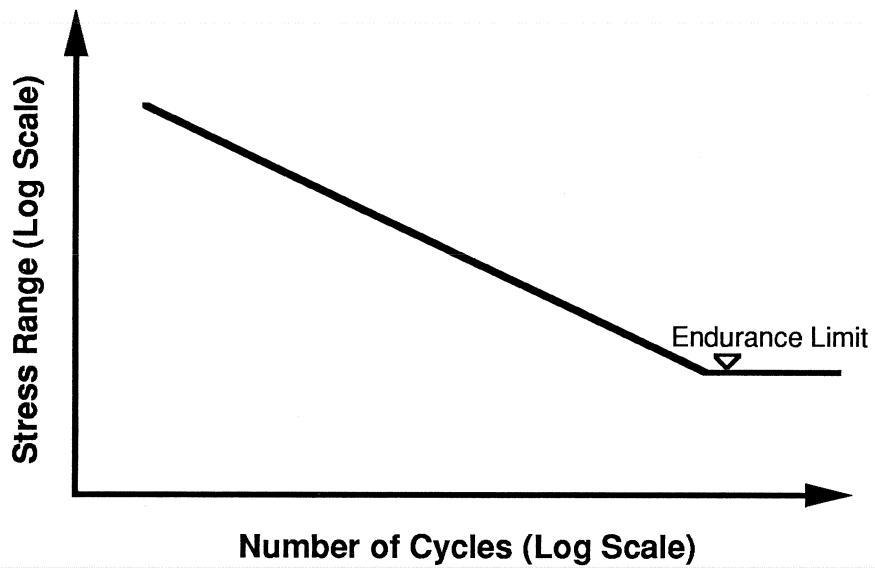
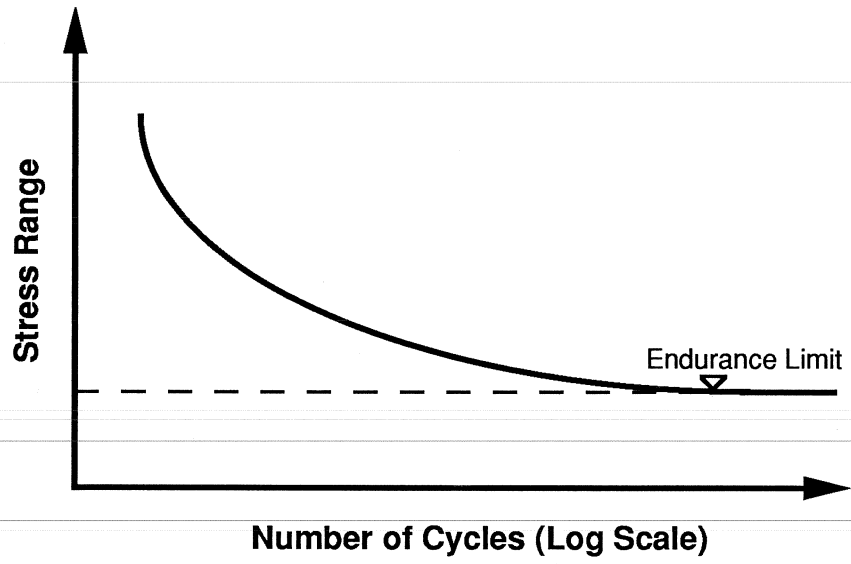


Figure 2.2 Typical Fatigue Strength Plots

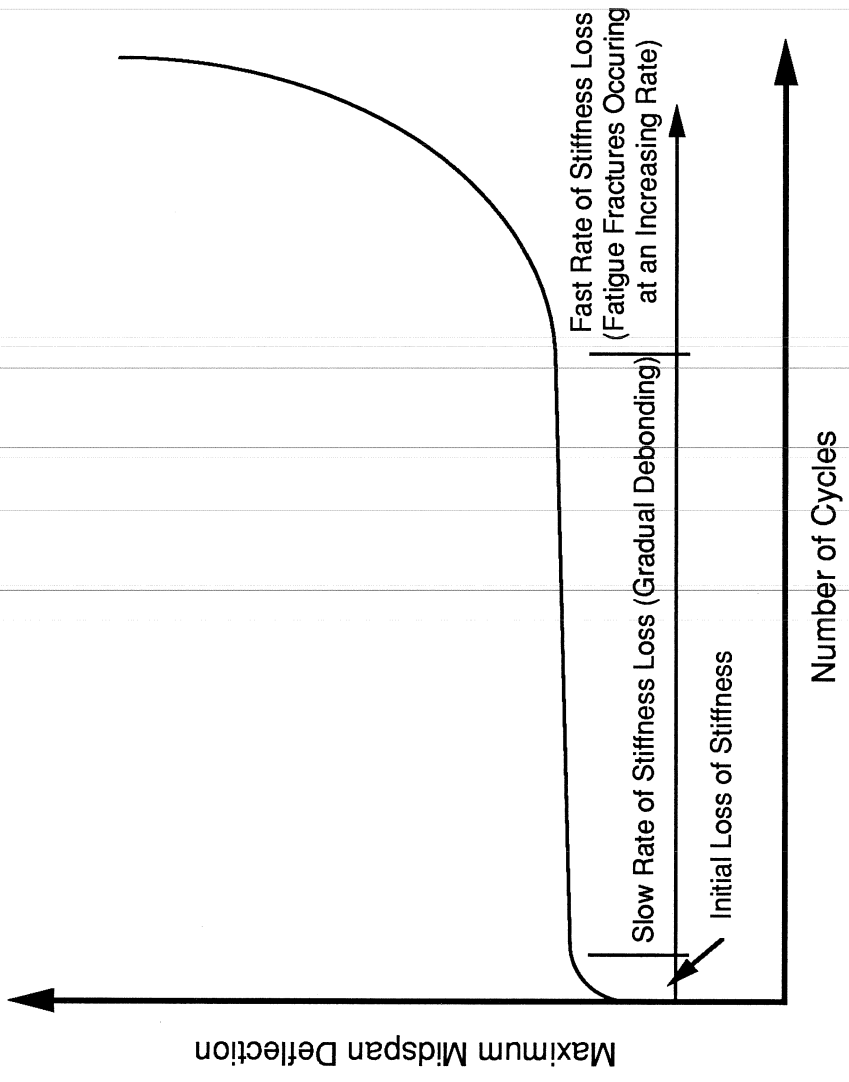


Figure 2.3 Typical Stiffness History

cracking cycles and the first wire break. In this region cracks propagate further and bond deterioration continues. As a result, additional deflection (loss of stiffness) occurs. The third region corresponds with the occurrence of wire fractures. The initial wire break is followed by the fracture of additional wires at an increasing rate resulting in a rapid loss of stiffness.

The fatigue behavior of prestressed concrete beams is influenced by the fatigue behavior of component materials which include concrete, prestressing steel, and non-prestressed reinforcement. The fatigue behavior of the prestressing steel (tendons) is considered the most important of the three in governing the fatigue behavior of the beams.

Fatigue behavior of pretensioned and post-tensioned beams was not differentiated until recently, when it was learned that the behavior differs significantly [14,20]. In the following sections of this chapter previous fatigue studies on pretensioned and post-tensioned specimens and their component materials are presented.

### **2.2.2 Fatigue of Prestressing Tendons**

The fatigue behavior of prestressing tendons is considered to significantly influence the overall

fatigue behavior of prestressed beams. Most of the fatigue research related to prestressed beams has been tests of "strands in air" (tests conducted in the relatively benign environment of air). The failure mechanism is the creation and propagation of cracks (as discussed in Section 2.2). Failure corresponds with fracture of the first wire.

A problem encountered during in-air fatigue tests of prestressing strand is failure of the strand in the gripping device. Gripping (anchorage) systems produce localized stress concentrations on the tendon which can result in creation of cracks and eventual failure within the gripping device [17].

Another factor related to the fatigue behavior of tendons is the length of the test samples. A longer test sample has higher probability of having surface irregularities and flaws which can lead to creation of cracks. Theoretically, the longer the test sample, the smaller is its fatigue life. This was confirmed in investigations conducted by Edwards and Picard [17] who tested three samples of different length.

An extensive investigation of over 700 individual strand fatigue tests was performed at The University of Texas at Austin by Paulson et al. [17]. He also

conducted his own strand fatigue tests, and developed a design model (shown in Fig. 2.4) for the fatigue life of prestressing strand.

### **2.2.3 Fatigue of Pretensioned Concrete Beams**

The majority of previous fatigue studies on prestressed concrete is related to pretensioned concrete. Overman et al. [16] give an extensive review of previous fatigue studies. Yates [27] gives a summary of previous studies along with his observations and conclusions. Many variables were considered, such as tendon stress range, concrete tensile stress, cross-section shapes, amount and detailing of passive reinforcement, degree of prestress, and others. The most important conclusion drawn was that the in-air fatigue properties of the prestressing tendons can be used to predict the fatigue life of pretensioned concrete beams. For more details related to this and other conclusions the reader should refer to the references cited earlier [16,27].

### **2.2.4 Fatigue of Post-Tensioned Concrete**

As was mentioned in Section 2.2.2, the fatigue behavior of prestressed concrete beams is greatly

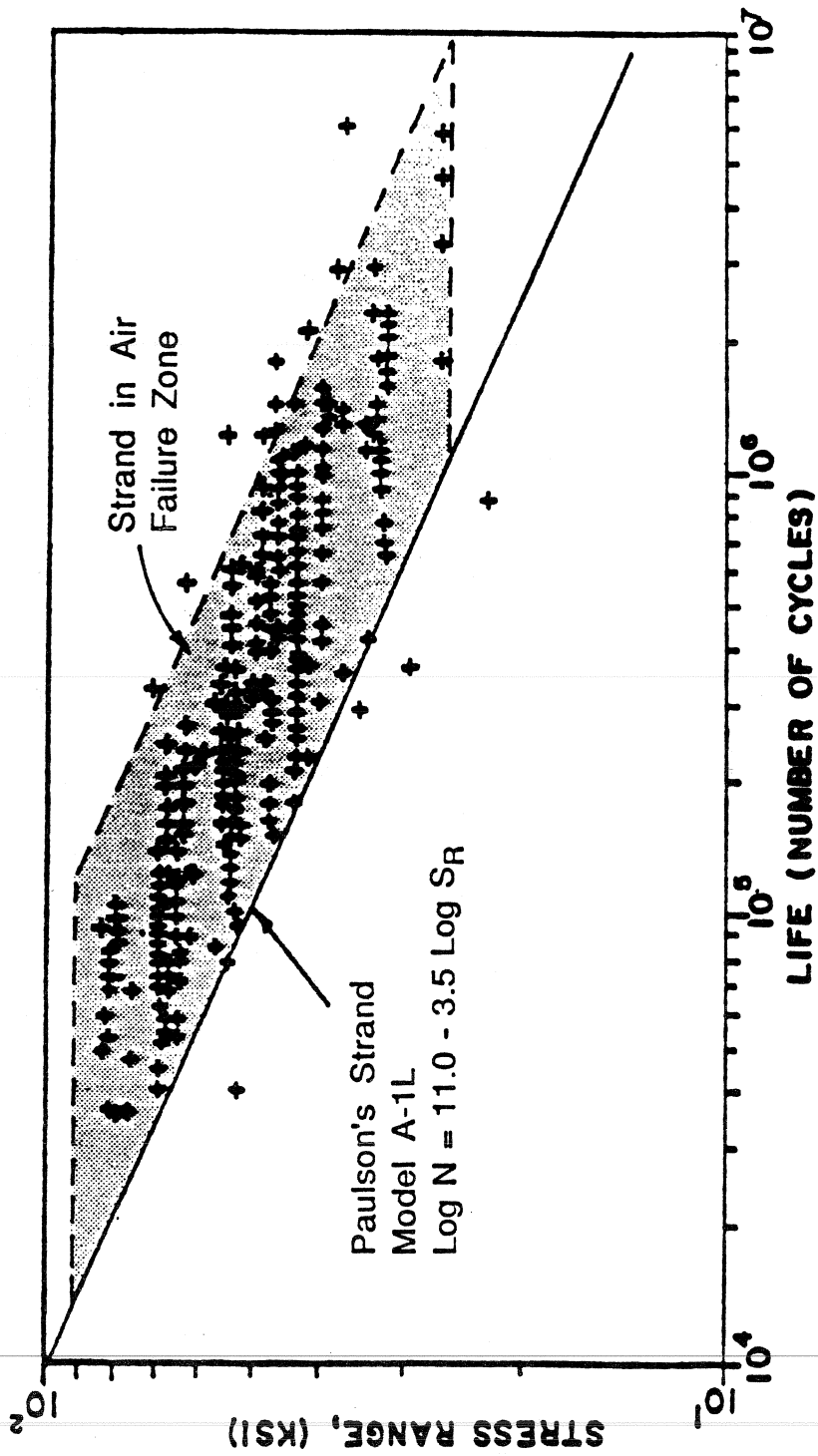


Figure 2.4 Strand In Air Failure Zone (from Paulson [17])

influenced by the fatigue behavior of the tendons. Tendon conditions in a post-tensioned concrete beam differ significantly from those of a pretensioned concrete beam, thus resulting in different fatigue behavior of the tendons in each case [6,26,27]. This is the primary reason leading to the differentiation of fatigue behavior in post-tensioned and pretensioned beams. In the case of a post-tensioned concrete beam, the tendons are inserted in a duct within the concrete beam (after the concrete has cured), tensioned, then grouted. The result is that the strands are brought into contact with the duct or with other tendons. While in the case of pretensioned concrete beams, the individual strands are surrounded by concrete. Once the post-tensioned beam is cracked, debonding of the tendon at crack locations occurs. The crack results in increased localized tendon stresses at the crack locations (Fig. 2.1) and slipping of the tendon relative to its surroundings when load is applied to the beam. This slip results in friction forces between the strand wires and the duct with which they are in contact, or between strands. This metal-to-metal rubbing combined with lateral forces induced by the curved tendon layout and fluctuating tendon stress when the beam undergoes



repeated loading can result in abrasive wear and corrosion of the strand and duct at the crack locations, accelerated formation and propagation of cracks, and eventually reduction in the fatigue life of the tendon and post-tensioned beam. This sequence of events is called fretting fatigue [27]. In the case of pretensioned concrete beams, fretting fatigue is not a problem. Since individual strands are surrounded by concrete, there is no metal-to-metal rubbing. Fretting fatigue is discussed in more detail in the following section.

### **2.3 Fretting Fatigue**

In general terms fretting is the process that two elements (usually metals) in contact undergo when they move repeatedly relatively to each other [25,27]. During this process, rubbing between the two elements can result in abrasive wear, corrosion, and fatigue cracking. In more detail, the application of lateral force between the two elements (metals) can result in high local stresses because the area of contact is very small. These local stresses, combined with the rubbing action between the two elements when cyclic relative displacements are imposed, destroy the protective oxide

film present on the steel. The exposed surface without the protective oxide film goes through a process called "cold welding". Further relative displacements between the elements result in the destruction of the cold welds and creation of new ones. During this process, cyclic surface shear stresses are induced which are combined with existing fluctuating stresses. The result is a stress state that initiates cracks. The corrosion of the metal which results from the destruction of the oxide film and the abrasive wear due to the friction forces acting during rubbing also contributes to the initiation of a crack [25]. When the crack reaches a critical width it becomes unstable resulting in brittle fracture of the element.

Figure 2.5 shows schematically the characteristics of an ordinary fatigue crack and a fretting fatigue crack. Within the zone of surface shear stresses the fretting fatigue crack follows an inclined path corresponding to a plane of principal tension. Beyond the zone where surface shear stresses have an influence, the fretting fatigue crack propagates due to existing tensile stresses in the same way as an ordinary fatigue crack propagates. The existing tensile stresses help in accelerating initiation of fretting fatigue cracks

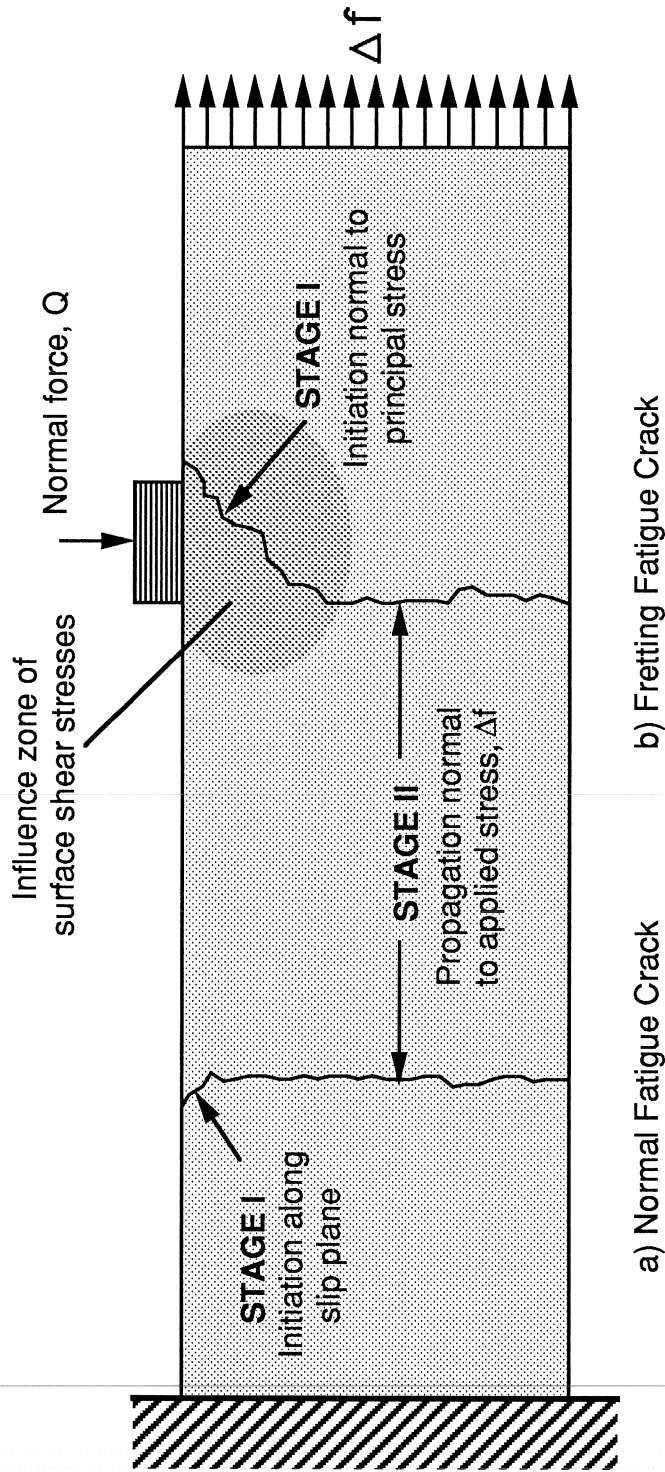


Figure 2.5 Fatigue Crack Characteristics ( from Waterhouse [24] )

and in causing crack propagation. When the element is thick, the effect of fretting fatigue (or surface shear stresses) is not so critical because the influence zone of the surface shear stresses is relatively small. In this case, fretting fatigue is not very different from normal fatigue of the element. However, if the element is thin (like wires of a prestressing tendon) the surface-shear influence zone is considerably larger and dominates the crack initiation and propagation [24].

Figure 2.6 shows schematically the difference between fatigue life for normal fatigue, fretting fatigue of a thick element, and fretting fatigue of a thin element.

### **2.3.1 Factors Affecting Fretting Fatigue**

The factors affecting fretting fatigue are many and can be grouped into three categories as shown in Table 2.1. There is no clear way to precisely determine the contribution of each factor to fretting fatigue because most of them are interrelated. However, trends in fretting fatigue associated with some of the factors listed in Table 2.1 are discussed in the following sections.

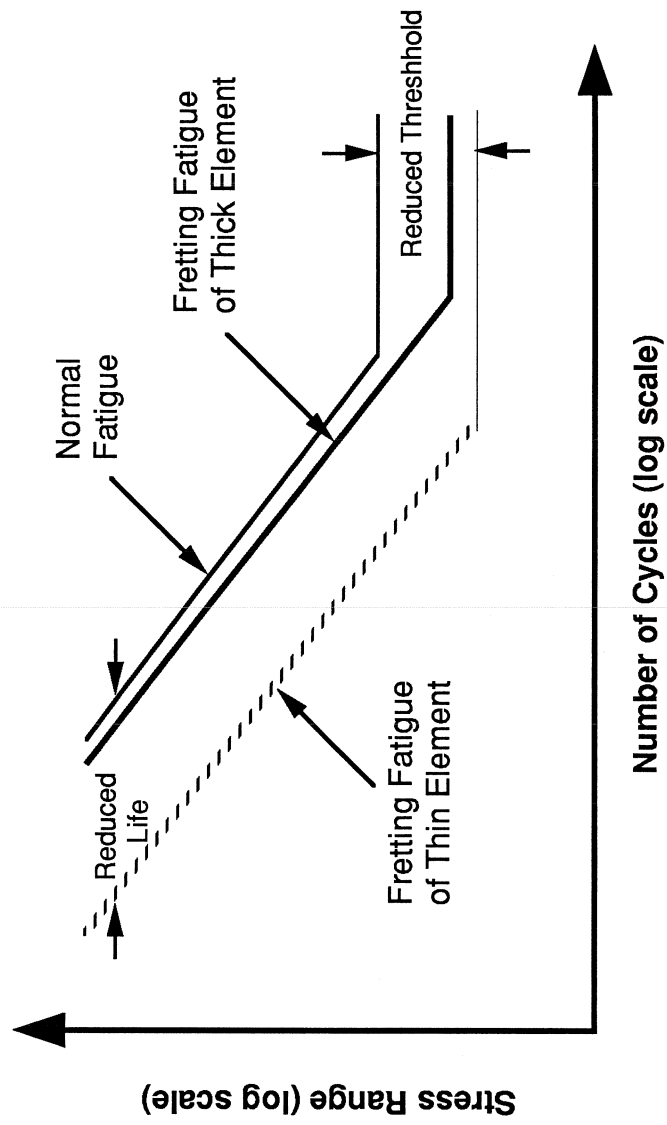


Figure 2.6 Effect of Fretting on Fatigue Life ( from Waterhouse [24] )

Table 2.1 Factors Affecting Fretting Fatigue ( from Yates [27] )

Stress Conditions	Material Properties	Environmental Conditions
Stress Range	Fatigue Characteristics	Adjacent Materials
Lateral Pressure	Friction Coefficient	Atmospheric Chemistry
Slip Amplitude	Strength and Ductility	Humidity
Geometry	Fracture Toughness	Temperature
Frequency	Corrosion Resistance	

### **2.3.1.1 Stress Range**

Stress range is considered to be one of the most important, if not the most important, factor influencing fretting fatigue, as well as normal fatigue. The crack growth is influenced considerably by the magnitude of the stress range. Increasing stress range results in an accelerated crack growth and decreased fatigue life of the element.

### **2.3.1.2 Slip Amplitude**

The slip amplitude is interrelated with other factors influencing fretting fatigue. However, there is a general trend describing the effect of slip amplitude on fretting fatigue as indicated in previous studies [2,8,9]. This general trend is shown schematically in Fig. 2.7. Krueger [8] suggests that if the slip is small enough, it can be accommodated by elastic deformation, and no fretting fatigue damage will take place. If the slip is large enough to wear away any already existing surface microcracks by abrasion before they propagate, no new cracks will form from fretting, and the result will be normal wear. Between these two extremes, fretting fatigue damage is very probable. Within this region an increase in the slip

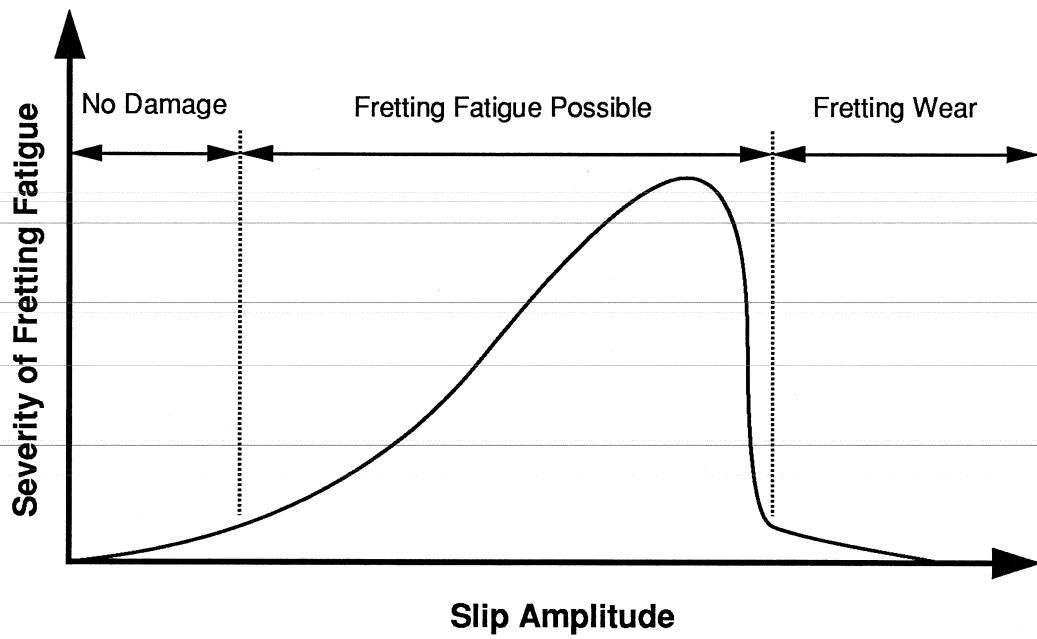


Figure 2.7 Effect of Slip Amplitude on Fretting Fatigue ( from Yates [27] )



amplitude results in an increase in fretting fatigue damage.

One strange aspect of the relationship between slip amplitude and fretting fatigue is that fretting fatigue was encountered at practically immeasurable slip amplitudes [8]. According to Waterhouse [24] this can be explained by the fact that even when gross slip does not occur, micro-slip can occur between points of contact, resulting in locally high stresses of sufficient magnitude to cause crack nucleation.

#### **2.3.1.3 Lateral Pressure**

The effect of lateral pressure on fretting fatigue is not very clear because lateral pressure is interrelated with other factors affecting fretting fatigue. For example, in the case of post-tensioned beams, lateral pressure depends on the stress range, prestress level, curvature of the duct, type of prestressing steel and duct material and size. However, a previous investigation [24] has shown a general trend of increased crack growth rate and likelihood of fatigue failure with increased lateral pressure.

#### **2.3.1.4 Material Properties**

Properties of the prestressing steel and the duct are thought to have an effect on fretting fatigue, although no proof is yet available. In more detail, the fatigue and corrosion resistance of the prestressing steel are believed to have an important role on fretting fatigue. However, these factors are interrelated with other factors making it difficult to clearly establish their effects on fretting fatigue.

Grout and concrete properties have an effect on fretting fatigue, but their importance is thought to be minor [3].

#### **2.3.1.5 Environment**

Environmental factors that influence mechanical and chemical reactions involved in the fretting process can have an important effect on fretting fatigue. Humidity is one of these factors. Bill [18] has shown that humidity can influence fretting at various levels depending on the type of prestressing steel used, as indicated in Fig. 2.8.

The presence of oxygen is another important factor. Waterhouse [24] has shown that the crack growth rate is greatly retarded in an environment free of oxygen.

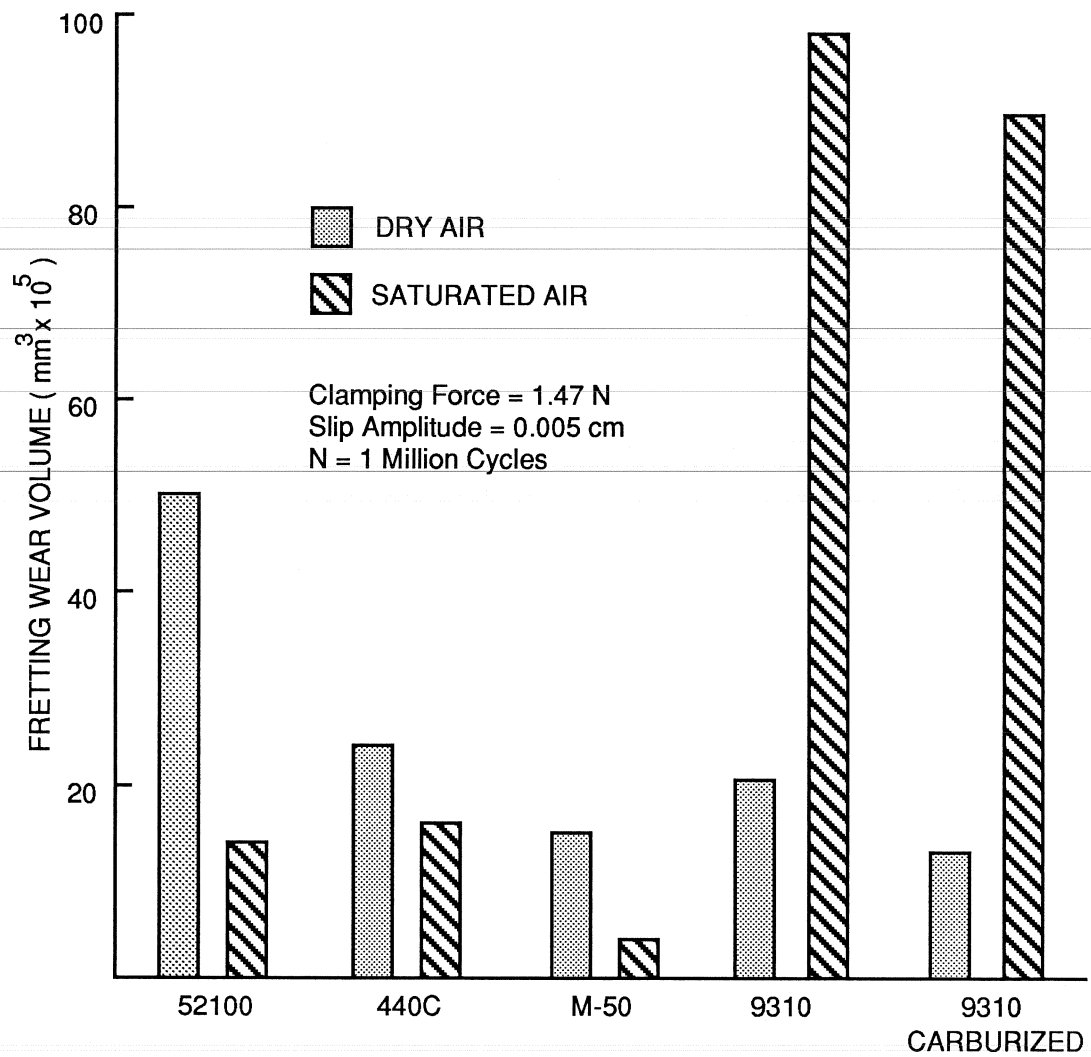


Figure 2.8 Influence of Humidity on Fretting Wear for Several Steels (from Bill [2])

The effect of corrosive agents, which is somehow interrelated to the presence of oxygen, was also examined by Waterhouse who concluded that corrosive agents have little effect on fretting fatigue.

#### **2.4 Fretting Fatigue of Post-Tensioned Beams**

As mentioned earlier, the factors affecting fretting fatigue are many, and are often interrelated. The same situation applies in the specific case of fretting fatigue of post-tensioned beams. There is no clear answer as to how much any particular factor affects fretting fatigue. Only general trends are available. Figure 2.9 shows a schematic representation of the interaction of important variables that affect the state of stress in a post-tensioned tendon, and consequently affect fretting fatigue of the whole post-tensioned beam.

#### **2.5 Previous Studies**

The number of previous studies related to fatigue of post-tensioned concrete beams is small compared to that of pretensioned concrete beams. The research studies on post-tensioned concrete beams are summarized in the remainder of this chapter.

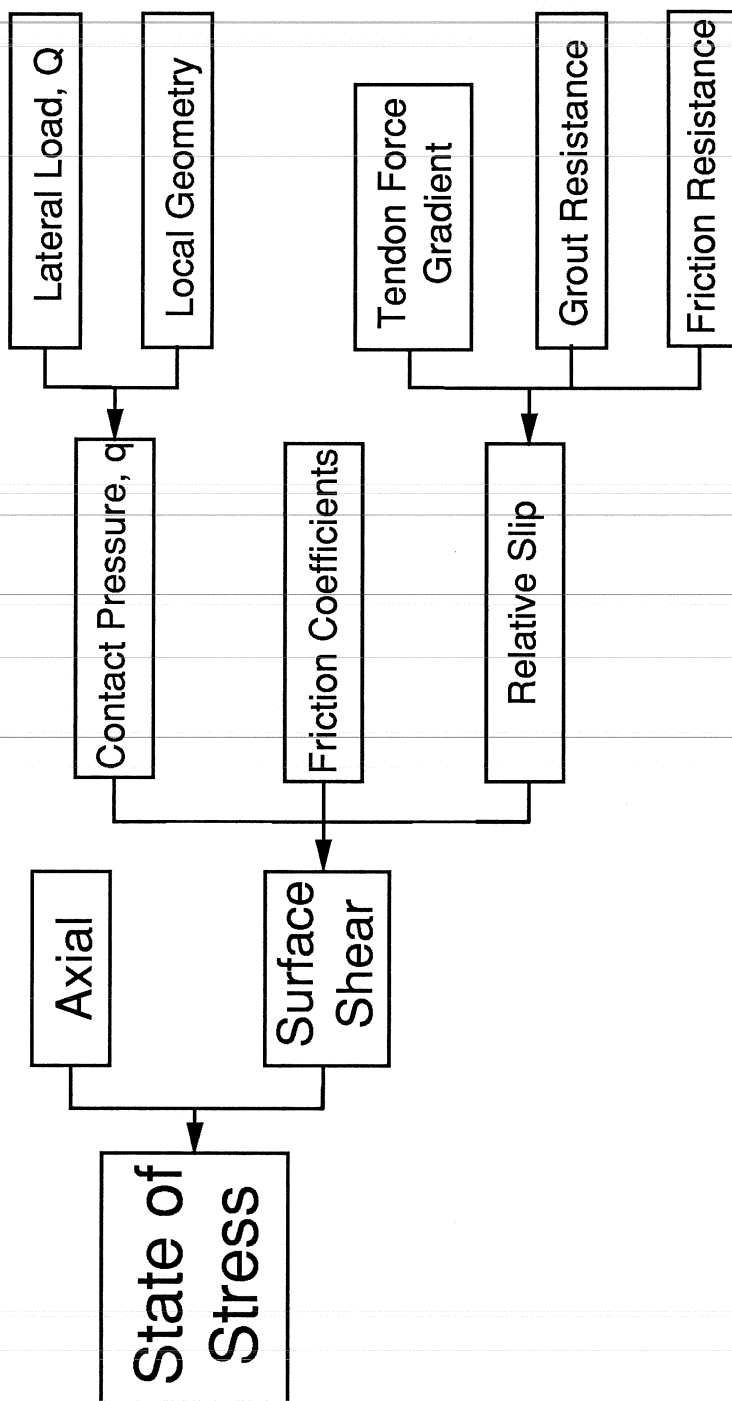


Figure 2.9 Interaction of Local Variables Affecting Fretting Fatigue of a Post-Tensioned Tendon (from Yates [27])

### 2.5.1 Magura and Hognestad

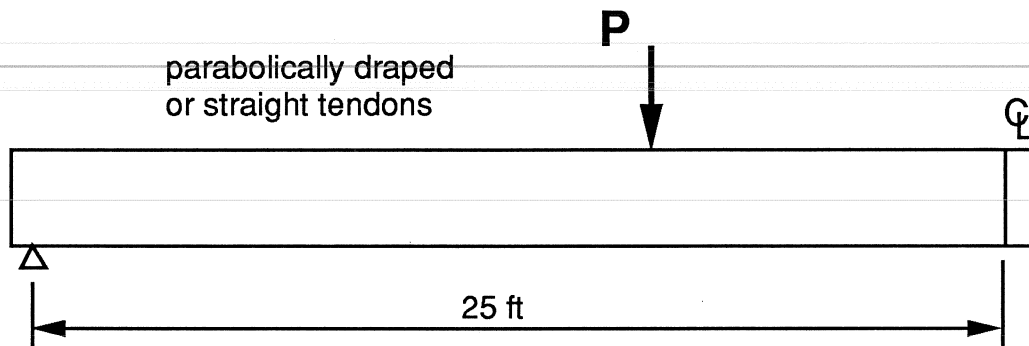
Magura and Hognestad [10] fatigue tested two post-tensioned and two pretensioned concrete girders (Fig. 2.10). The most important conclusion of these tests was the following:

Pretensioned girders which were subjected to maximum concrete tensile stresses of approximately  $7\sqrt{f'_c}$  "showed no significant detrimental effects from flexural cracks under repeated loading, whereas similarly stressed and cracked post-tensioned bridge girders showed serviceability distress and reduced capacity from load repetitions." [10]

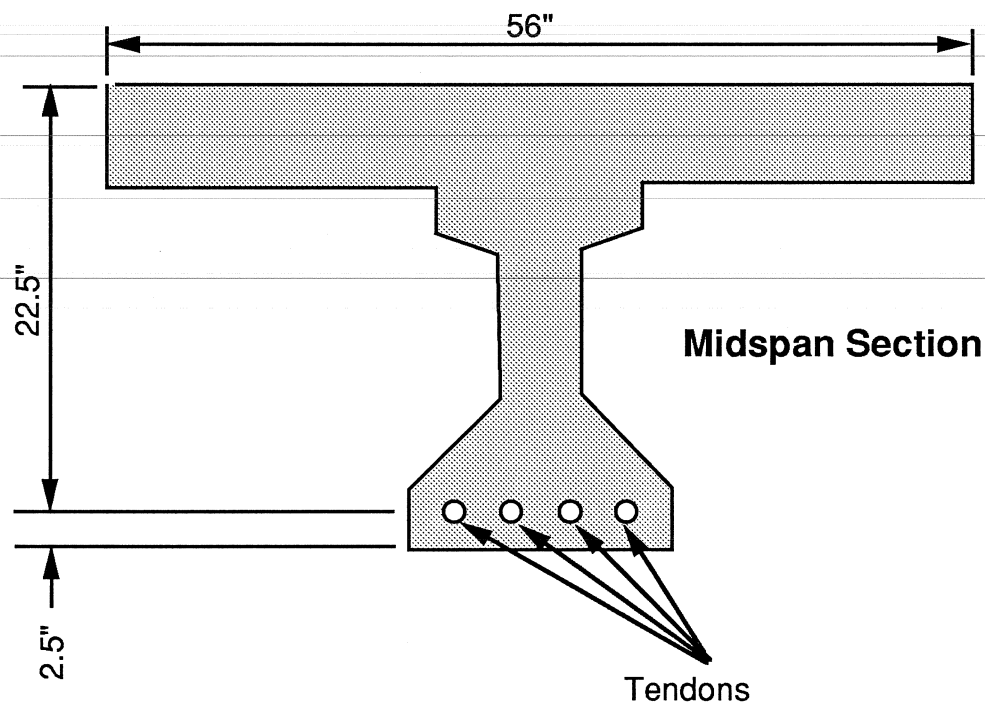
This statement implies that an uncracked prestressed girder does not deteriorate from fatigue. However, if the girder is cracked and subjected to repeated loading, fatigue can significantly reduce the life and capacity of a post-tensioned girder, whereas in the case of a pretensioned girder the capacity is not significantly affected. An explanation for this behavior was offered in Section 2.2.4.

### 2.5.2 Rigon and Thurlimann

Rigon and Thurlimann [20] fatigue tested fifteen post-tensioned concrete beams, the details of which are



Elevation



Midspan Section

16 or 20 - 3/8 in dia 7 Wire Strands  
 10 - 0.916 in dia Parallel Wires per  
 Tendon (4 to 6 Tendons)  
 Draped or Straight Tendons  
 Metal Duct

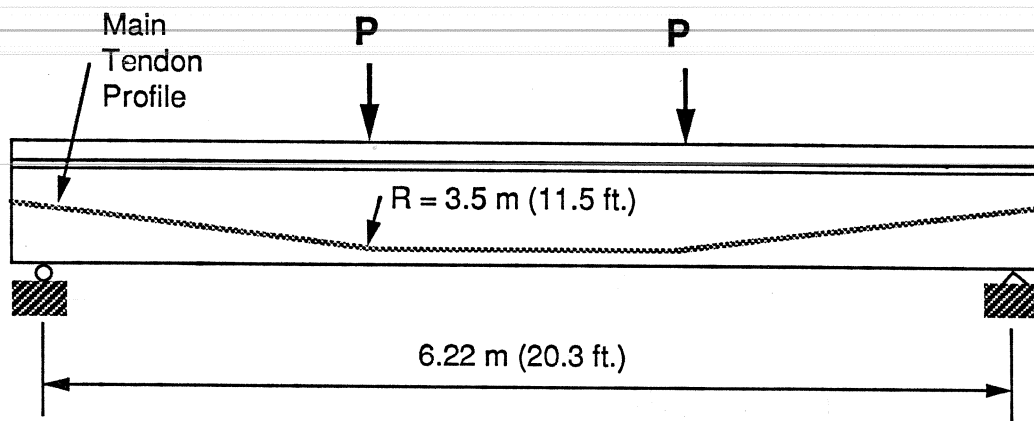
Figure 2.10 Beams Tested by Magura and Hognestad [10]

shown in Fig. 2.11. One of the variables considered was the type of tendon. Eight beams were post-tensioned with 16-7.0 mm diameter parallel wires, and the remaining seven with 4-0.6 in. diameter seven-wire strands. Another variable was the duct material. Metal duct was used in all beams except in one of the eight beams with parallel wires. Plastic duct was used in that one. The last variable considered was the tendon stress range.

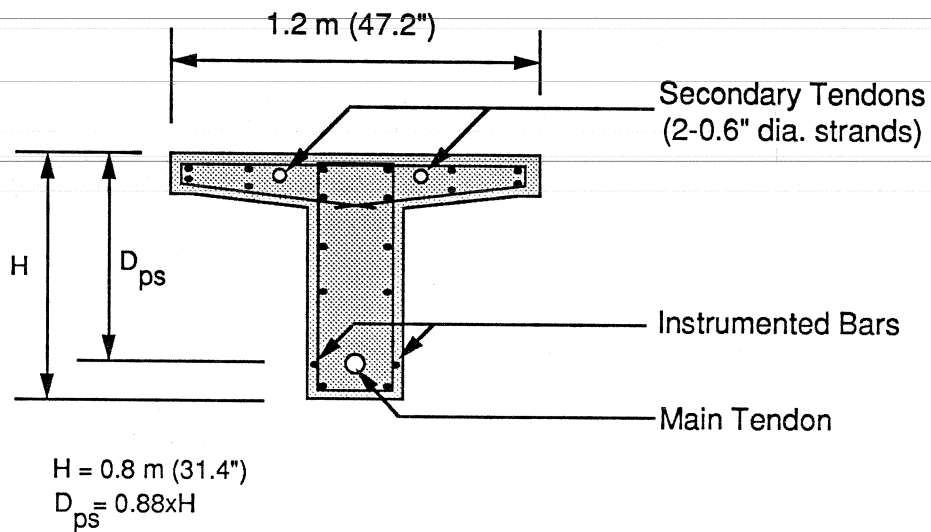
Many important observations and conclusions were made during this study. Some of these are:

- Both metal and plastic ducts were fractured at the location of the cracks.
- The inner surfaces of the ducts showed signs of rubbing between the ducts and the tendons or wires. In the case of metal ducts, signs of corrosion were visible on both the inner surface of the duct and wires at the points of contact. The beams with parallel-wire tendons suffered more corrosion than the beams with multi-strand tendons.
- The beams with metal ducts had the majority of fatigue fractures which occurred primarily in the curved sections of the tendons.
- In both strand and parallel-wire tendons, once a wire





a) Elevation



b) Midspan Section

Figure 2.11 Beams Tested By Rigon and Thurlimann [20]

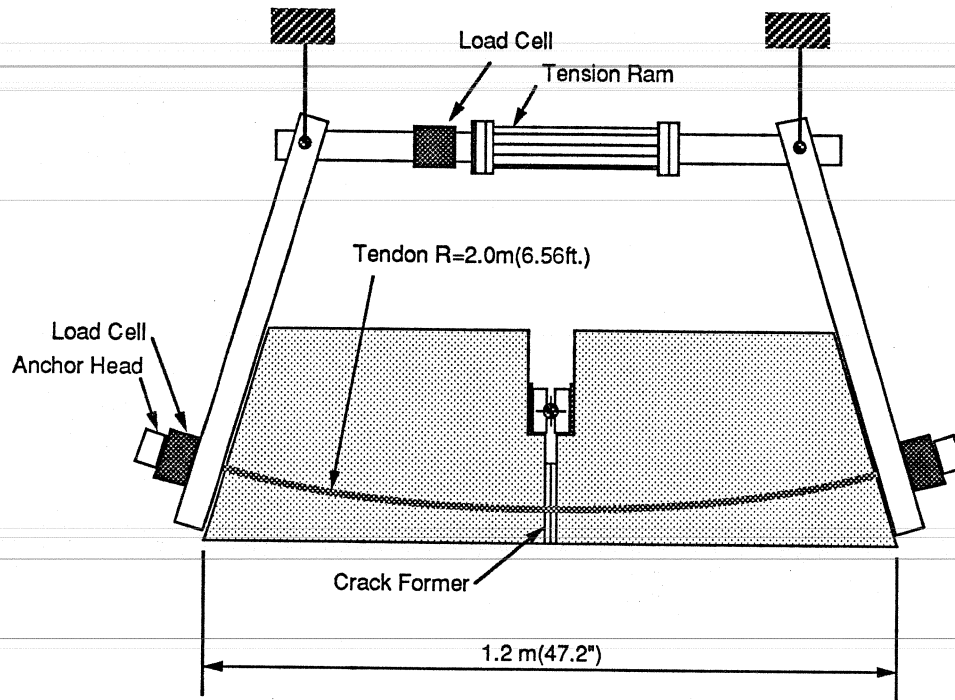
fractured, fretting action between the fractured wire and undamaged wires became more severe leading to additional crack initiation and eventually additional wire fractures.

- The beam with plastic duct had an improved fatigue life compared to those with metal duct.

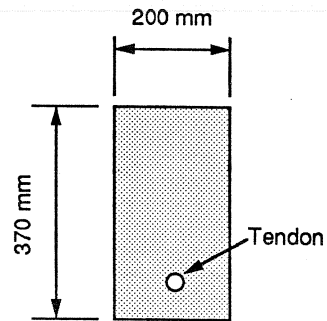
### **2.5.3 Oertle, Thurlimann and Esslinger**

During this study the investigators developed a reduced post-tensioned beam (Fig. 2.12) [13,14,15]. In addition to the fifty-six reduced beam specimens they also tested four large-scale post-tensioned beams identical to those tested by Rigon and Thurlimann [20]. The investigators studied the effects of tendon type (single wires, multiple wires, and strand), duct type (metal or plastic), and the presence or absence of grouting on the fatigue behavior of post-tensioned beams. Some of the observations made during this study include the following:

- In grouted beams with metal duct, failure resulted from fracture of the wires in contact with the steel duct.
- In ungrouted beams with a steel duct, failure resulted from fracture of wires away from contact



a) Elevation



b) Section

Tendon	Duct	Grouted	Ungouted
1-7 mm dia Wire	Metal	●	●
	Plastic	●	
5-7 mm dia Parallel wires	Metal	●	
	Plastic	●	
1-0.6 in dia 7 wire strand	Metal	●	●
	Plastic	●	●

c) Test Program

Figure 2.12 Reduced Beams Tested by Oertle, Thurlimann and Esslinger [14]

points.

- Fretting fatigue reduced the fatigue life of the post-tensioned tendons.
- The use of plastic ducts resulted in an increased fatigue life for post-tensioned tendons.

#### **2.5.4 Cordes, Lapp-Emden and Trost**

During this study, the investigators fatigue tested post-tensioned tendons with and without simulated fretting conditions [4,5]. The apparatus used to simulate fretting conditions is shown in Fig. 2.13. The variables considered were the type of tendon, the tendon stress range, and the magnitude of lateral pressure. Most of the fractures occurred at the contact points between strand and duct. The general conclusion drawn from this investigation was that the fatigue life of post-tensioned tendons was significantly reduced due to fretting.

#### **2.5.5 Muller**

Muller [12] fatigue tested a series of grouted post-tensioned beams with tendons composed of parallel wires, or strands, or a single threaded-bar (Fig. 2.14). Metal duct was used for all beams.

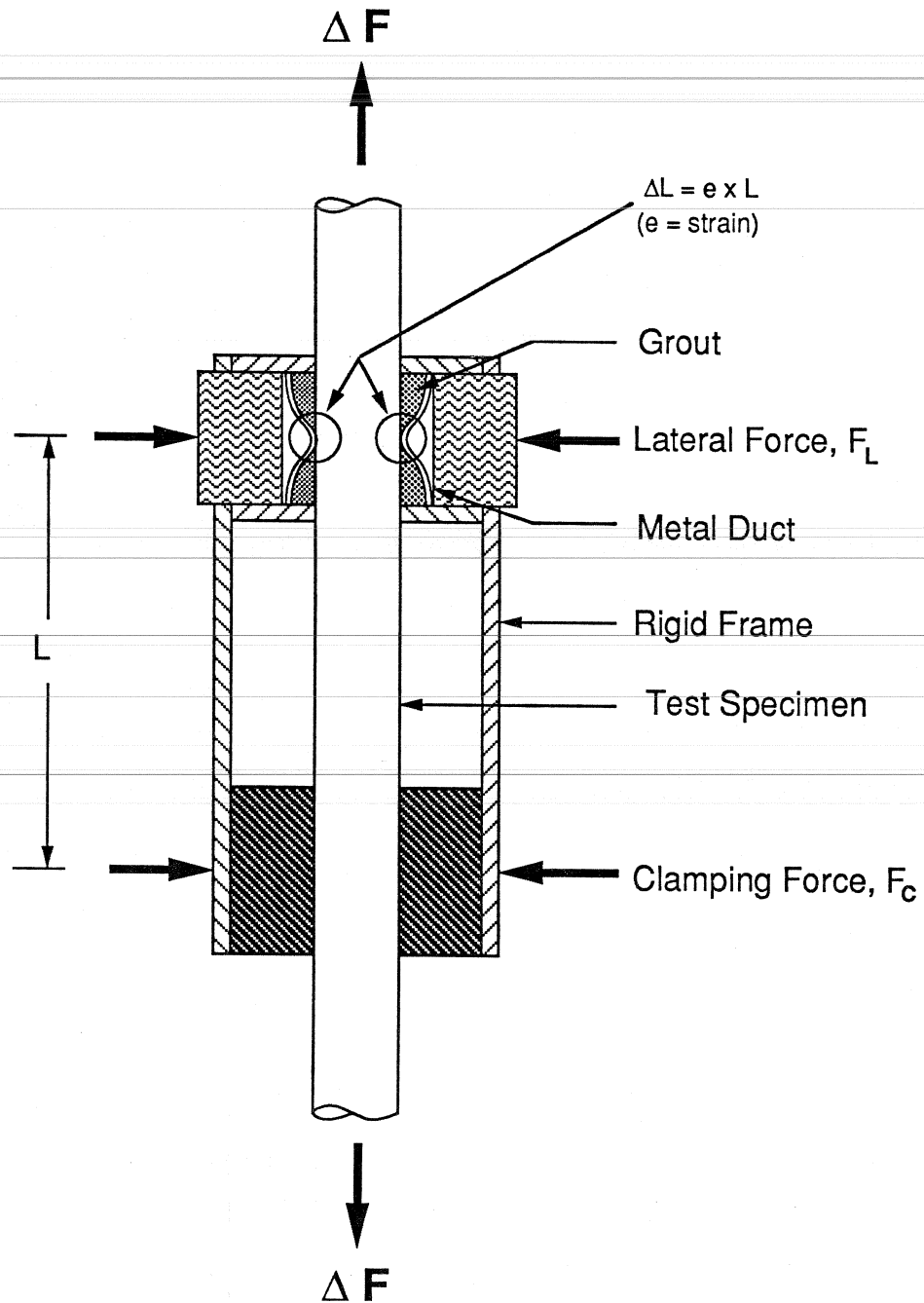
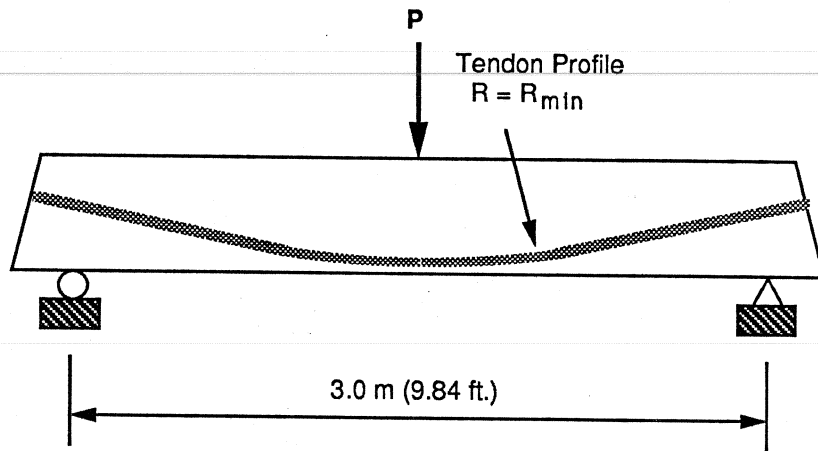
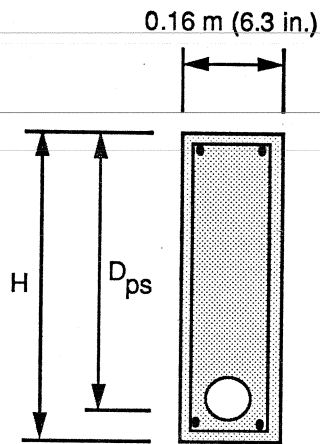


Figure 2.13 Fretting Simulation Apparatus Used by Cordes, Lapp-Emden and Trost [4]



a) Elevation



$H = 0.5 \text{ m (19.7 in.)}$

$D_{ps} = 0.87 \times H$

b) Midspan Section

Tendon Type	Minimum Radius, $R_{min}$ m (ft.)
Dywidag 26.5 mm dia 1-Threaded bar	8.90 (29.2)
Sawoe 12.2mm dia 3-Parallel wires	3.50 (11.5)
Dywidag 0.6 in. dia 3-7 wire strands	4.80 (15.8)

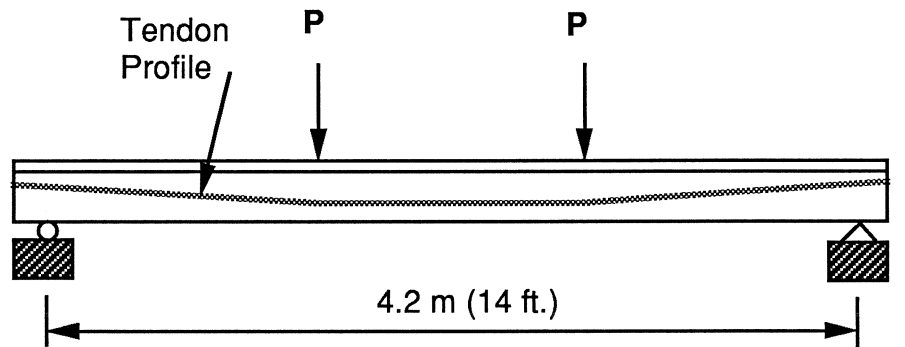
c) Tendons

Figure 2.14 Beams Tested by Muller [12]

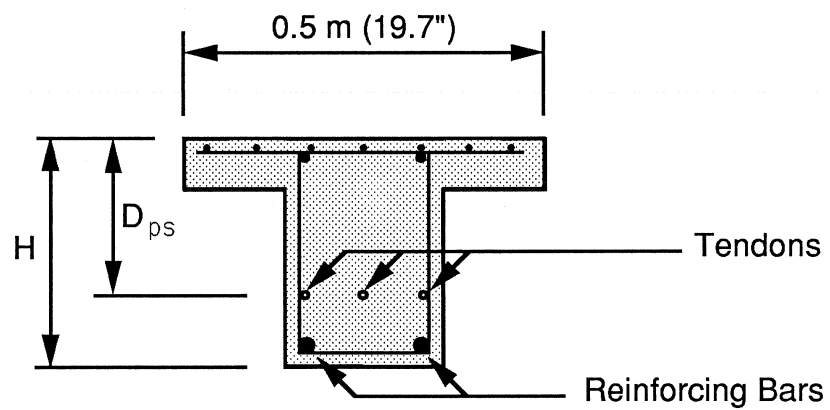
Different tendon crack initiation patterns were observed by Muller. In the case of parallel-wire tendons, the fatigue cracks initiated at contact points between tendon and duct in two of the beams, and at a contact point between adjacent wires in the third beam. In the case of strands, the fatigue cracks initiated from inside the strand due to fretting between adjacent wires of the strand. In the case of threaded-bar tendons, the fatigue cracks initiated at the outside of the tendon curvature.

#### **2.5.6 Shahawi and Batchelor**

During this study, Shahawi and Batchelor [21] fatigue tested eight bonded post-tensioned T-beams, the details of which are shown in Fig. 2.15. The primary variable considered was the degree of prestress, which is defined as the ratio of the force carried by the prestressed reinforcement to the force carried by the total reinforcement (prestressed and non-prestressed) at ultimate conditions. One of the interesting observations made was that six out of the eight beams tested failed by successive fracture of the non-prestressed reinforcement at crack locations due to fatigue, while the post-tensioned tendons did not



a) Elevation



$$H = 0.32 \text{ m (12.6")}$$

$$D_{ps} = 0.70 \times H$$

b) Section

Figure 2.15 Beams Tested by Shahawi and Batchelor [21]



fracture. This observation contradicts all other fatigue studies discussed previously where fracture of tendons was present and was the primary reason for failure. Yates [27] gives the following explanation:

"The difference in modes of failure could be due to the difference in location of prestressed reinforcement relative to non-prestressed reinforcement in a section."

Furthermore, Yates stated that the cross-section of the beams tested by Shahawi and Batchelor was relatively inefficient in terms of its use of prestressing reinforcement.

#### **2.5.7 Brondum - Nielson**

Six post-tensioned beams were fatigue tested during this study [3]. The primary variable considered was the presence or absence of grouting within the duct. In the case of beams without grouting (unbonded), the fatigue lives were short and failure resulted from fractures of the tendons near the end anchorages. In the case of grouted (bonded) beams, the fatigue lives were much longer compared to those of the unbonded beams.

### 2.5.8 Yates

The investigation by Yates [27] was part of a larger study conducted at The University of Texas at Austin. The research that is the subject of this report and the investigations by Diab [6] and Wollmann [26] constitute the other parts of this study. Yates fatigue tested fourteen grouted reduced-beam specimens with single-strand tendons. The primary variables considered were the tendon stress range, the level of prestress, and the type of duct (metal or plastic). Details of the reduced-beam specimen are shown in Fig. 2.16. The reduced beam specimen has several advantages compared to the conventional post-tensioned beam. As Yates stated, "the reduced-beam specimen accurately models the fretting fatigue actions that occur in a conventional cracked post-tensioned beam". It was also more economical and less time-consuming to construct and test.

The reduced-beam specimens were constructed, post-tensioned, grouted, and tested at FSEL. Each specimen was cracked during the initial static load cycles, and the response to these static loads was recorded. This response was used to determine the flexural decompression load which was used to determine the

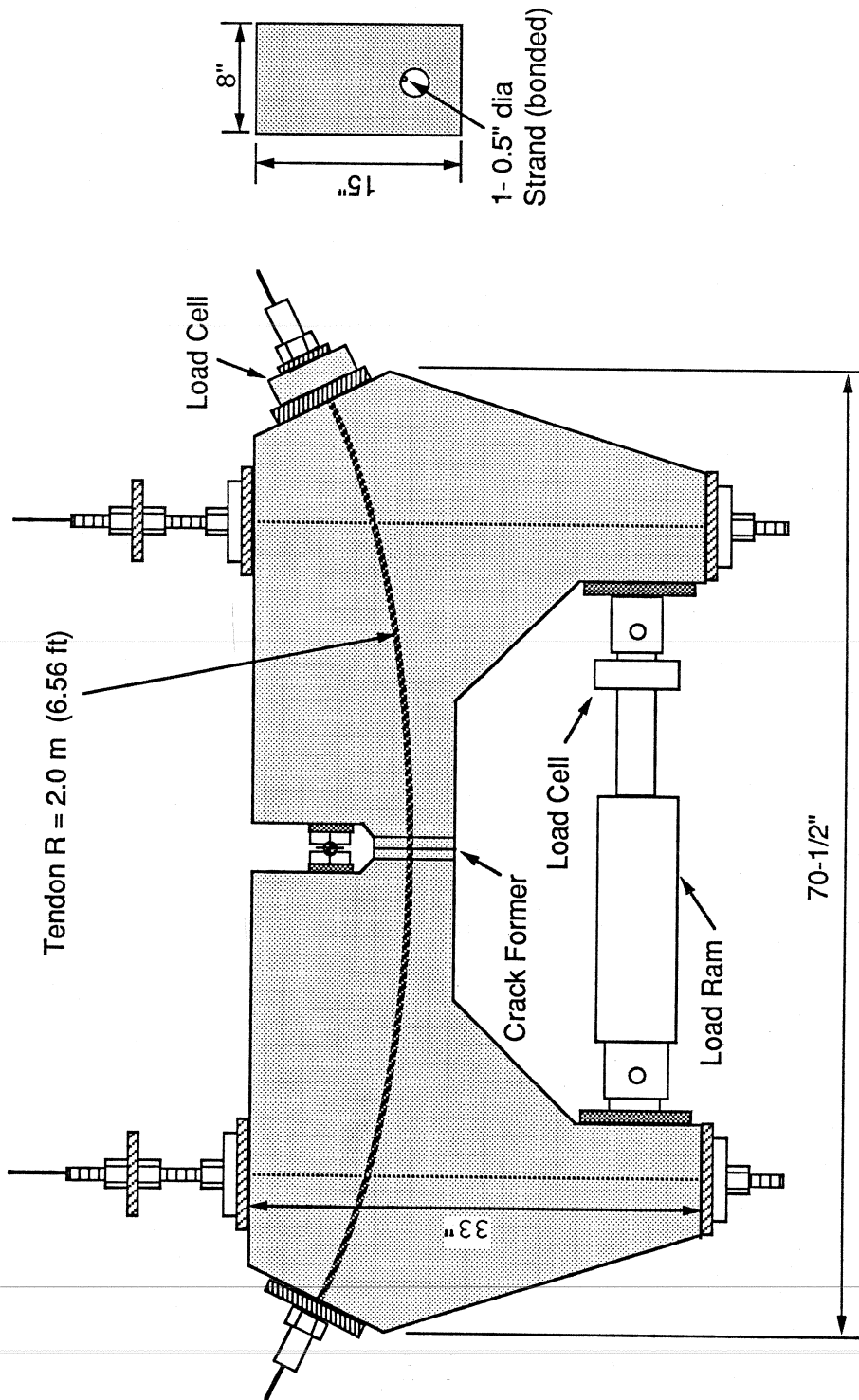


Figure 2.16 Reduced Beams Tested by Yates [27]

effective tendon stress vs. ram load relationships. Then, each specimen was subjected to cyclic loading. The ram loads used were larger than the decompression load in order to have the cracks open during testing. Sufficiently large loads were used to ensure that the beams were internally statically determinate. The cyclic loading was stopped periodically to apply additional static load cycles to each specimen. During static load cycles the specimen response was recorded. Usually load vs. crack width or load vs. ram extension was recorded to describe the specimen response to static load cycles. These plots were used as indicators of the stiffness history of each specimen. When a sudden change in specimen stiffness occurred, the specimen was considered to have failed. After that, a static flexural strength test was performed. Then, the concrete surrounding the duct was chipped away, and the duct was removed from the specimen for a more detailed inspection. The duct was cut open and wire fractures, as well as other fretting signs were examined.

Many interesting observations were made during this post-mortem investigation. Some of these follow:

- All metal ducts were fractured at the locations of concrete cracks.

- The plastic ducts showed much less damage than the metal ducts.
- Deterioration of the grout occurred in the vicinity of cracks.
- The interior surface of the ducts had indentations at the strand contact points. In the case of metal ducts, the contact points showed signs of corrosion or abrasion (which are fretting signs) while in the case of plastic ducts there were no signs of corrosion or abrasion.
- Fretting between metal duct and strand caused initiation of some wire fractures.
- Fretting between wires of the same strand caused some fractures.
- Ordinary fatigue fractures were identified as well as ultimate-strength fractures.

#### **2.5.9 Wollmann**

This investigation by Wollmann [26] was a continuation of the study performed by Yates [27]. Wollmann fatigue tested nine reduced-beam multiple-strand tendon specimens similar in design to those tested by Yates. The primary variables considered were the type of tendons (uncoated strands, or

epoxy-coated strands), the type of duct (metal or plastic), the nominal contact load, and the tendon stress range. The experimental program was similar to the one followed by Yates.

The observations made during the post-mortem investigation were similar to those Yates made. In addition, Wollmann concluded that epoxy coated strands improved the fatigue behavior of a post-tensioned beam. The reason behind this conclusion is that epoxy coating prevents strand-to-strand or strand-to-duct rubbing until the coating is worn through.

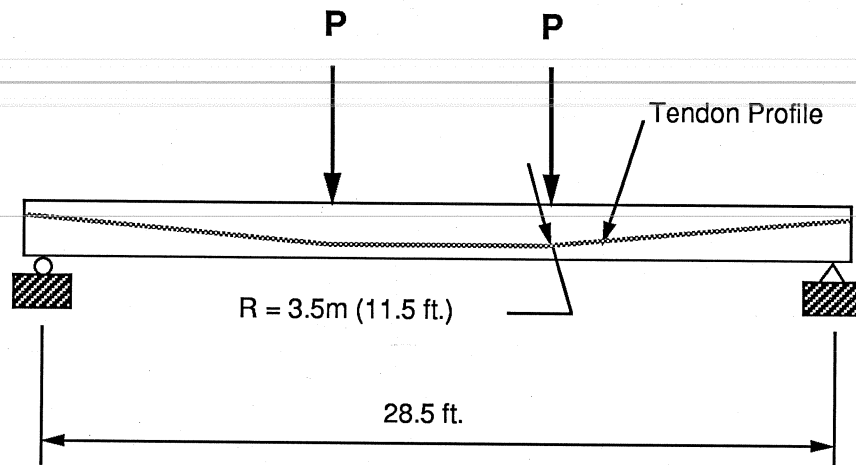
In the case of one specimen with reduced nominal contact load (achieved with a reduced tendon curvature) the test results were surprising. The specimen showed poor fatigue performance which contradicts previous studies in which it was indicated that reduced lateral contact increased fretting fatigue life. The post-mortem investigation of this specimen offered an explanation to this surprising situation. It was found that two strands were twisted in the tendon resulting in an increased concentrated contact load between the strands. This increased concentrated contact load is believed to be the reason for the poor fatigue performance of the specimen.

### 2.5.10 Diab

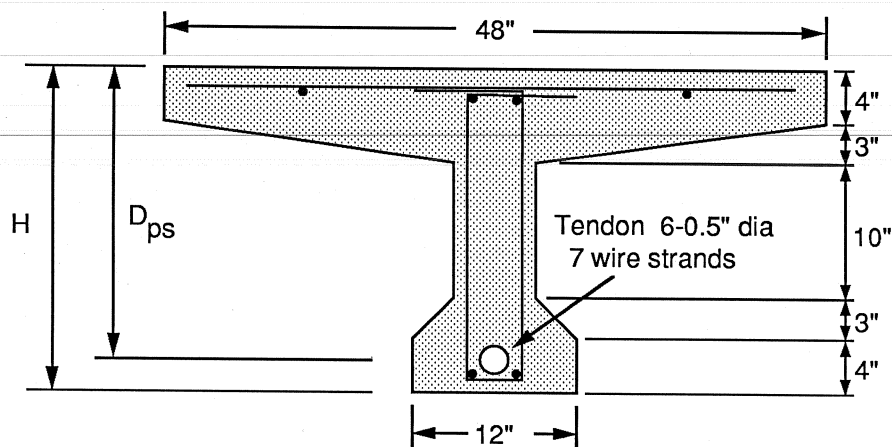
The investigation conducted by Diab [6] was intended to complement the work by Yates and Wollmann, and was the precursor of the research that is the subject of this thesis. Diab fatigue tested three post-tensioned beams whose details are shown in Fig. 2.17. The primary variable considered was the tendon stress range. All the specimens had a single metal duct with a tendon that consisted of 6-0.5 in. diameter, 7-wire strands.

Each specimen was first cracked during initial static load cycles. Load vs. midspan deflection and load vs. crack width curves were plotted during these initial static load cycles. Based on these curves the decompression load was determined. Relationships between load and tendon stress range were computed.

After the initial static load cycles, the specimen was subjected to cyclic loads. The lower load level was always chosen to be below the decompression load in order for the cracks to close during each load cycle. Periodically, cyclic loading was interrupted and additional static load cycles were conducted during which ram load vs. midspan deflection and ram load vs. crack-width curves were plotted. These curves served



a) Elevation



$$H = 24 \text{ in.}$$

$$D_{ps} = 0.86 \times H$$

$$\text{SECTION AREA} = 408 \text{ sq. in.}$$

$$\text{MOMENT OF INERTIA} = 21,831 \text{ in.}^4$$

b) Midspan Section

Figure 2.17 Beams Tested by Diab [6]



as indicators of the specimen stiffness. When a specimen experienced sudden reduction in stiffness, it was believed to indicate fracture of one or more wires, and a static flexural strength test was conducted. During this test, one or two cracks at, or near, the drape points opened up considerably causing additional wire or strand fractures and flexural failure of the specimen.

After the static flexural strength test was completed, the concrete surrounding the duct, between the outside of the drape points, was chipped away and the duct was removed from the specimen for further inspection. The duct was cut open in order to examine the tendon condition. Several observations were made during this post-mortem investigation. It was noticed that most of the wire fretting fractures occurred due to strand-against-duct rubbing. Some of the fractures were caused from wire against wire rubbing. It was also noticed that most of the fractures occurred at the drape points due to the presence of high lateral pressure.

## CHAPTER 3

### EXPERIMENTAL PROGRAM

#### **3.1 Introduction**

The purpose of the experimental program was to study the effects of repeated cyclic loads on the fatigue life and behavior of post-tensioned beams. Five large-scale post-tensioned beams were fabricated, post-tensioned, and tested at FSEL. The variables considered were the duct layout, tendon stress range, and duct material. One beam had a metal duct with a parabolic profile, two beams had a double-draped metal duct, and the remaining two beams had a double-draped plastic duct.

The basic objective of the tests was to obtain fatigue data that would allow development of a tendon stress range vs. number of cycles (S/N) curve.

#### **3.2 Strand in Air Tests**

Two different spools of strand were used in the fabrication of the large-scale post-tensioned beams. The first one is referred to as "Strand B" and the second one as "Strand C". Strand B was used in previous

studies at FSEL and was used in the fabrication of the first two specimens. When Strand B was depleted, Strand C was used in the fabrication of the remaining three specimens.

Stress-strain curves for both strand types were provided by the manufacturer. Additional laboratory tests confirmed the validity of the information provided by the manufacturer. Consequently, Yates [27] and Wollmann [26] fatigue tested samples of Strand B and Strand C in air in order to determine fatigue characteristics for the strand.

### **3.2.1 Fatigue Tests**

A set of 10 Strand B samples and a set of four Strand C samples were fatigue tested in air by Yates [27] and Wollmann [26], respectively. The fatigue equipment and test set-up are described in detail by Paulson [17]. A simple schematic of the strand fatigue test set-up is shown in Fig. 3.1. The results of the tests are listed in Table 3.1. The results are also plotted in Fig. 3.2, along with Paulson's strand in air failure zone developed based on results of over 700 strand in air fatigue tests [17] and the AASHTO fatigue model. Comparison of the results and the data points in

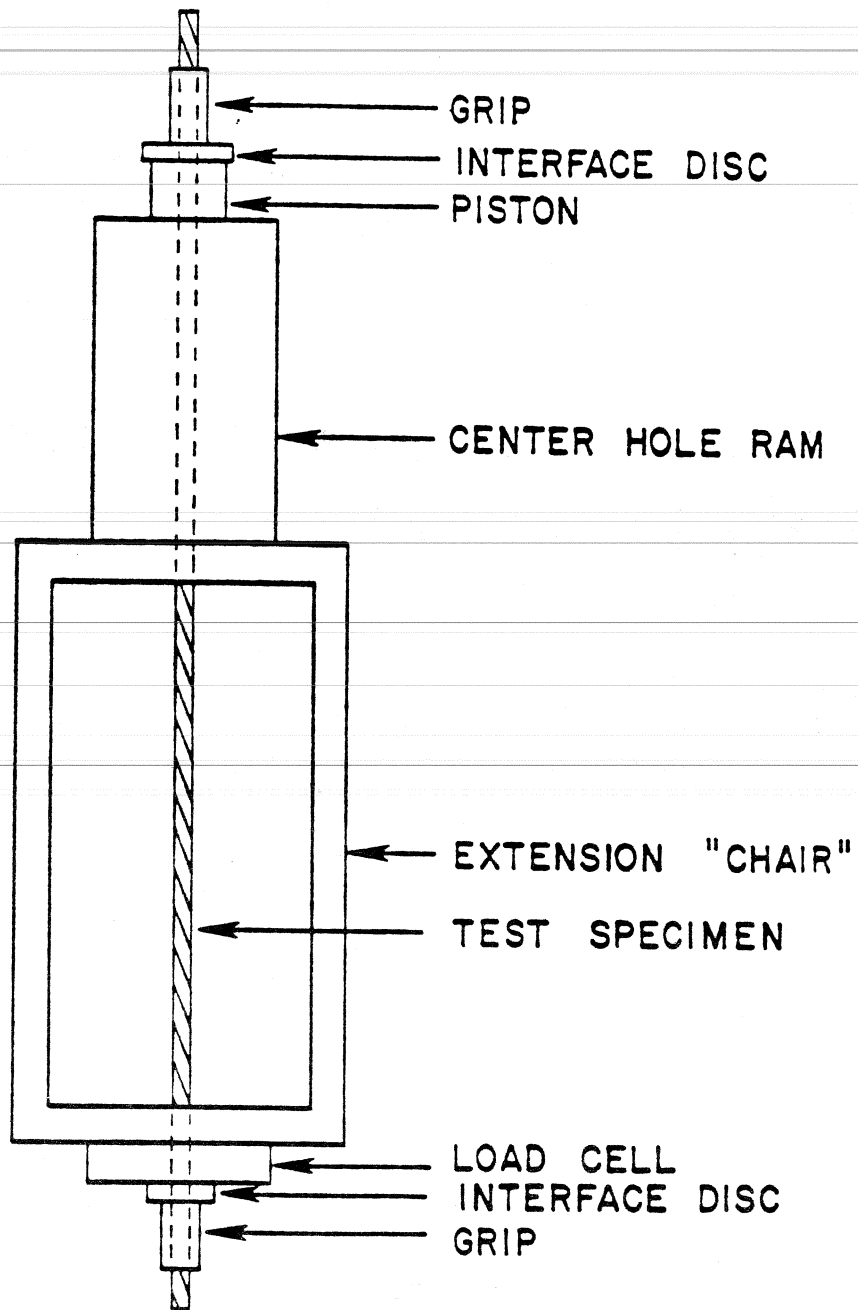


Figure 3.1 Schematic Representation of the Strand Fatigue Test Set-Up (from Paulson [17])

Table 3.1 Strand In Air Fatigue Test Results

Strand Type	Sample No.	Stress Range (ksi)	Fatigue Life (No. of Cycles x 1000)
Strand A	1	40.5	306
	2	40.5	468
	3	40.5	1746 *
	4	40.5	684
	5	40.5	265 *
	6	30.0	925
	7	30.0	406 *
	8	30.0	1298
	9	30.0	1797 *
	10	30.0	2175 *
Strand B	1	40.0	289
	2	40.0	782
	3	30.0	3057
	4	30.0	9000 #

\* Failure occurred in the grip region

# Runout

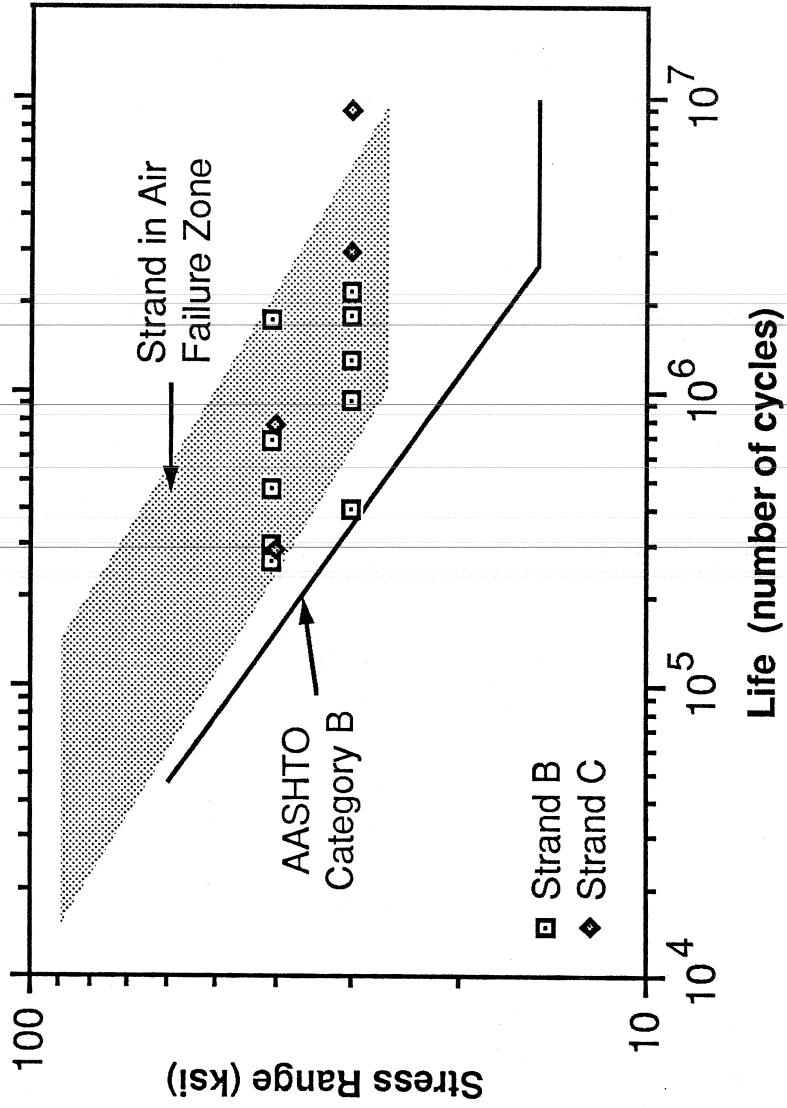


Figure 3.2 Comparison of Strand-In-Air Fatigue Test Results, Paulson's Strand-In-Air Failure Zone and AASHTO Fatigue Model

Fig. 3.2 shows that the data points for Strand B and C fall within the bounds of Paulson's strand in air failure zone and above the AASHTO fatigue model.

### **3.2.2 Static Tests**

Two static tests were conducted with samples of Strand C to confirm the mechanical properties of the strand. Yates conducted similar tests for Strand B [27]. Elongation of the strands was measured electronically with deflection transducers. Load vs. elongation curves were plotted with an X-Y plotter. The test results showed no significant differences in the mechanical properties for Strand C compared to Strand B. Properties of both strands compared well with their respective mechanical properties provided by the strand manufacturers. The gage length chosen was 24 in., and the average modulus of elasticity for Strand B and Strand C was determined to be 28,770 ksi and 28,100 ksi, respectively.

### **3.3 Large-Scale Beam Tests**

The primary objective of this report was to study the fatigue behavior of large-scale post-tensioned beams, and to develop a stress range vs. number of

cycles (S/N) curve.

An alphanumeric label was assigned to each specimen. Each label consists of two letters and two numbers. The first letter is either a "P" or a "D" indicating whether the specimen had a parabolic duct or a draped duct. The second letter is either an "M" or a "P". An "M" indicates that the specimen had a metal duct, and a "P" indicates that the duct used was plastic. The third character is a number, and indicates the beam's testing sequence. The beam with a "1" as the third character was tested first. The fourth character indicates the tendon stress range in ksi applied during testing. Using the labelling system described above, the five beams tested were labelled as follows:

P-M-1-25

D-M-2-40

D-M-3-30

D-P-4-30

D-P-5-30

### **3.3.1 Specimen Description**

A T-shaped cross-section was chosen for the large-scale beams. The efficiency factor for this



cross-section, defined by Equation 3.1 is approximately 0.44. The actual dimensions and details of the specimen are shown in Fig. 3.3.

$$\text{Equation 3.1} \quad R = I / (A * C_t * C_b)$$

where  $R$  = Efficiency Factor

$I$  = Moment of Inertia of  
Cross-Section

$C_t$  = Distance of Neutral Axis to  
Top Concrete Fiber

$C_b$  = Distance of Neutral Axis to  
Bottom Concrete Fiber

The width of the bottom flange of the specimen is increased at the ends to accommodate the embedded anchorage plate and the spiral reinforcement. Figures 3.4 and 3.5 show the location of the draped and parabolic tendons within the specimen.

The draped ducts had a radius of curvature of 3.5 m or 11.5 ft for the curved section of the tendon. This curvature is the same as used in post-tensioned beams tested at the Swiss Federal Institute of Technology in Zurich [20] and at the Technical

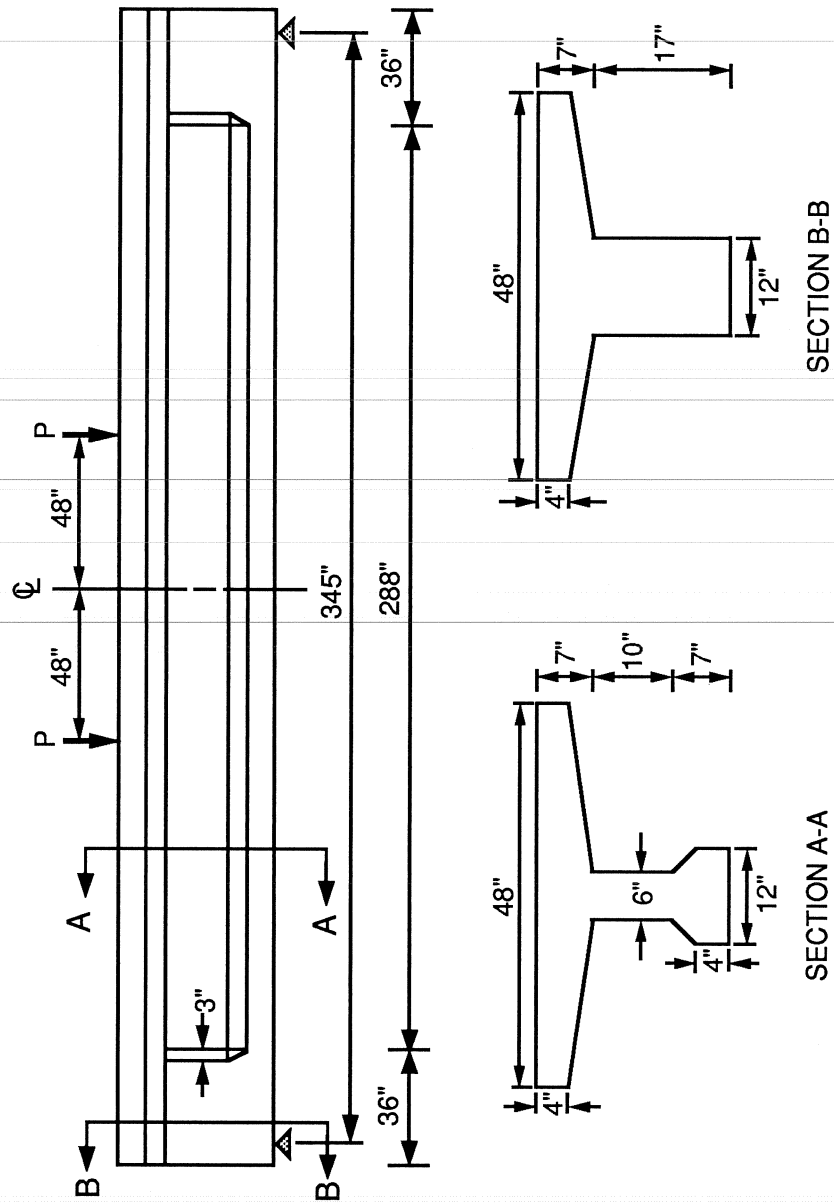


Figure 3.3 Actual Dimensions and Details of Large-Scale Beam

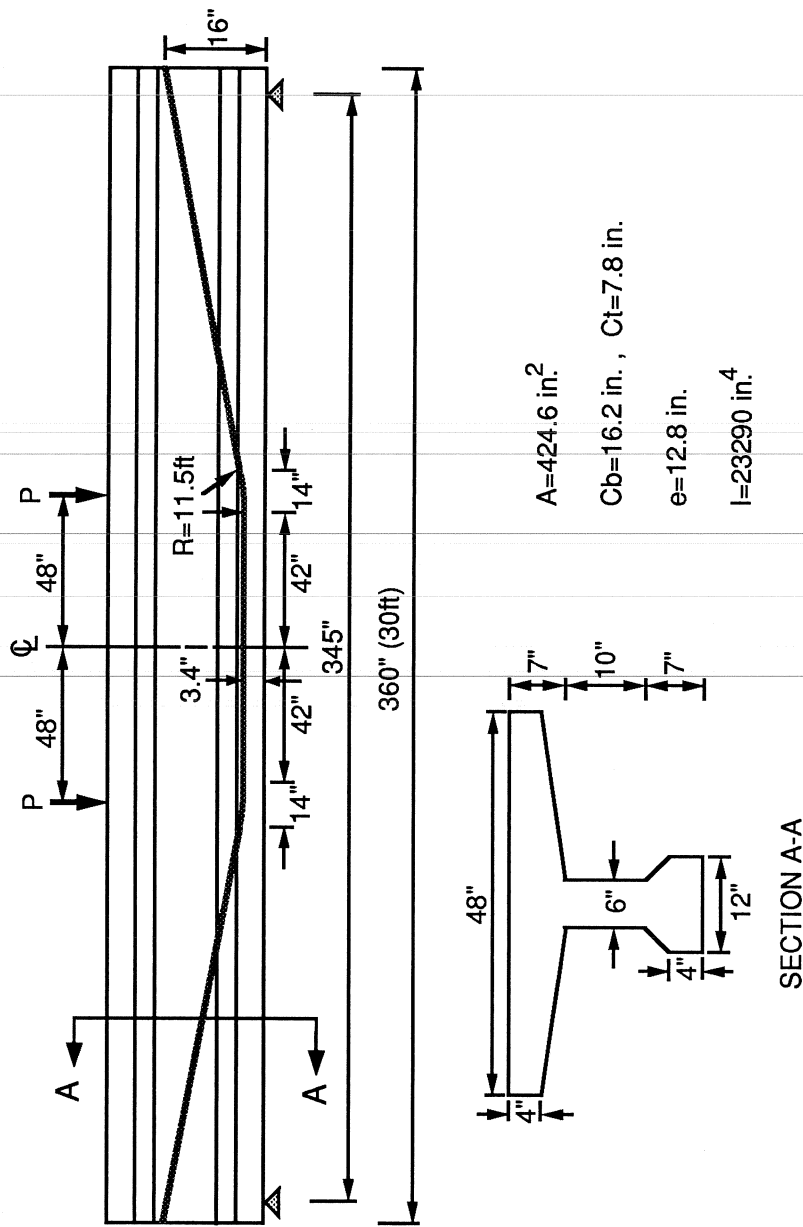


Figure 3.4 Large-Scale Beam with Draped Tendon  
(Non-Prestressed Reinforcement Not Shown)

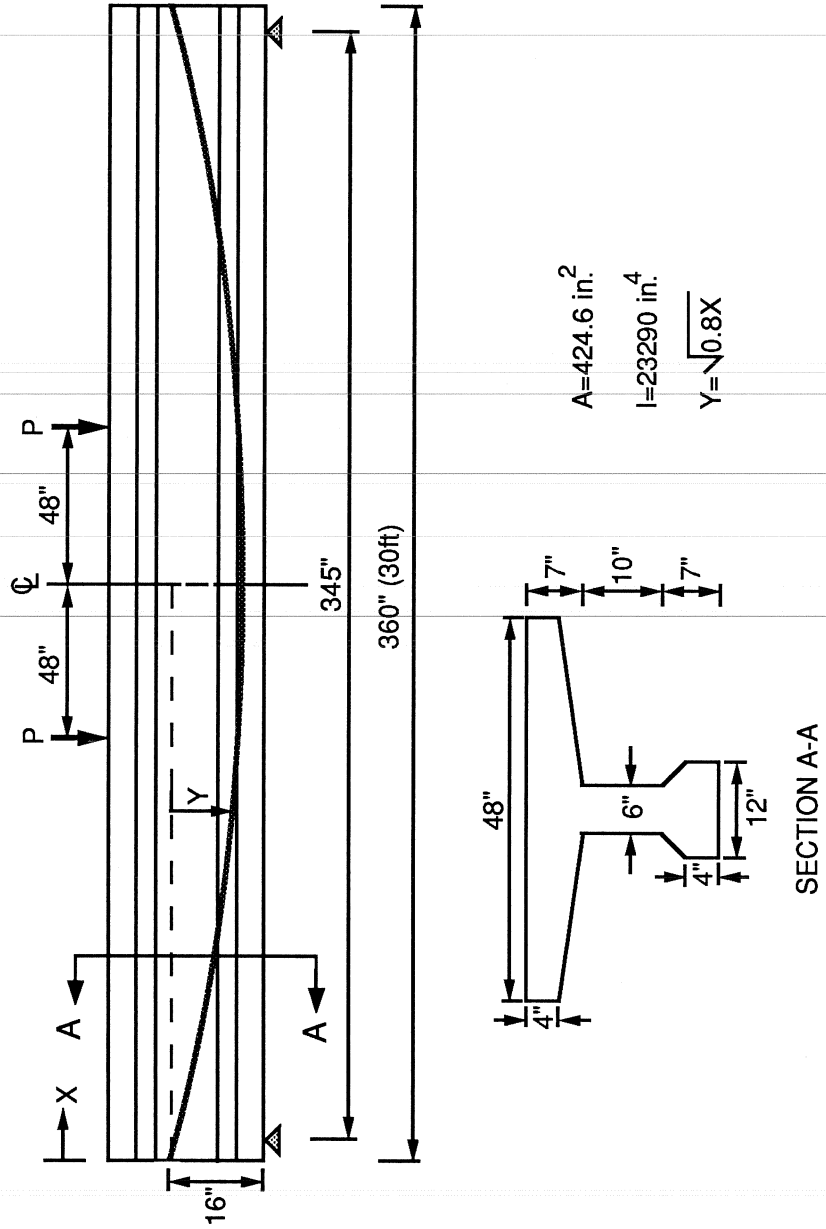


Figure 3.5 Large-Scale Beam with Parabolic Tendon  
(Non-Prestressed Reinforcement Not Shown)

University of Munich [12] for the sake of comparison.

### **3.3.2 Test Variables**

Since the number of specimens tested was limited, the three most important variables were considered. The first of those variables was the duct layout. One specimen was fabricated with a parabolic duct, and the remainder with draped ducts. The second variable was the duct material. Three specimens had standard metal post-tensioning duct, and the remaining two had plastic duct. The last variable was the tendon stress range. The five specimens were tested with a tendon stress range varying from 25 to 40 ksi.

### **3.3.3 Materials**

#### **3.3.3.1 Concrete**

Concrete for all five large-scale beams was delivered by a commercial concrete supplier. It had a target 28-day compression strength of 6000 psi and was without air entrainment. The maximum size aggregate was 3/8 inch. The concrete consisted of Type I Portland cement, Colorado river sand, and crushed limestone coarse aggregate. The 6000 psi compressive strength concrete was required so that post-tensioning could take

place at an early age.

Concrete compressive strengths were determined from compression tests of 6.0 x 12.0 in. cylinders. Tests were conducted at seven days, at the time of post-tensioning, at 28 days, and at the time of testing. Measured compressive strengths are shown in Table 3.2.

#### **3.3.3.2 Passive Reinforcement**

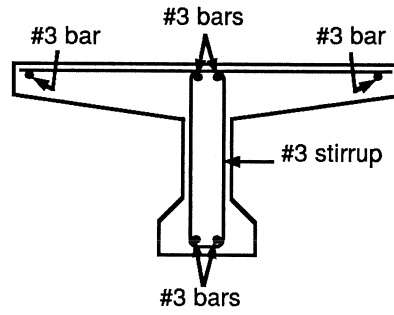
Each specimen had a minimum amount of longitudinal unstressed (passive) reinforcement which consisted of ASTM A615, Grade 60 steel. The top flange was reinforced with 4-#3 bars and the bottom flange with 2-#3 bars. Minimum shrinkage and temperature reinforcement was also provided in the top flange perpendicular to the longitudinal axis of the beam.

The top flange passive reinforcement was placed to permit transportation of the specimen to the place where post-tensioning was performed without cracking the specimen. The purpose of the bottom flange passive reinforcement was to control crack width and reduce creep losses. Passive reinforcement details are shown in Fig. 3.6.

Table 3.2 Concrete Compressive Strengths

Specimen	Concrete Compressive Strengths (psi)			
	At 7 Days	At 28 Days	At Post-Tensioning	At Testing
P-M-1-25	N.A.	N.A.	N.A.	5380
D-M-2-40	5450	6290	6340	6350
D-M-3-30	5690	6540	6650	6690
D-P-4-30	5200	6220	6530	6620
D-P-5-30	6450	7140	7180	7200

Typical Non-Prestressed Reinforcement in the Center Region



End Region with 5 Stirrups at 8 in. Spacing

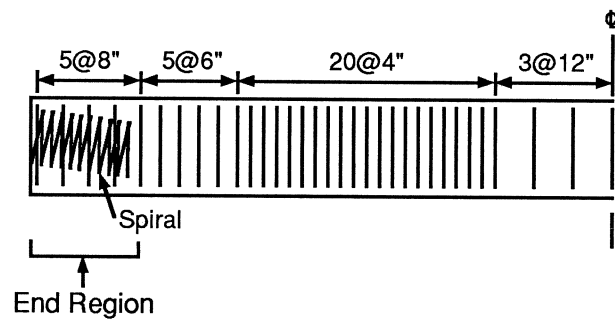
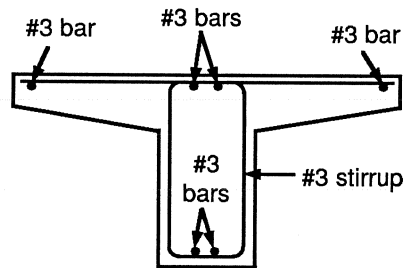


Figure 3.6 Passive, Longitudinal, Transverse, and Confining Reinforcement in Large-Scale Beams



### **3.3.3.3 Shear and Confining Reinforcement**

The shear and confining reinforcement consisted of ASTM A615, Grade 60 steel and was bent and delivered by a local supplier. The design of the transverse reinforcement was done in accordance with ACI 318-83 by Diab [6]. The shear reinforcement consisted of #3 stirrups. The shape of the stirrups was the same along the length of the specimen except in the end regions of the beam. The spacing varied along the length of each specimen as shown in Fig. 3.6.

At the ends of each specimen, spiral reinforcement (shown in Fig. 3.6) was provided as recommended by Stone and Breen [22]. The purpose of the spiral reinforcement was to resist splitting forces imposed by the post-tensioning anchorage devices.

### **3.3.3.4 Prestressing Steel**

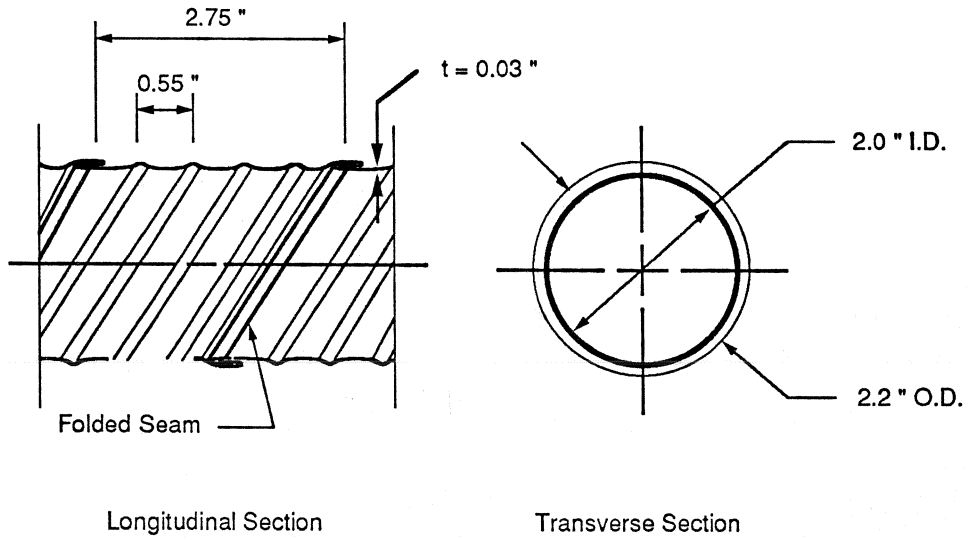
The post-tensioning tendons consisted of 1/2 in. diameter, ASTM A416, Grade 270, stress-relieved seven wire strand. The tendons were cut from two different spools of strand, as discussed in Section 3.2. Each specimen contained one tendon made up of six strands. The location of the tendon is shown in Fig. 3.4 or Fig. 3.5.

### 3.3.3.5 Post-Tensioning Duct

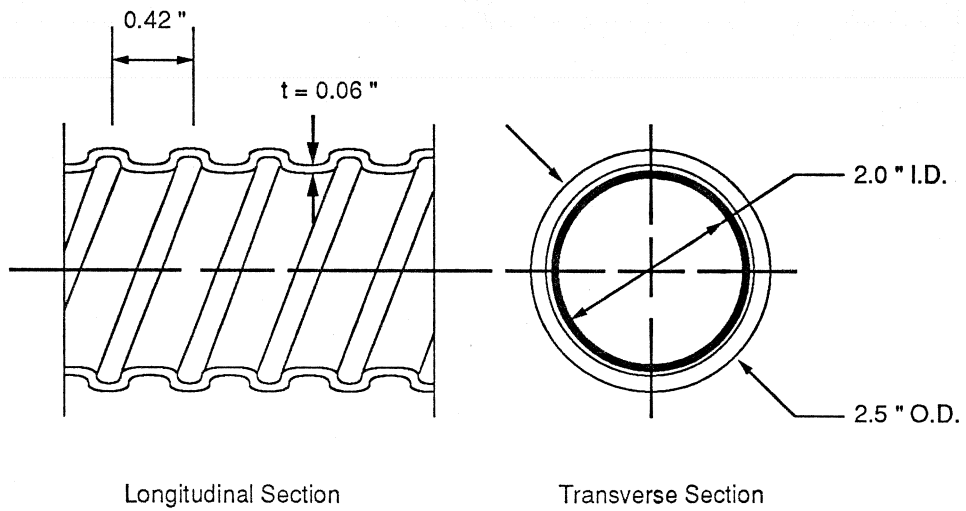
Two types of post-tensioning duct with a nominal diameter of 2 1/8 in. were used. One was galvanized folded metal duct and the other was polypropylene corrugated plastic duct. Both of them were purchased from commercial suppliers. The metal duct was delivered in 20-foot pieces, while the plastic duct came in a continuous coil. Pieces of metal duct were joined together using a one-foot length of duct that was one size larger than the duct being spliced. The shape and the actual dimensions of the metal and plastic duct are shown in Fig. 3.7.

### 3.3.3.6 Grout

The grout mix design was derived from the Texas State Department of Highways and Public Transportation (TDHPT) Standard Specifications. The grout mix consisted of one bag of Type I Portland cement, 5-1/2 gallons of water (which yielded a water/cement ratio of 0.5) and 0.94 lbs Interplast expansive agent (one percent by weight of cement). The water/cement ratio used exceeded the maximum value of 0.45 which is recommended by the Post-Tensioning Institute [18] and AASHTO [1].



(a) Metal Duct



(b) Plastic Duct

Figure 3.7 Measured Dimensions of Duct

Grout compressive strengths were obtained from compression tests of 2.0 in. cube samples conducted prior to testing of the specimen. Average compressive strength of the grout used in each specimen was determined from three cube samples. These values are shown in Table 3.3.

#### **3.3.3.7 Prestressing Hardware**

The prestressing hardware was loaned to FSEL by Prescon Corporation. It included a 100-ton, center hole, double action hydraulic ram, a seven-strand prestressing anchor with wedges, and a pressure plate with mechanical rubber springs. Other hardware used during post-tensioning included anchorage hardware, a steel chair, and a hand-pump.

The anchorage hardware consisted of a Prescon embedded anchorage plate with 1/2 in. diameter grout tubes, and a seven-strand anchor with T13 Freyssinet wedges.

A three-leg steel chair was built for the second stage of the post-tensioning operation. A 10,000 psi RP40DR Templeton Kenley hand-pump was used to provide hydraulic pressure. Figure 3.9 shows most of the prestressing hardware in place during post-tensioning.

Table 3.3 Grout Compressive Strengths

Specimen	Grout Compressive Strengths (psi)
P-M-1-25	2664
D-M-2-40	3180
D-M-3-30	2656
D-P-4-30	2909
D-P-5-30	2760

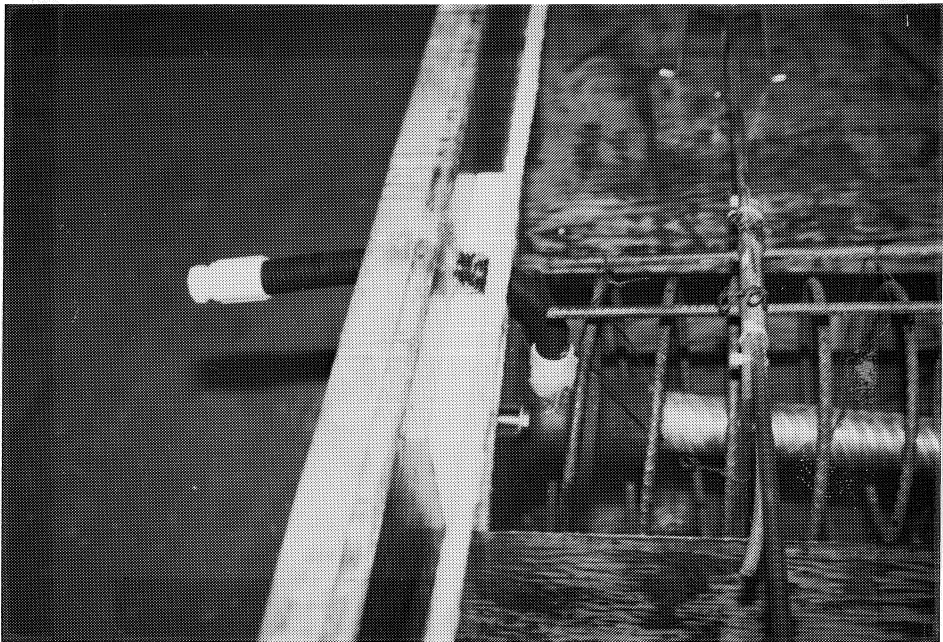


Figure 3.8 Embedded Anchorage Plate and Spiral Reinforcement in Place Before Casting

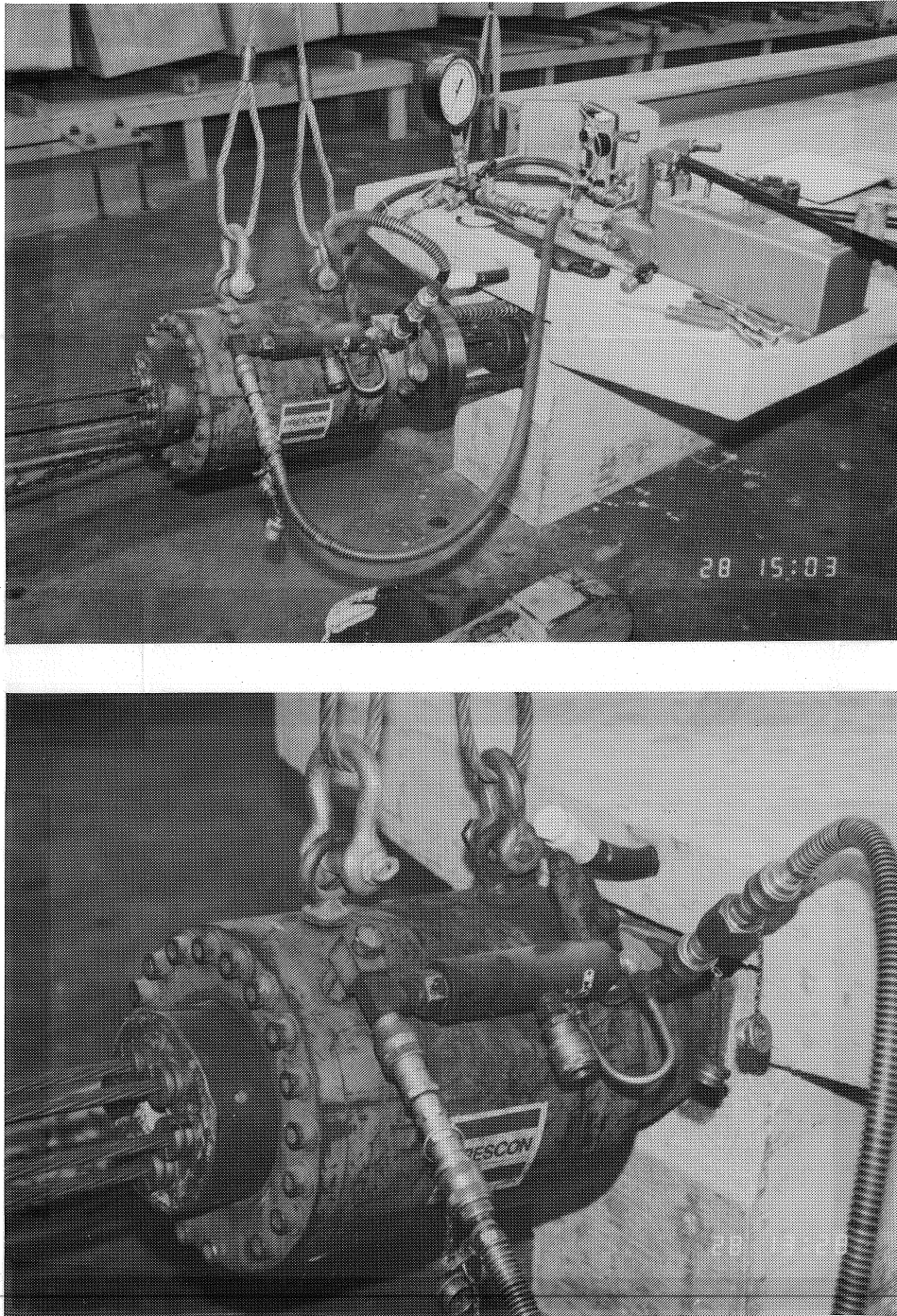


Figure 3.9 Photographs of Post-Tensioning Procedure

### **3.3.4 Fabrication**

All five large-scale beams were fabricated at FSEL. The fabrication time schedule was such that when one specimen was being tested another one was fabricated and made ready for post-tensioning. As soon as the specimen being tested failed, the other specimen was post-tensioned, grouted, and placed in the test setup. Post-tensioning was performed as late as possible to reduce time-dependent prestress losses before testing.

#### **3.3.4.1 Formwork**

Formwork for the large-scale beams was designed and constructed at FSEL by Diab [6]. The wood used was 1/2 and 3/4 in. plywood and 2x4 in. ribs. The formwork consisted of eight side panels (four on each side), two end panels (one at each end) and a continuous bottom platform. The whole assembly was held together using threaded rods. The formwork was used for casting of all large-scale beams tested in this program.

Before the placement of concrete, the formwork was thoroughly cleaned using sand paper, then assembled. Any gaps existing between the panels were sealed with silicon and/or duct tape to prevent concrete from leaking. Three to four layers of lacquer mixed with



thinner were then applied to the formwork for protective purposes. The final step was the application of form oil to prevent any adhesion of concrete to the formwork thus protecting the formwork and making the stripping off of the formwork easier.

#### **3.3.4.2 Reinforcing Cage**

The reinforcing cage, excluding the spiral reinforcement, was assembled and then the post-tensioning duct was placed. Installation of the duct included aligning and bending it to the proper curvature. Placement of the duct was made more difficult when plastic duct was used, because of increased flexibility. The duct was secured to the reinforcing cage with cable and plastic ties. Two pick-up hooks were then attached to the reinforcing cage at approximately the third points. The location of the hooks was such that when the specimen was lifted and transported before post-tensioning, the tensile stresses induced in the top flange were not large enough to crack the specimen.

Next, the reinforcing cage was placed inside the formwork using an overhead crane. The spiral reinforcement was then placed at the ends of the

reinforcing cage, and the end panels of the formwork with the embedded anchorage hardware (Fig. 3.8) were attached to the formwork making it ready for the placement of concrete.

#### **3.3.4.3 Concrete Placement**

Concrete from a local ready-mix plant was used for the fabrication of the specimens. A concrete slump test was performed according to ASTM before placement. Usually, some water was added in order to achieve the desired slump of six inches. Concrete was loaded from the truck into a one cubic yard bucket, and was transported to the formwork with an overhead crane. Casting of the concrete was done in three layers, and 3/4 and 1-1/2 in. pencil vibrators were used to consolidate the concrete. The top surface of the beams was trowelled to a smooth finish. About one hour after casting, the concrete was covered with wet burlap and a plastic sheet. The cover remained in place for two days to maintain the humidity and heat needed for curing.

Fifteen 6.0 x 12.0 in. test cylinders were cast with each beam specimen. They were covered with plastic caps during the curing period and were stripped at the same time when the plastic, burlap, and formwork were

removed from the beam.

#### **3.3.4.4 Post-Tensioning**

Six 40-ft long strands were cut from the spool and passed through the duct, extending five feet on each side of the specimen. One strand had nine electrical strain gages attached to it, as shown in Fig. 3.17, in order to determine the prestress force applied to the tendon during post-tensioning. A seven-strand prestressing anchor was placed at each end of the beam. Wedges were inserted around the strands in the anchor devices, and mechanical rubber springs were inserted around each strand at one end of the specimen (live end), pushing against the wedges. A pressure plate was placed next, pushing against the mechanical rubber springs. A Prescon double-action 200 kip capacity ram was placed against the pressure plate with the strands passing through the ram. The strands were passed through another seven-strand anchor which was placed against the back side of the ram, and were secured by inserting wedges in the anchor plate. A Templeton Kenley hand pump was then connected to the ram using high-pressure hydraulic hoses. A pressure transducer, which was calibrated in advance, and a pressure gage

were installed between the hand pump and ram to measure and cross-check the pressure levels applied to the ram. The electrical response of the pressure transducer was read using a strain indicator box. The electrical wires coming from the strain gages were also connected to a switch and balance box that was connected to a strain indicator box.

The ram force was applied to the tendon in increments. At each load increment the strain gage, pressure gage, pressure transducer, and ram extension readings were recorded. The ram force was increased until a maximum stress of  $0.75f_{pu}$  was applied to the tendon.

During the post-tensioning procedure described above, the prestressing anchor and the wedges were held in place by the pressure plate and the mechanical rubber springs so that anchorage seating losses were minimized.

The ram force was slowly released, and the stressing hardware was removed and then placed back at the other end of the beam on a three-legged steel chair that replaced the pressure plate and the mechanical rubber springs as shown in Fig. 3.9. The ram force was again applied in increments and the same readings as before were taken. During this step the prestressing

anchor at the former "dead end" was pulled away from the embedded anchorage plate. When the maximum stress of 0.75fpu was again reached, semicircular steel shims with different thicknesses were used to fill the gap between the prestressing anchor and the embedded anchorage plate. The anchor head was released onto the semicircular shims by unloading the post-tensioning ram.

#### **3.3.4.5 Grouting**

The grouting operation was done as soon as possible after the post-tensioning procedure was finished in order to minimize losses due to relaxation of the strands.

First, silicon caulk was used to seal the unused open hole of the prestressing anchor and any gaps around the prestressing anchor and wedges to prevent grout from leaking outside the duct. This was done immediately after post-tensioning was finished. The following day the grout ingredients (proportions are discussed in Section 3.3.3.6) were placed and mixed for ten minutes in a commercial grout pump. The grout was then pumped into the duct through plastic hoses. A photograph of the grout pump is shown in Fig. 3.10.

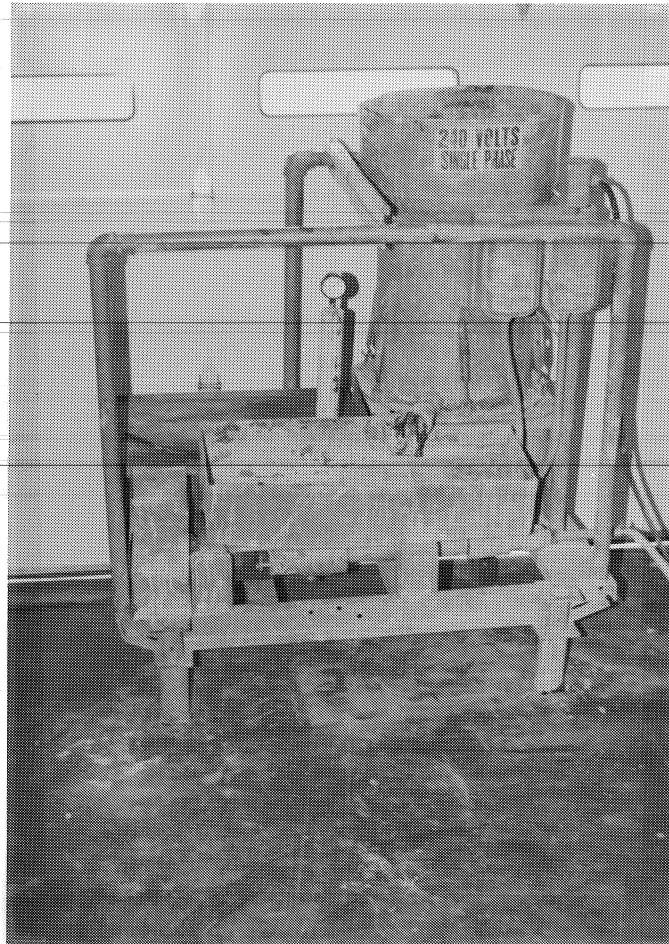


Figure 3.10 Photograph of the Grout Pump

### 3.3.5 Test Set-Up

#### 3.3.5.1 Loading System

The loading system consisted of two wide-flange steel columns tied to the test floor, a cross beam bolted to the two columns, and two diagonal steel angles bracing the steel columns for stability purposes. Details of the loading frame are shown in Fig. 3.11.

Steel pedestals tied to the test floor provided the supports at the ends of the specimens. In order to allow some longitudinal and rotational movement of the specimen, 16 x 9 x 1 in. neoprene pads were placed between the specimen ends and the supports. To avoid any possible excessive longitudinal and transverse movement of the specimen, steel angles were used as shown in Fig. 3.12. This figure shows a steel pedestal and neoprene pad as well.

The top of the ram used to load the specimen was pinned to the cross beam, and the bottom was attached to a spreader beam through a "cup and dish" system as shown in Fig. 3.13. The spreader beam transferred load to the specimen through a pair of "cup and dish" assemblies as shown in Fig. 3.14. To avoid any transverse movement of the spreader beam, it was braced against one of the steel columns. The longitudinal

Moved to  
465-25  
Pg 59



Figure 3.11 Photographs of the Loading Frame



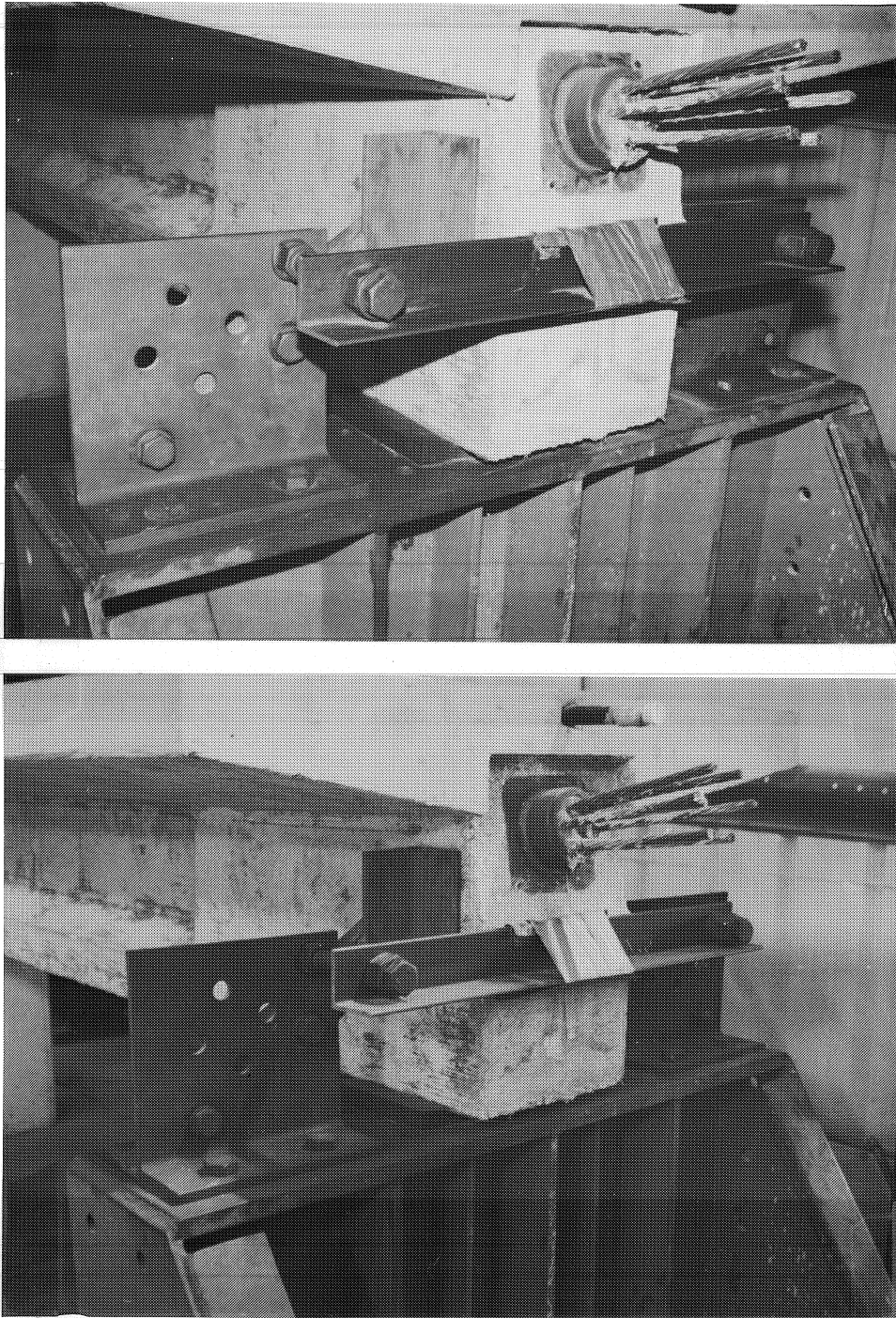


Figure 3.12 Photographs of Steel Pedestals, Neoprene Pads, and End Restraints

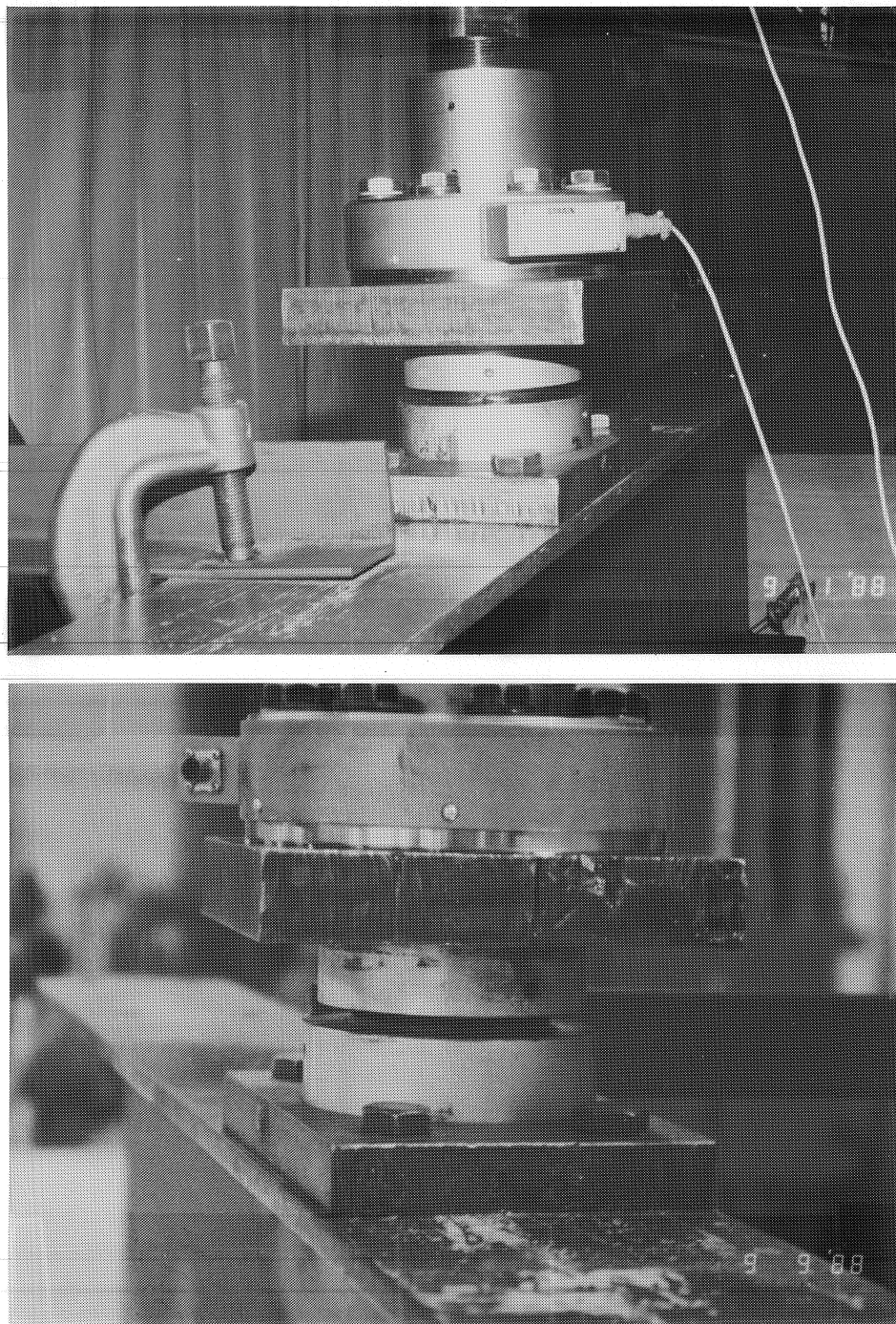


Figure 3.13 Cup and Dish Assembly Between the Ram and Spreader Beam

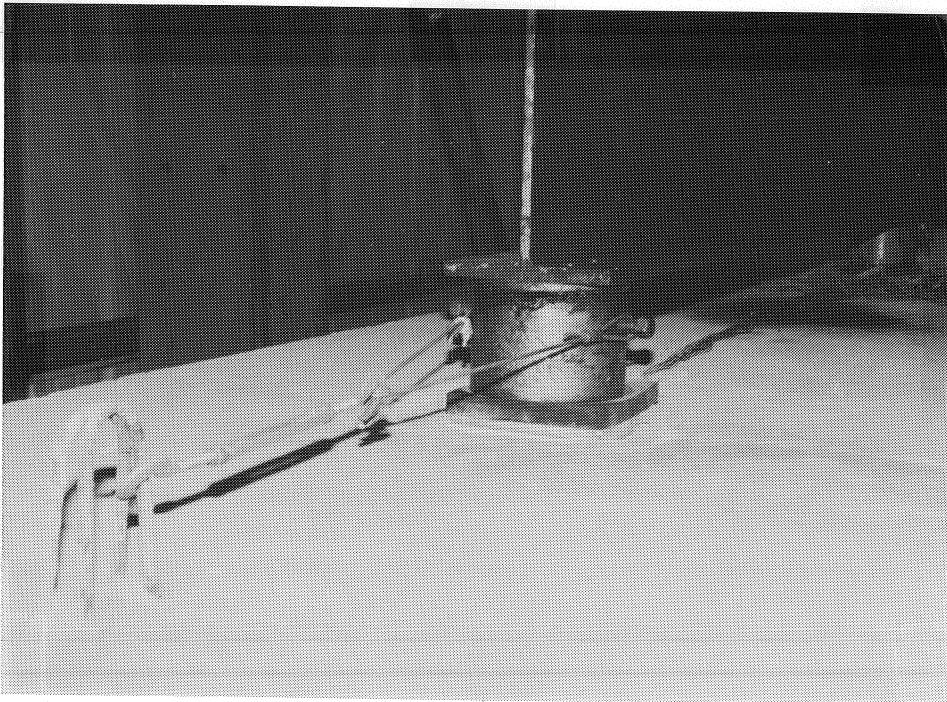
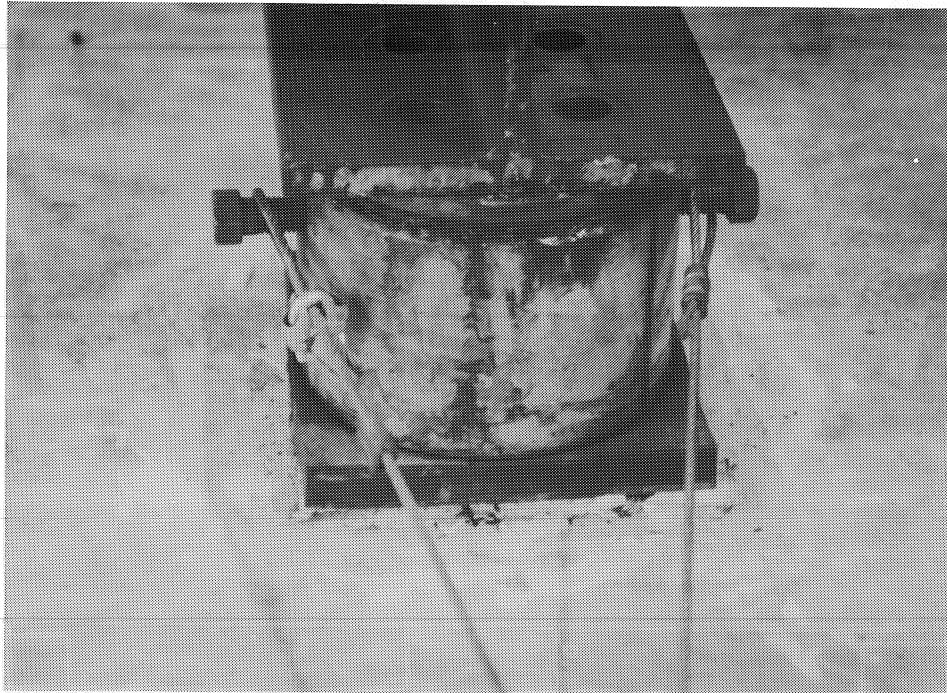


Figure 3.14 Cup and Dish Assembly, Neoprene Pad, and Hydrastone Layer Between Spreader Beam and Specimen

movement of the spreader beam was prevented by tying the cup and dish assemblies beneath the spreader beam to the pick-up hooks by using cables as shown in Fig. 3.14. To achieve a smooth transfer of the load from the cup and dish assemblies to the specimen, a layer of hydrastone and a 7 x 7 x 1 in. neoprene pad were placed between each dish and the beam specimen.

Loading was controlled with a closed-loop servo control system (Fig. 3.15). Two Shore Western pumps, with 20 gpm and 50 gpm capacities, connected in series provided the hydraulic pressure in the system. The first three specimens were tested using both pumps, while the last two were tested using only the smaller capacity pump while the larger pump was undergoing repairs.

Load was applied using a Miller 192 kip capacity ram with a 7 in. bore and 12 in. stroke. Flow of oil to the ram was controlled by a Moog A076-104 15 gpm servo-valve installed on top of the ram as shown in Fig. 3.11. Voltage signals which corresponded to load levels were monitored by a Pegasus Hydraulic Servo Controller (Fig. 3.16) and a 100 kip capacity Universal Flat Load Cell attached at the bottom of the ram. These signals (loads) were continuously read and displayed on

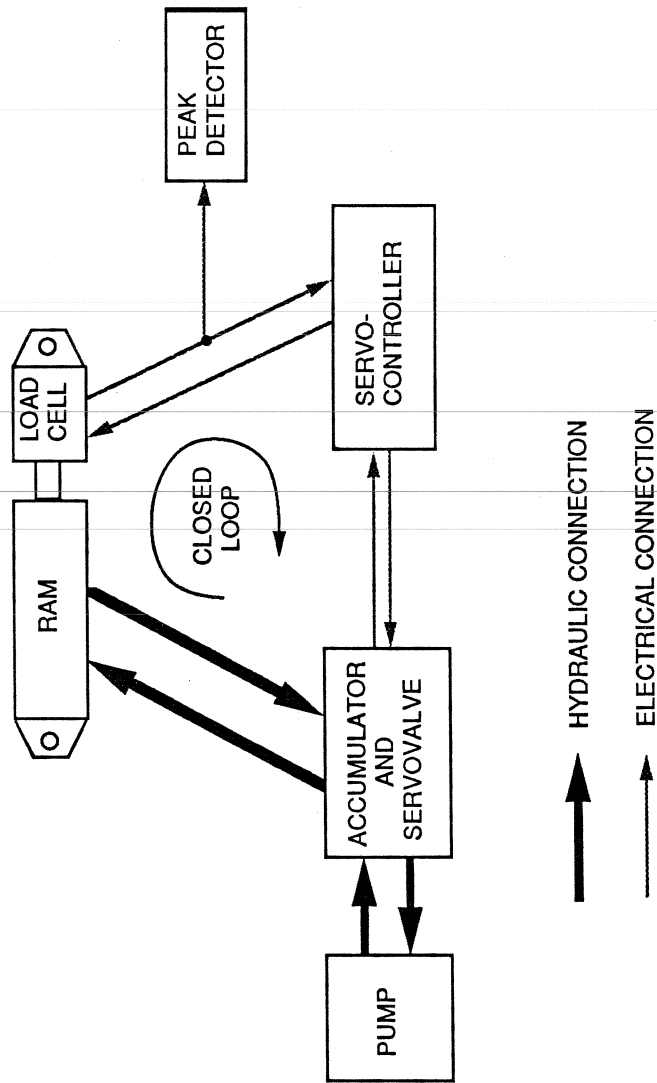
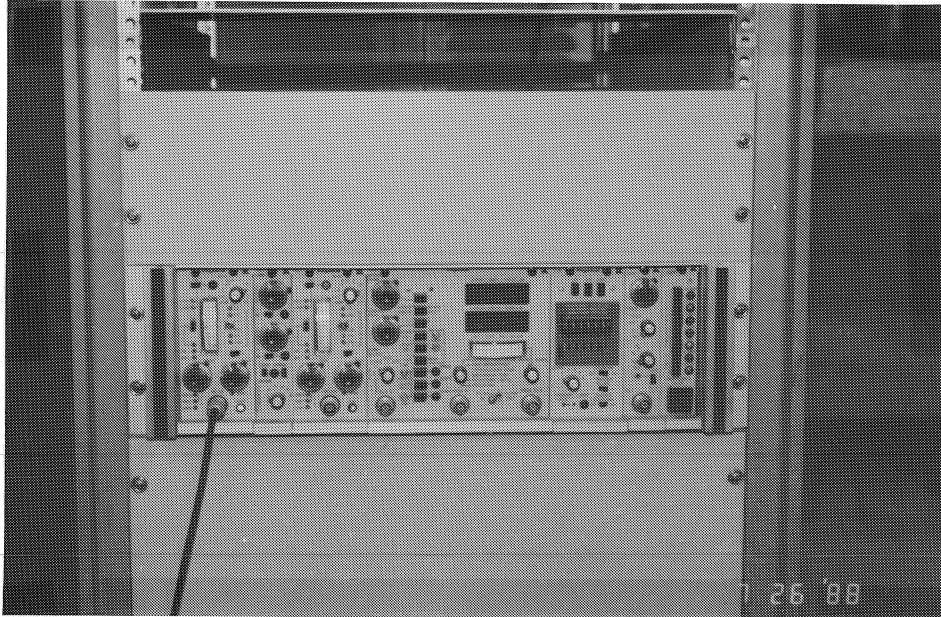
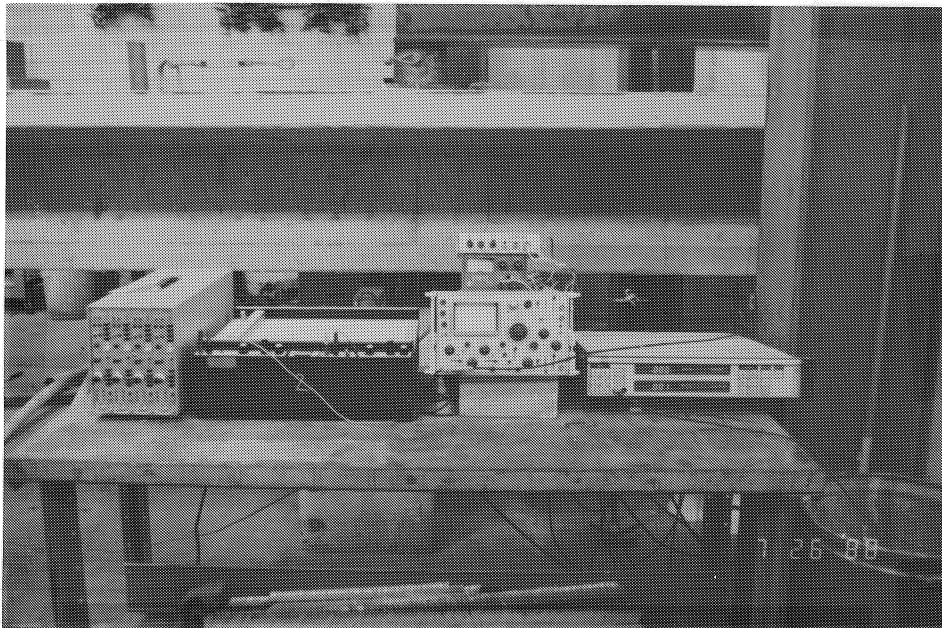


Figure 3.15 Schematic Representation of Closed Loop Servo Control System (from Yates [27])



a) Pegasus Hydraulic Servo Controller



b) Equipment Used for Deformation Measurements

Figure 3.16 Some of the Equipment Used During Testing

an MTS peak detector.

Several fail-safe mechanisms were incorporated in the closed-loop test set-up to shut down the fatigue test if the girder response or vital signs for the closed-loop system exceeded pre-set values. These mechanisms included:

- oil temperature in the pumps
- oil level in the pumps
- excessive deflection of the specimen
- number of cycles
- upper load level
- lower load level
- fluctuations in the power supply.

### **3.3.5.2 Instrumentation**

#### **3.3.5.2.1 Displacements**

Equipment used to monitor deformations during testing included an X-Y plotter for recording ram load vs. midspan deflections or crack widths, displacement transducers (potentiometers) for monitoring vertical displacements of the beam specimen and crack opening widths, an amplifier for amplifying signals from the crack opening transducers, and a Hewlett-Packard power supply. This equipment is shown in Fig. 3.16.

### 3.3.5.2.2 Strain Gages

Strain gages were used during post-tensioning and testing. Readings of the strain gages were taken using strain indicator and switch and balance boxes.

Before post-tensioning the tendon, nine strain gages were placed on one of the strands at different locations as shown in Fig. 3.17. The gages were placed to avoid damage to them when the tendon was stressed and lateral forces were induced between strands, or between the strands and the duct. During post-tensioning strain gage readings were taken at different intervals to measure the tendon prestress force. (These readings were cross-checked using a pressure gage and a pressure transducer on the stressing ram). Typically a couple of strain gages stopped functioning properly as the prestress force approached the maximum stress.

The primary problem with the strain gages occurred after the duct was grouted. Grout or water entered the protective cover over each strain gage and damaged all gages. Yates [27] offered a solution to this problem which can be found in Section 3.2.6.1 of the cited reference.

Strain gages were also placed on the passive reinforcement that was located in the bottom flange.



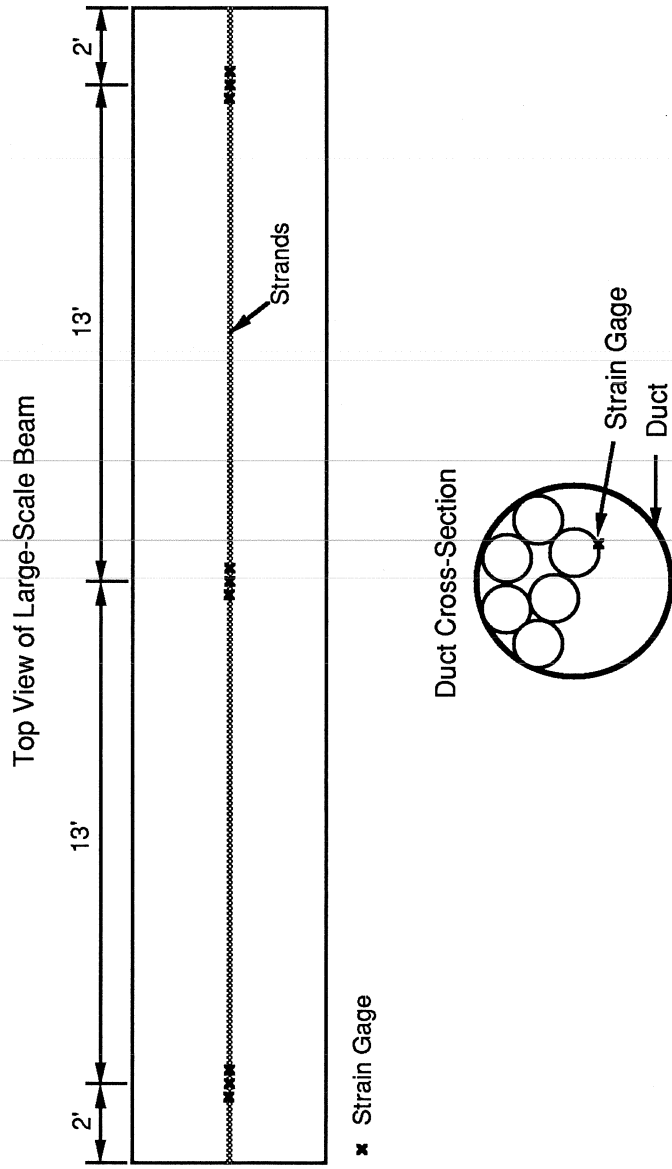


Figure 3.17 Locations of Strain Gages on the Strands

Nine strain gages were placed on each of the #3 bars as shown in Fig. 3.18. Readings were taken during the initial cracking cycle and during the periodic static cycles. No systematic problem was encountered with these strain gages.

#### **3.3.5.2.3 Other Instrumentation**

Additional instrumentation was used to determine whether any of the bottom-flange passive reinforcing bars had fractured. The two bottom #3 bars were cleaned with sand paper near the ends. An electrical wire was then soldered and clamped onto each sanded location of each bar. The regions of the stirrups which touched the bottom bars were epoxied and covered with plastic material in advance so there was no conductivity between any of the bottom bars and the stirrups or the duct. The two electrical wires connected to each bar were connected to an Ohm meter. If a bar was not broken, the bar's resistance was very close to zero. If it was broken, the electrical resistance was quite high. With this instrumentation, knowledge about the condition of bottom passive reinforcement could be obtained at any time.

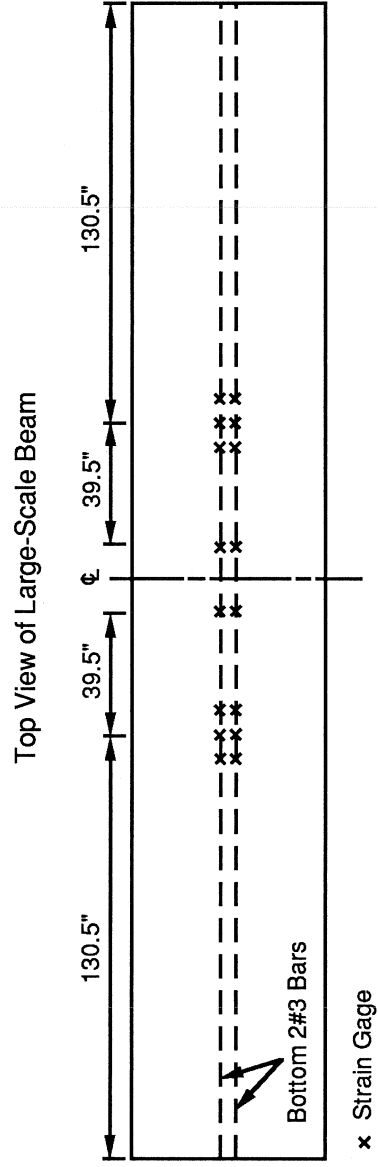


Figure 3.18 Location of Strain Gages on Bottom Passive Reinforcing Bars

### **3.3.6 Test Procedure**

#### **3.3.6.1 Initial Static Cycles - Cracking of Specimen**

Each specimen was initially subjected to a monotonically increasing load until it cracked. Additional loads, which were larger than the initial cracking load by five percent, were applied to fully crack the specimen, increase the number of cracks, and get a more accurate evaluation of the initial stiffness of the specimen. During these initial static cycles, deflection transducers were used to measure the crack widths and the midspan deflection of the specimen. This information was plotted against the ram load using an X-Y plotter. The plots were used to cross-check the cracking load displayed on the peak detector when first cracking occurred, and to evaluate the specimen's decompression load ( $P_0$ ). The decompression load is the ram load at which the concrete bottom fiber stresses were estimated to be zero, or in other words, the load which initiated opening of cracks in the bottom of the specimen. A typical ram load vs. midspan deflection curve is shown in Fig. 3.19 and a typical ram load vs. crack-width curve is shown in Fig. 3.20.

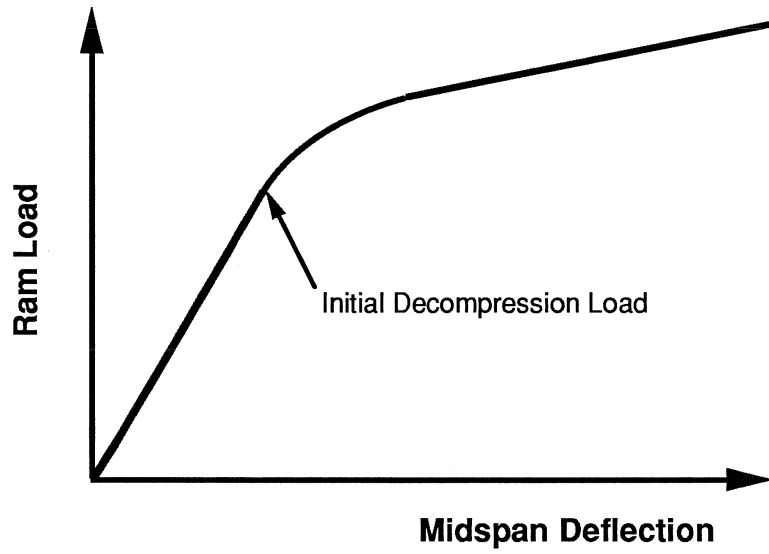


Figure 3.19 Typical Ram Load Vs. Midspan Deflection Curve

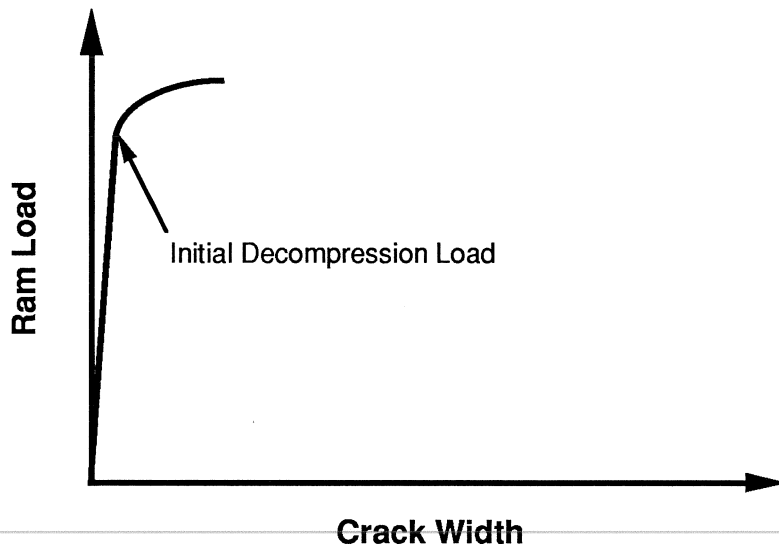


Figure 3.20 Typical Ram Load Vs. Crack-Width Curve

### **3.3.6.2 Determination of Effective Prestress Force**

The first step in the determination of the effective prestress force is the determination of the decompression load. The decompression load was obtained using the plots in Figures 3.19 and 3.20. The load which corresponded to the points where the curves in the figures started deviating from the linear behavior is the decompression load. Careful judgement was needed in the determination of the decompression load because the calculated tendon stress range was influenced considerably by small changes in the decompression load. The ram load vs. midspan deflection plot was considered more reliable than the ram load vs. crack-width plot which was used as a cross-check. The decompression load was then used in a basic flexural analysis to back-calculate the effective prestress force at midspan. As mentioned in Section 3.3.5.2, strain gages placed on one of the strands before post-tensioning were destroyed by the grouting process. They also would have been used in the determination of the effective prestress force at midspan if they had remained active.

### **3.3.6.3 Determination of Ram Load Vs. Tendon Stress Relations**

Once the effective prestress force was determined, an analysis was conducted to obtain ram load vs. tendon and passive reinforcement stress diagrams. Assuming a concrete strain in the top fiber of the beam, a trial and error technique was followed to find the location of the neutral axis for which the internal compressive forces were equal to the internal tensile forces. The ram load, tendon stress, and passive reinforcement stress were then calculated. This method was repeated for different concrete strains until the ram load vs. tendon stress and the ram load vs. passive reinforcement stress curves were well defined. These curves are shown in Figures 4.4 and 4.5 respectively.

### **3.3.6.4 Cyclic Loading**

The maximum and minimum ram loads applied during the fatigue tests were intended to achieve the following:

- 1) Produce the desired tendon stress range;

This was done by obtaining the corresponding ram loads for the desired tendon stress range from the plot in Fig. 4.4.

- 2) Not yield any of the bottom passive reinforcing steel before the expected life of the girder was reached; This was done by referring to Fig. 5.3 in Matsumoto's thesis [11] which showed the stress range vs. number of cycles for the passive reinforcement. The stress range in the passive reinforcement was obtained using Fig. 4.4. In case the fatigue life for the passive reinforcement had not been long enough, the ram loads would have been adjusted to produce the desired tendon stress range but with a longer fatigue life for the bottom passive reinforcement.

The applied loading was sinusoidal with a frequency that varied from 2.5 Hz when both pumps were running to as low as 0.5 Hz when only the smaller capacity pump was used. The wave was displayed on an oscilloscope to make sure it was a smooth sinusoidal wave. The upper and lower applied loads, as well as the mean load were displayed continuously on an MTS peak detector. As the stiffness of each specimen decreased, it was not possible to maintain the load at the original loading frequency. In such cases a lower frequency was required to maintain the desired upper load.

Table 3.4 shows the tendon stress range, tendon mean stress, effective prestress force at midspan, upper



Table 3.4 Cyclic Test Loads and Tendon Stresses

Specimen	Cyclic Test Load (kips)			Tendon Stress Range (ksi)	Tendon Mean Stress (ksi)	Effective Tendon Prestress Force (kips)
	Lower Load	Upper Load	Mean Load			
P-M-1-25	10	35	22.5	25	168.5	141.7
D-M-2-40	10	40	25.0	40	144.0	112.0
D-M-3-30	10	45	27.5	30	175.5	145.6
D-P-4-30	10	45	27.5	30	180.7	150.5
D-P-5-30	10	51	30.5	30	202.7	170.0

load, lower load, and mean load for all large-scale beams.

#### **3.3.6.5 Periodic Static Cycles**

Every time any of the fail-safe mechanisms described in Section 3.3.5 shut down the test or when a desired number of cycles was reached, the cyclic loading was stopped and static load cycles were performed.

During a static cycle the load was applied monotonically in two to five-kip increments until the upper load was reached. Midspan and end deflections were measured using displacement transducers placed under the specimen. Transducer response was displayed on an MTS peak detector, and was recorded at each load increment. Readings of the strain gages placed on the bottom passive reinforcement were obtained at each load increment using a strain indicator and two switch and balance boxes. Crack widths were also measured using a displacement transducer.

After all the readings were taken, the load was released and applied again at a steady rate. This time the ram load vs. mid-span deflection was plotted using an X-Y plotter. This was the most reliable way to monitor the variation of the specimen's stiffness with

increasing number of applied load cycles. A typical plot of the ram load vs. midspan deflection for different number of cycles is shown in Fig. 4.6. A sudden and progressive drop in the decompression load, as shown in Fig. 4.6 indicated breaking of strand wires. Eventually, very rapid deterioration of the specimen's stiffness indicated failure of the specimen. This was cross checked by plotting selected crack widths vs. number of cycles as shown in Fig. 3.20, or by plotting the maximum midspan deflection (corresponding to the upper load) vs. number of cycles as shown in Fig. 4.7. A sudden increase in the crack width and/or midspan deflection confirmed the failure of a test specimen.

#### **3.3.6.6 Static Flexural Strength Test**

When a rapid deterioration of the specimen's stiffness was observed the specimen was assumed to have reached the end of its life, and a static flexural strength test was conducted.

The load was applied monotonically in five-kip increments until the specimen failed. Concrete blocks and wood were stacked under the specimen near midspan to prevent collapse of the specimen. Some distance between the bottom of the specimen and the top of the

wood stack was provided during the test. As the load was increased along with the specimen's deflection, pieces of wood were removed to allow the specimen to deflect freely while at the same time keeping the cribbing a close distance from the specimen.

During the static flexural strength test, midspan deflections were measured using a surveyor's level. Displacement transducers were used to measure the deflections at the two ends of each specimen. Strain gage readings for the bottom passive reinforcement were also taken. As the load approached the failure load, some strain gages typically stopped functioning. Propagation of existing cracks and new cracks were marked, and the corresponding loads were recorded.

At the time of failure a loud noise was typically heard which was associated with breaking of strand wires. The remaining load was immediately released.

#### **3.3.6.7 Post-Mortem Investigation**

After the static flexural strength test was completed, the specimen was moved outside the laboratory and a post-mortem investigation was conducted. The concrete at the bottom of the specimen between the locations of the two cracks furthest from midspan was

chipped away using a jack hammer, the stirrups were cut with a disc grinder and the duct section was removed from the specimen and moved inside the laboratory.

The duct was cut open along its sides using a disc grinder. The duct, grout, and strands were carefully examined. Locations of cracks in the duct, wire breaks in the strands, and fretting points were recorded and photographed.

## CHAPTER 4

### LARGE-SCALE BEAM TEST RESULTS

#### 4.1 Introduction

This chapter is devoted presenting test results for the five large-scale post-tensioned concrete beam tests. These specimens showed similar aspects of fatigue behavior. Therefore, general test results as well as more specific results indicating effects of the primary variables on fretting fatigue are presented in this chapter.

The five specimens (identified with the alphanumeric labels assigned in Section 3.3) are divided into the following three groups:

1. Group PM consists of specimen P-M-1-25 in which parabolic tendon and metal duct were used.
2. Group DM consists of specimens D-M-2-40 and D-M-3-30 in which a draped tendon and metal duct were used.
3. Group DP consists of specimens D-P-4-30 and D-P-5-30 in which a draped tendon and plastic duct were used.

## **4.2 Static Behavior**

### **4.2.1 Initial Static Load Cycles**

Each specimen was first subjected to initial static load cycles. During the first cycle the load was increased until a flexural crack was formed in the concrete. The load causing formation of the first flexural crack is called the "cracking load". During the initial static load cycles ram load vs. midspan deflection and ram load vs. crack-width curves were plotted. The ram load vs. midspan deflection curve plotted during the first static load cycle was used to confirm the observed cracking load. The response curves plotted during the remainder of the initial static load cycles were used to graphically determine the value of the decompression load. The decompression load corresponds with zero flexural stress at the extreme flexural fibers, and was identified as the transition point between the lower linear portion and the curved portion of the ram load vs. midspan deflection curve shown in Fig. 4.1. An accurate estimation of the decompression load and cracking load for each specimen was very important because they were used in the determination of the effective tendon stress for each specimen. The effective tendon stress was used in

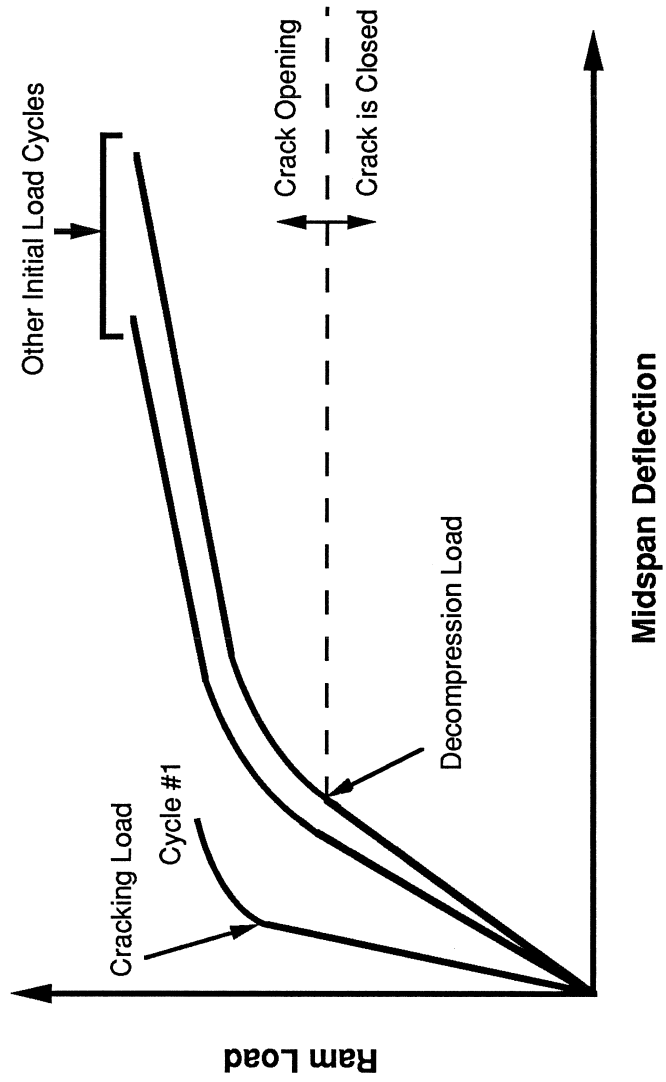


Figure 4.1 Typical Specimen Response to Initial Static Load Cycles



developing a theoretical load vs. tendon-stress relationship for each beam, which was then used to select upper and lower fatigue loads that corresponded with the desired tendon-stress range for each test. Useful information collected during initial static load cycles is presented in Table 4.1.

#### **4.2.2 General Characteristics of the Static Behavior**

All specimens displayed similar characteristics during the static load cycles. These characteristics were also observed by Yates [27], Wollmann [26] and Diab [6], and are discussed in Sections 4.2.2.1 and 4.2.2.2.

##### **4.2.2.1 Hysteretic Behavior**

All specimens exhibited hysteretic behavior during static loading, as shown in Fig. 4.2. Deflections during unloading were greater than deflections for corresponding loads during loading most likely as the result of tendon friction between the tendon and adjacent materials. This results in dissipation of energy by the beam during each load cycle.

Time has some effect on this hysteretic behavior. This is illustrated by the unloading path of the response curve in Fig. 4.2. When the load is brought

Table 4.1 Information From Initial Static Load Cycles

Specimen	No. of Cycles	Cracking Load (kips)	Decompression Load (kips)
P-M-1-25	N/A	N/A	21.0
D-M-2-40	6	34	21.0
D-M-3-30	9	48	30.0
D-P-4-30	7	49	31.0
D-P-5-30	9	48	37.0

N/A Not Available

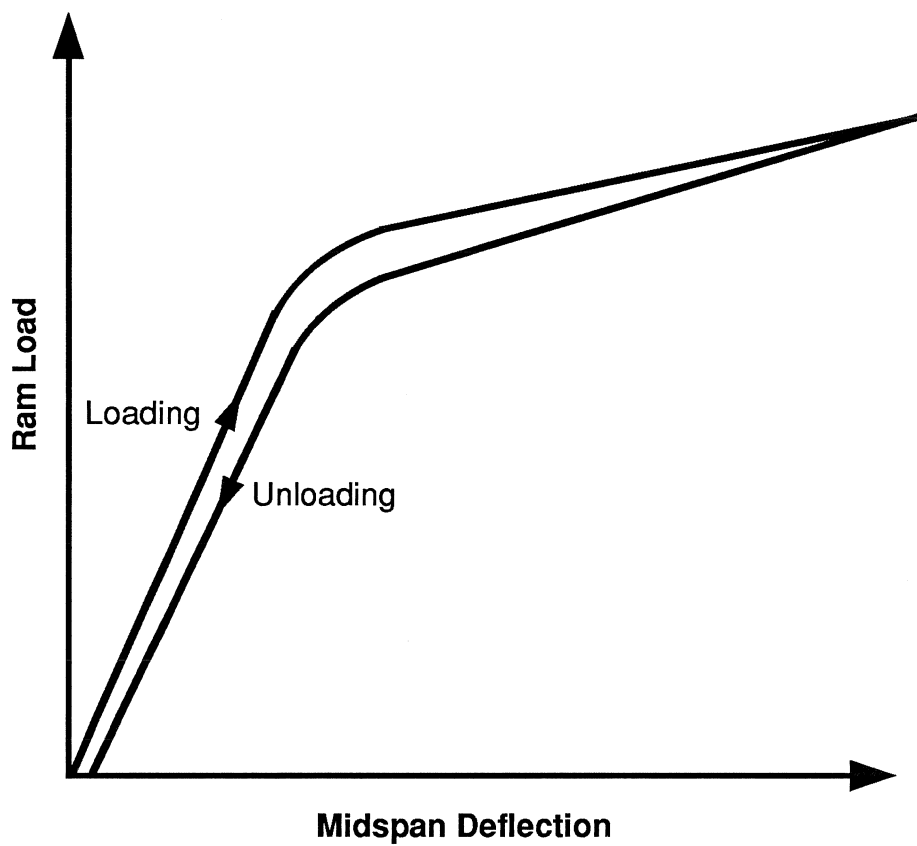


Figure 4.2 Typical Hysteretic Behavior during Static Load Cycles

back to zero a residual deflection exists. However, after some time deflection returns to zero.

#### **4.2.2.2 Time Dependence of Displacements**

It was observed that time had an effect on displacements during static load cycles, as shown in Fig. 4.3. For a constant load, displacements increased with time. It was also observed that higher sustained loads resulted in larger increases in displacement with time.

#### **4.3 Determination of Cyclic Test Loads**

An accurate estimate of the effective prestress force for each beam was dependent upon the quality of the estimate of the decompression load for each beam. An attempt was made to determine each effective prestress force using readings from strain gages that were placed on tendons at different locations during the fabrication process. However, most of the strain gages were destroyed during post-tensioning. Any strain gages that survived the post-tensioning process were destroyed after each specimen was grouted. The last resort was to calculate the effective prestress force using the decompression load, section dimensions, and

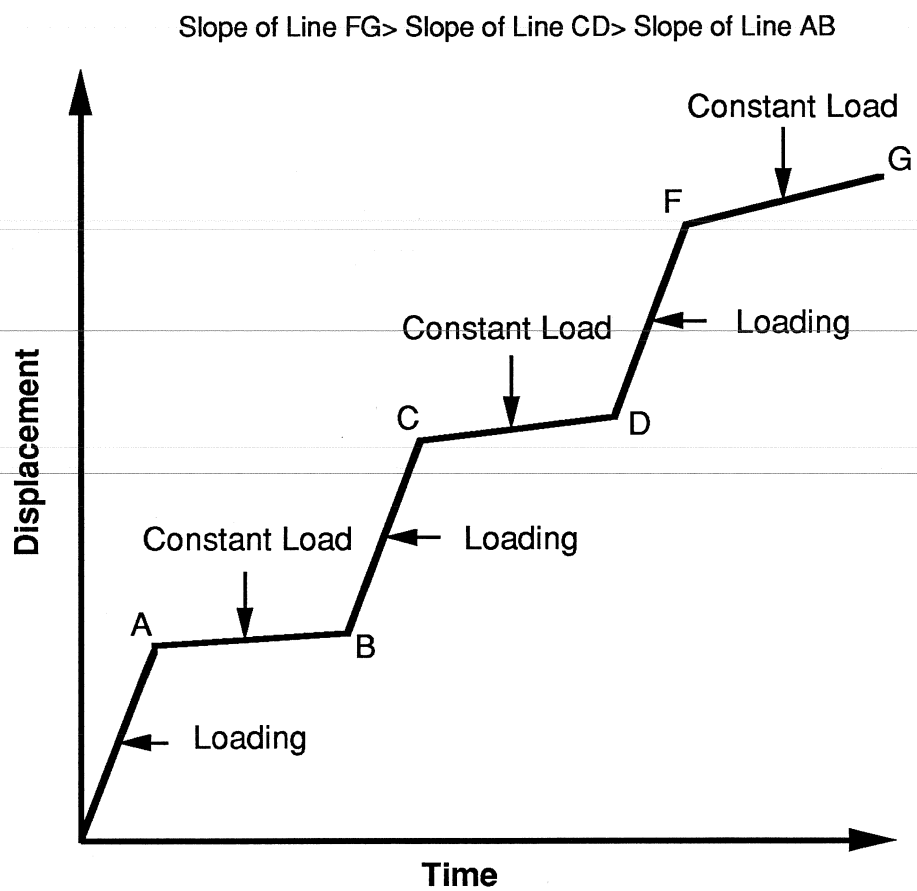


Figure 4.3 Typical Plot of Time Dependence of Displacement

statics. The calculated effective prestress force values are presented in Table 4.2.

The decompression load, section dimensions, and beam dimensions were also used to determine ram load vs. tendon stress and ram load vs. passive reinforcement stress relationships which are shown in Fig. 4.4 and Fig. 4.5. Using these plots the cyclic test loads were chosen to produce the desired tendon stress range while maintaining passive reinforcement stresses low enough to preclude fractures of passive reinforcement before wire fractures occurred in each tendon. A summary of the cyclic test loads and corresponding tendon stresses is given in Table 4.3.

#### **4.4 Fatigue Behavior**

The load-deflection response and maximum midspan deflection vs. number of load cycles for each specimen were used to identify when wire breaks occurred. The two types of response plots, shown in Figures 4.6 and 4.7, were constructed from data collected during periodic static-load cycles.

Typical specimen response was generally characterized by initial deterioration in stiffness due to crack propagation and depending of tendons. This is

Table 4.2 Calculated Effective Tendon Prestress Force and Stress

Specimen	Effective Tendon Prestress Force (kips)	Effective Tendon Stress (ksi)
P-M-1-25	141.7	154.4
D-M-2-40	112.0	122.0
D-M-3-30	145.6	158.6
D-P-4-30	150.5	163.9
D-P-5-30	170.0	185.2

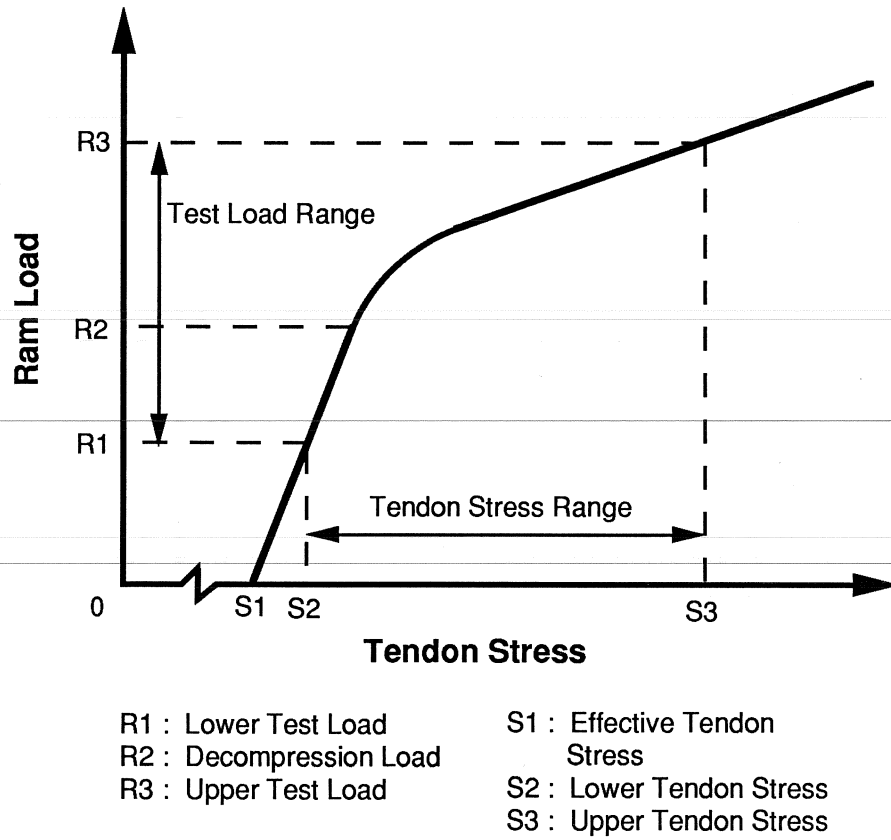


Figure 4.4 Typical Ram Load Vs. Tendon Stress Relationship



Table 4.3 Cyclic Test Loads and Tendon Stresses

Specimen	Cyclic Test Load (kips)		Tendon Stress Range (ksi)	Tendon Stresses (ksi)		Tendon Mean Stress (ksi)
	Lower Load	Upper Load		Lower Stress	Upper Stress	
P-M-1-25	10	35	25	156.0	181.0	168.5
D-M-2-40	10	40	40	124.0	164.0	144.0
D-M-3-30	10	45	30	160.5	190.5	175.5
D-P-4-30	10	45	30	165.7	195.7	180.7
D-P-5-30	10	51	30	187.7	217.7	202.7

illustrated by increases in the maximum midspan deflection during initial static load cycles (Fig. 4.7). The initial stiffness loss was followed by a stage of slow stiffness decrease (Fig. 4.7). The last stage was initiated by the first wire fracture, and was followed by rapidly increasing maximum midspan deflection (decreasing stiffness) due to additional fractures. Each wire fracture also was typically accompanied by a decrease in the decompression load. This is illustrated schematically in Figures 4.6 and 4.7.

For specimen P-M-1-25 the situation was somehow different. The first wire fracture (detected because of a reduced decompression load) did not cause a very large stiffness loss, and the second wire fracture did not follow before a considerable number of additional load cycles were applied. However, the second wire fracture was not the critical one. It took many cycles for the third wire fracture which was accompanied by a large stiffness loss and was followed by many additional wire fractures.

#### **4.5 Static Flexural Strength Test**

After each specimen had reached its useful fatigue

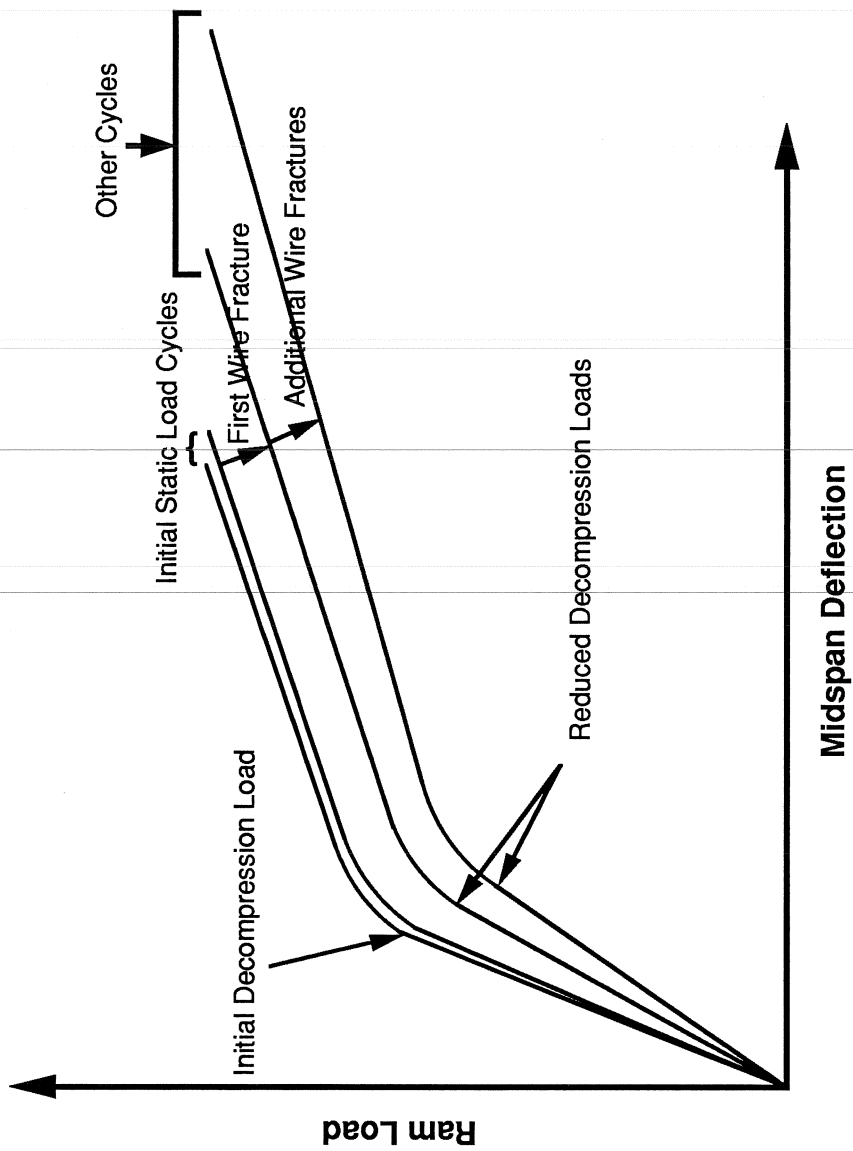


Figure 4.6 Typical Ram Load Vs. Midspan Deflection History

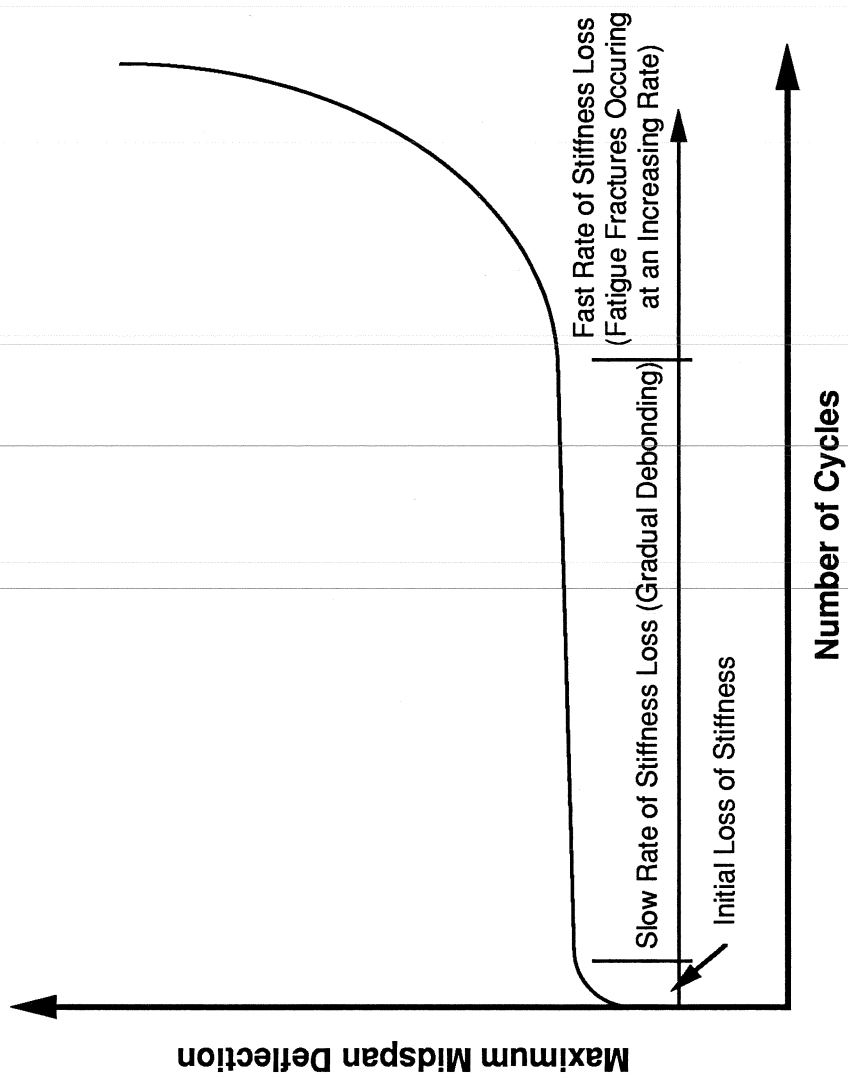


Figure 4.7 Typical Stiffness History

life, a static flexural strength test was conducted. Each specimen was loaded incrementally to failure. During the test, additional wires (sometimes entire strands) were fractured, and some cracks propagated into the top flange. Usually one or two cracks opened much wider than the rest causing wire fractures to occur within the vicinity. The load at which each specimen failed is referred to as "Ultimate Load". The ultimate loads for all specimens are given in Table 4.4.

#### **4.6 Crack Patterns**

The formation and propagation of most of the cracks followed an expected pattern which was similar for all specimens. A typical crack pattern is shown in Fig. 4.8. During the initial static load cycles three to six flexural cracks that extended into the web formed between the drupe points. These cracks were not inclined. During cyclic loading the existing cracks propagated more and new cracks formed. Cracks outside the loading points started deviating from vertical and developed inclinations towards the loading points (Fig. 4.8). The inclined cracks developed as a result of the interaction between shear and flexure. Inclined cracks that originated as flexural cracks are called

Table 4.4 Ultimate Loads for Large-Scale Beams

Specimen	Ultimate Load (kips)
P-M-1-25	46
D-M-2-40	58
D-M-3-30	55
D-P-4-30	78
D-P-5-30	63

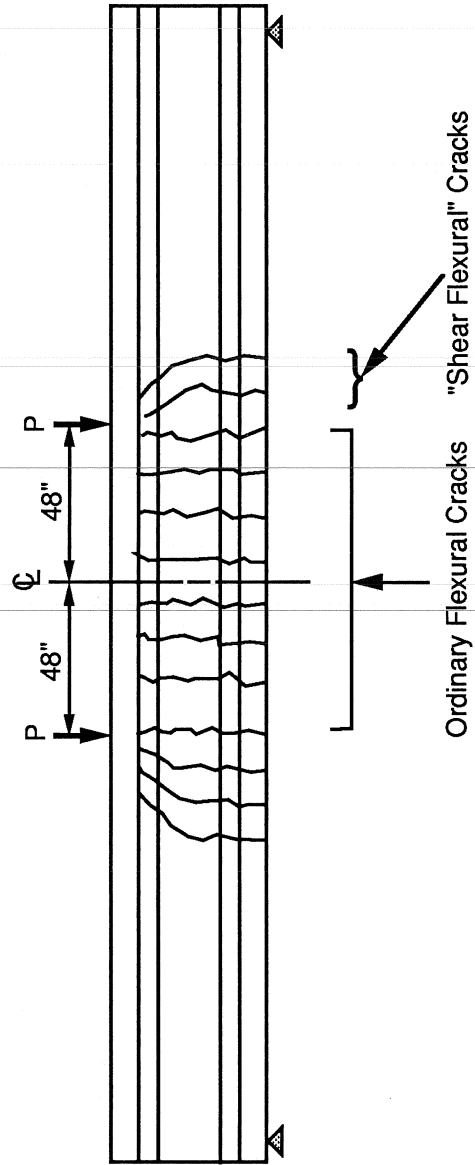


Figure 4.8 Typical Crack Patterns (before Static Flexural Strength Test)

"shear-flexural cracks" in Fig. 4.8. Flexural cracks that formed in the vicinity of the tendon draped regions usually dominated fatigue behavior of the specimen. Debonding and fretting action in the vicinity of these cracks resulted in most of the wire fractures and eventual failure of the specimen.

An interesting observation was made regarding the two specimens with plastic duct. A horizontal crack formed between the loading points at the bottom of the web as shown in Fig. 4.9. This type of crack was also encountered during a previous research study on flexural fatigue behavior of pretensioned concrete girders by Overman [16]. However, there is no proven explanation concerning the formation of these splitting cracks.

#### **4.7 Post-Mortem Investigation**

After completion of the static flexural-strength test, a post-mortem investigation was conducted for each specimen. The bottom-flange concrete between the extreme crack locations or the ends of the drape region (whichever was larger) was chipped away and the duct was removed for further examination. The exterior damage on the duct depended on many factors like the tendon stress range, the contact pressure, and the duct material.



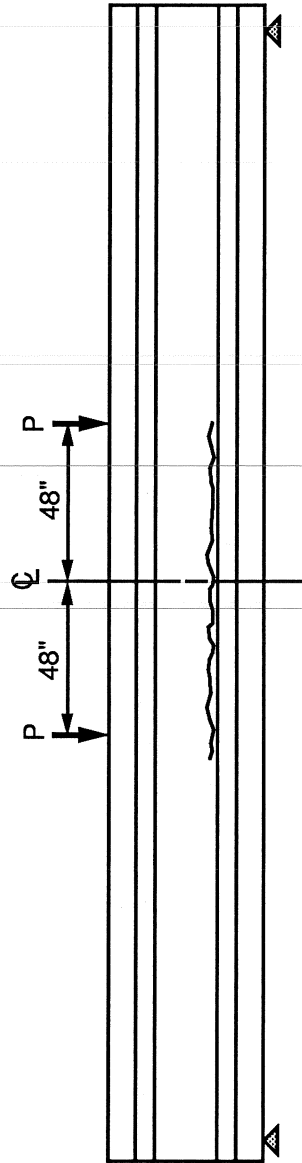


Figure 4.9 Horizontal Crack at Bottom of Web

Metal duct suffered severe damage compared to the plastic duct. The fractures in metal ducts were many and occurred at the locations of the corresponding concrete cracks. In many locations the fractures passed through the entire metal sheath. On the other hand, plastic ducts were not fractured at all. Ductility of the plastic duct, among other reasons (chemical constitution, friction coefficient) contributed a great degree to preventing the formation of cracks. Figure 4.10 shows photographs of fractured metal ducts.

After inspection of the exterior surface of the ducts, they were cut open for further inspection. All ducts had longitudinal indentations at the contact points with the strand caused by the rubbing action between duct and strand, and the lateral pressure. The indentations were more severe in the vicinity of a crack. In the case of metal ducts, the indentations were either corrosion or abrasion signs. Figure 4.11 shows the condition of the inside surface of a metal duct. In the case of plastic ducts, the situation was much different. The indentations at the contact points showed no signs of corrosion or abrasion. The indentations were simply signs of strand rubbing through the plastic. In some cases the strand had rubbed



Figure 4.10 Photographs of Fractured Metal Duct

through the duct and had come into contact with the concrete. This is shown in Fig. 4.12.

The grout showed deterioration signs as well. The deterioration was in the form of fractures in the vicinity of duct cracks or contact points. There is no evidence of a direct relationship between the severity of grout deterioration and the stress range as Yates [27] suggested. Specimen P-M-1-25 was tested at the lowest tendon stress range and its grout suffered the most deterioration. However, it had a much longer fatigue life and larger crack widths than the rest of the specimens. An explanation for the severity of the grout deterioration in specimen P-M-1-25 is that the extensive number of load cycles combined with large crack widths (large tendon slip amplitude) could have fractured the grout due to normal fatigue. More information is needed to reach a definite conclusion about the effect the above factors have on the severity of grout deterioration.

During the post-mortem investigation of the tendons five types of wire fractures were observed:

1. Fractures caused by rubbing between strand and duct.
2. Fractures caused by rubbing between strands.
3. Fractures caused by rubbing between wires of the same

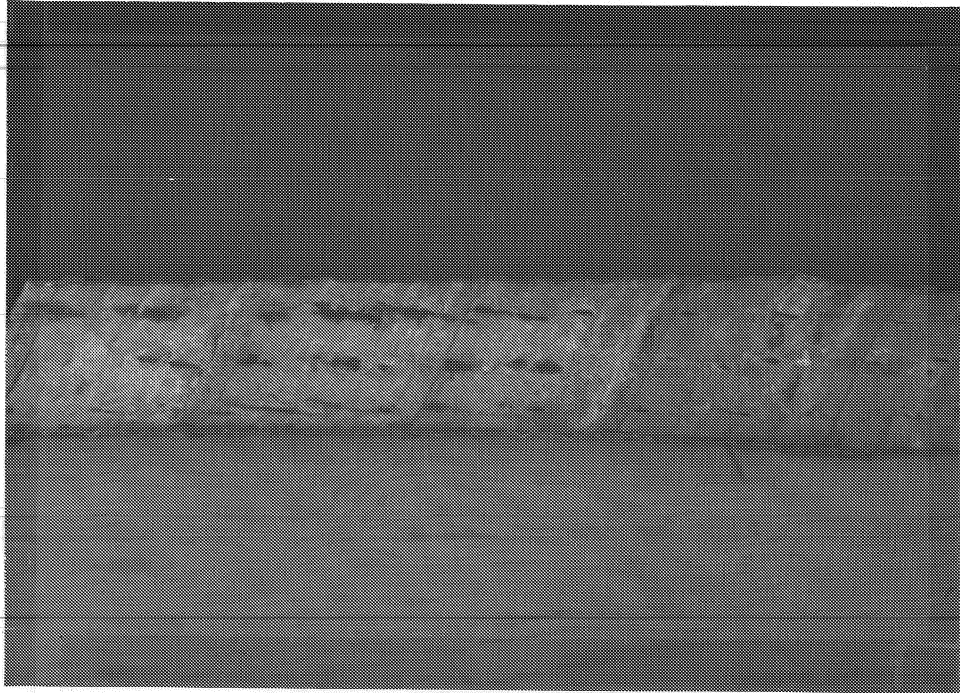


Figure 4.11 Condition of Metal Duct

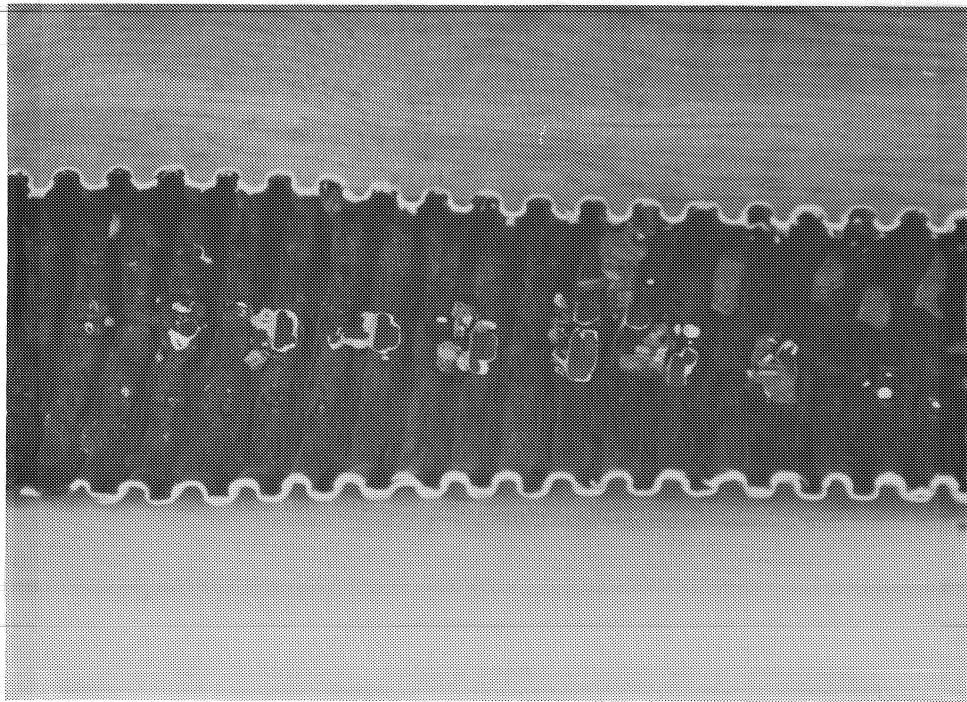


Figure 4.12 Condition of Plastic Duct

strand.

4. Ordinary fatigue fractures.
5. Ultimate-strength fractures.

The first three types of fractures are fretting fatigue fractures (Fig. 4.13). The path the crack follows is shown schematically in Fig. 4.14a. The crack forms and propagates for some distance at an inclined, smooth, and plane surface. Eventually, it becomes unstable at some depth and brittle fracture in the remaining wire section occurs.

The surface of ordinary fatigue cracks is perpendicular to the wire axis as shown in Fig. 4.14b. The fact that after each wire fracture there was an increased stress range in the remaining tendon led to ordinary fatigue fractures in wires in the vicinity of other fretting fatigue fractures. Imperfections (flaws) in the remaining wires increased the probability of development of ordinary fatigue cracks. A photograph of an ordinary fatigue fracture is shown in Fig. 4.15.

Ultimate-strength fractures of wires are the easiest to identify due to their unique characteristics. They are characterized by necking of the wires as shown in Figures 4.14c and 4.16. The necking of the wires is caused by yielding of the wires. Usually, this type of

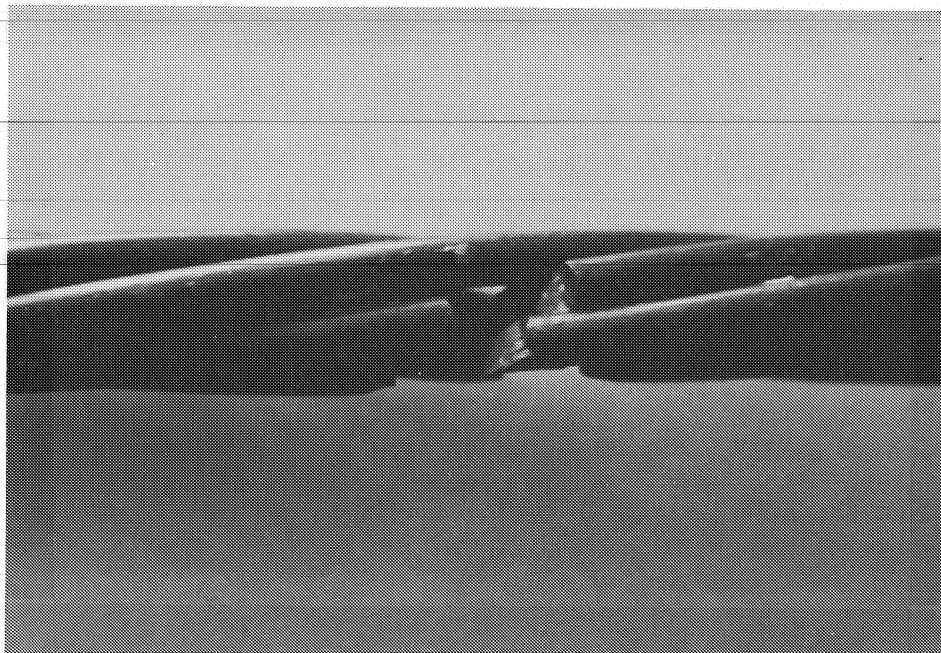


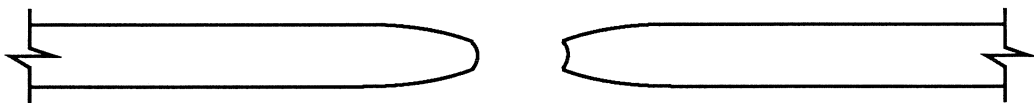
Figure 4.13 Photograph of a Fretting Fatigue Fracture



a) Typical Fretting Fatigue Fracture of Wire



b) Typical Ordinary Fatigue Fracture of Wire



c) Typical Ultimate-Strength Fracture of Wire

Figure 4.14 Typical Wire Fractures



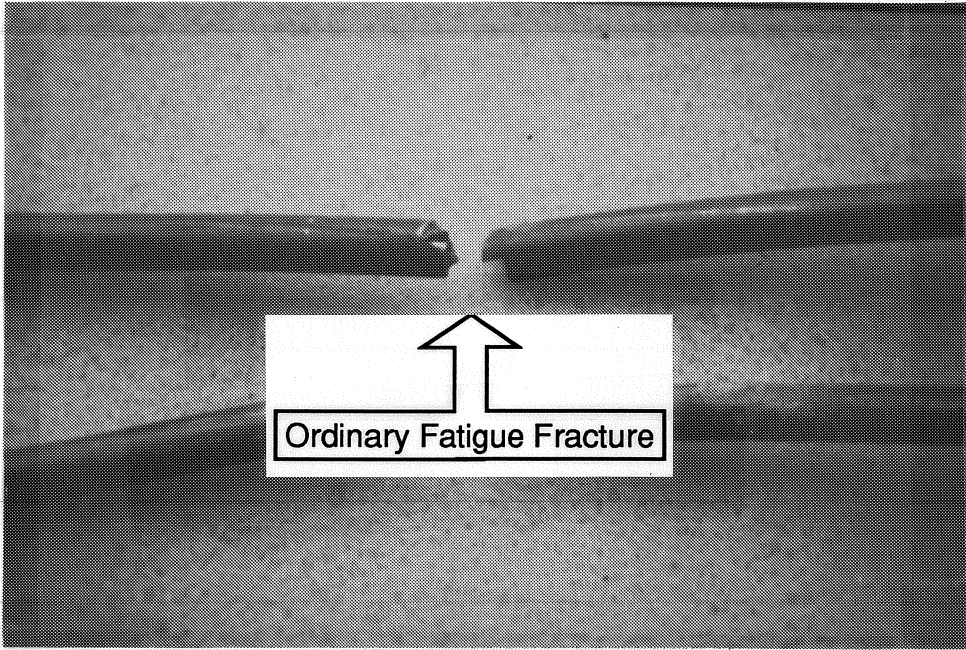


Figure 4.15 Photograph of an Ordinary Fatigue Fracture

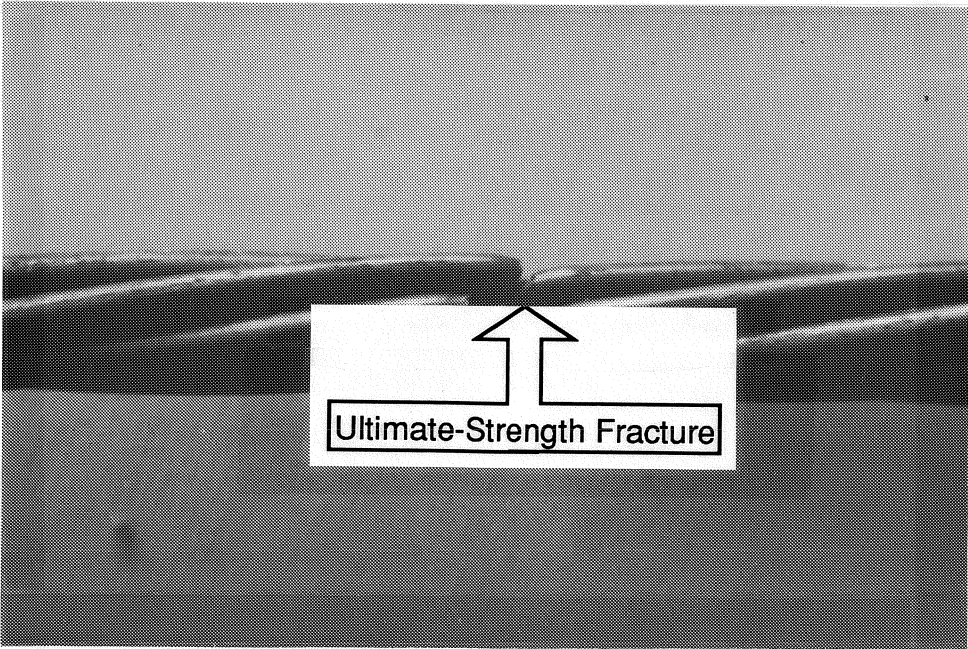


Figure 4.16 Photograph of an Ultimate Strength Fracture

wire fracture occurred during the static flexural strength test conducted after the completion of cyclic load testing.

#### **4.8 Specimens of Group PM**

##### **4.8.1 General**

One specimen (P-M-1-25) with parabolic tendon and metal duct was tested in fatigue at a tendon stress range of 25 ksi. The tendon mean stress was 168 ksi.

This specimen was used in previous tests of another study. After completion of that study, the old strands were removed and new strands were inserted in the duct. Then, the specimen was post-tensioned and grouted. However, the beam was cracked during previous tests so a determination of the cracking load was not possible. Initial static load cycles were conducted to estimate the initial stiffness and decompression load of the specimen. The decompression load was found to be 21 kips which was the lowest (together with that of specimen D-M-2-40) among the decompression loads of all specimens. This is attributed to relaxation of strands caused by the long period of time (30 days) that elapsed between post-tensioning and initial static load cycles.

The fatigue behavior of specimen P-M-1-25 was

interesting. After initial reductions in stiffness had occurred during the initial static load cycles, the stiffness was stable (decreased at a very slow rate) until 600,000 cycles where a significant reduction in stiffness occurred. This was attributed to a wire fracture. After that, cyclic loading was resumed. Stiffness remained relatively stable for another 1,200,000 cycles until additional wire fractures occurred. At 1,800,000 cycles another wire was fractured causing some more reduction in the specimen's stiffness. After that cycling loading was again resumed. At 2,200,000 cycles and at 2,235,000 cycles, additional wires were fractured causing large and rapid reductions in the specimen's stiffness, indicating that the specimen had exceeded its useful fatigue life. This specimen was the only one in which the first wire fracture did not cause a rapid deterioration in the specimen's stiffness leading to failure. The third wire fracture was the critical one leading to multiple fractures and failure. The stiffness history of the specimen is shown in Fig. 4.17. The fatigue life of the specimen is also listed in Table 4.5 and plotted in Fig. 5.6 along with the fatigue lives of the other specimens.

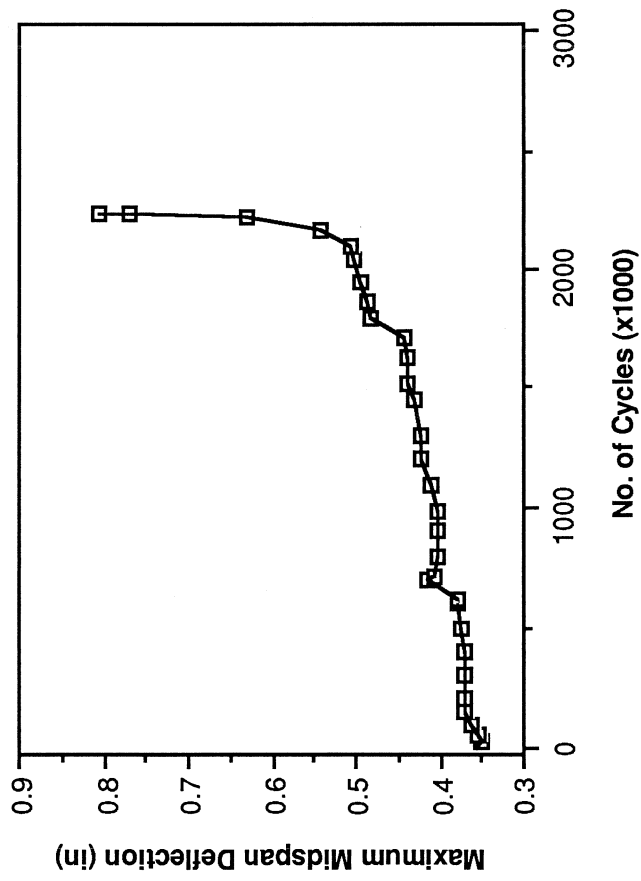


Figure 4.17 Stiffness History of Specimen P-M-1-25

Table 4.5 Fatigue Lives of Specimens

Specimen	Fatigue Life (no.of cycles x 1000)
P-M-1-25	2100
D-M-2-40	800
D-M-3-30	490
D-P-4-30	1300
D-P-5-30	700

#### 4.8.2 Post-Mortem Investigation

Some of the wire fractures initiated due to strand-to-duct fretting and some from strand-to-strand or wire-to-wire fretting. Almost all wire fractures occurred in the vicinity of concrete cracks. The uniform contact pressure due to the parabolic tendon profile contributed to having the wire fractures almost evenly distributed between the loading points. Abrasions and corrosion of the duct and strands were very visible and photographs of this are shown in Figures 4.18 and 4.19.

An entire strand was fractured at the location where a concrete crack opened most during the static flexural strength test. One out of seven wires of the strand was fractured due to strand-to-duct fretting during cyclic loading. Another one was fractured due to wire-to-wire fretting. The remaining five wire fractures were ultimate-strength fractures that occurred during the static flexural strength test.

The metal duct was cracked at many locations primarily in the vicinity of concrete cracks (Fig.4.20). When the concrete cracks were opening during cyclic loading, the metal duct was forced to elongate. In some cases, repeated elongation along with deterioration of

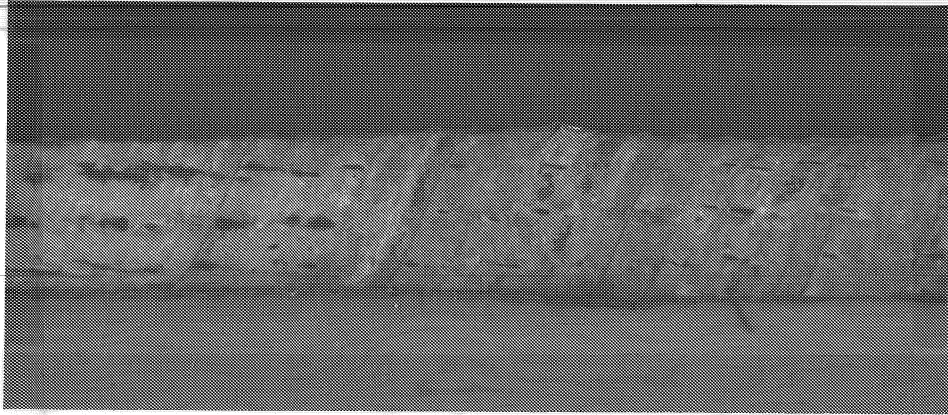


Figure 4.18 Fretting Signs on Metal Duct of Specimen P-M-1-25

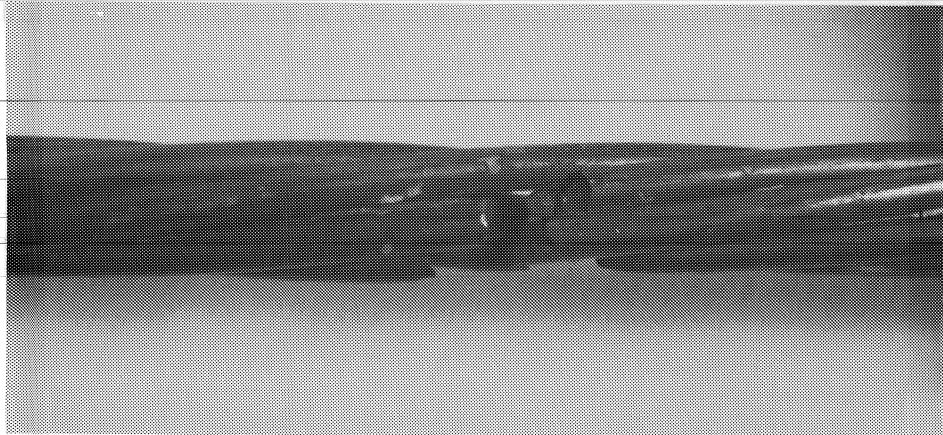


Figure 4.19 Fretting Fractures of Wires of Specimen P-M-1-25

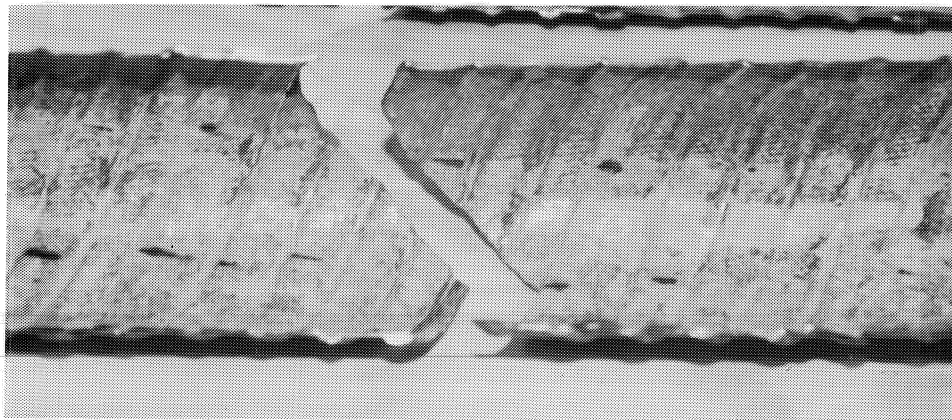


Figure 4.20 Fractured Metal Duct of Specimen P-M-1-25

the duct due to strand-to-duct fretting caused fracture of the duct.

#### **4.9 Specimens of Group DM**

##### **4.9.1 General**

Two specimens (D-M-2-40 and D-M-3-30) with a draped tendon and metal duct were tested in fatigue at a tendon stress range of 40 ksi and 30 ksi respectively.

At first, both specimens were subjected to initial static load cycles to estimate their initial stiffnesses and decompression load. The decompression load was found to be 21 kips for specimen D-M-2-40 and 30 kips for specimen D-M-3-30. Although both specimens were identical, the difference in their decompression loads was significant. The difference is mainly attributed to the different levels of time dependent losses that the specimens experienced. More time was elapsed between post-tensioning and initial static load cycles for specimen D-M-2-40 (25 days) than for specimen D-M-3-30 (10 days) due to problems encountered with some of the testing equipment.

No particular problems were encountered during testing of these two specimens. However, the fatigue lives of the two specimens were inconsistent with



expected results. The first specimen, which was tested at a 10 ksi higher stress range than the other specimen, experienced a much higher fatigue life. Its fatigue life was 800,000 cycles while that of the second specimen was only 490,000 cycles. A possible explanation is that although the first specimen was tested at a higher tendon stress range, its tendon mean stress and highest stress were much lower than those of the second specimen. Therefore, the contact pressure was much lower for the first specimen than for the second. The higher the contact pressure, the more severe is the rubbing action between strands and duct or between strands themselves, resulting in a lower fatigue life.

The stiffness history plots for both specimens followed a typical pattern and are shown in Figures 4.21 and 4.22. After initial losses in stiffness during initial static load cycles, stiffnesses were relatively stable until the first wire fracture. After that, additional wires started breaking at a fast rate causing rapid and significant losses in stiffness. Therefore, the first wire fracture was critical for both specimens, and the useful fatigue life for both beams was assumed to be the number of cycles corresponding to first wire

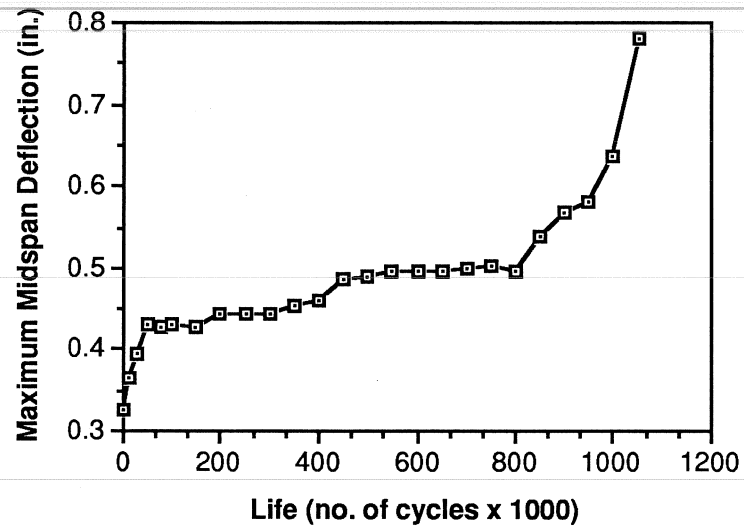


Figure 4.21 Stiffness History of Specimen D-M-2-40

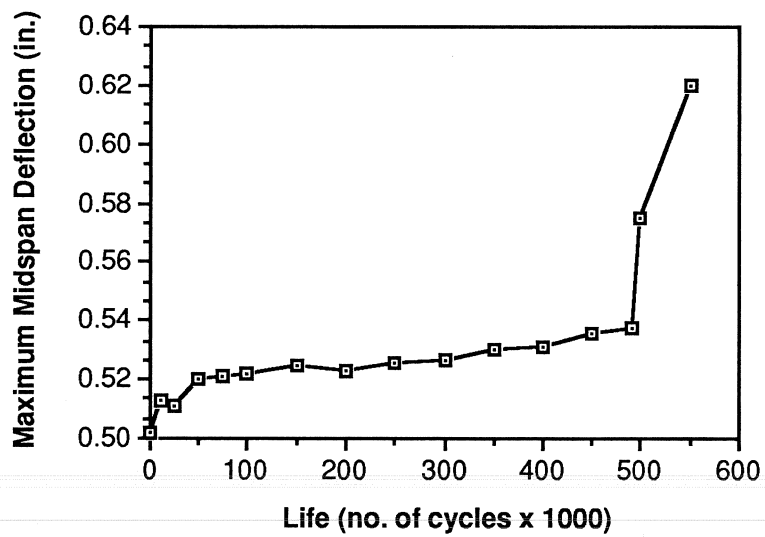


Figure 4.22 Stiffness History of Specimen D-M-3-30

fracture.

#### **4.9.2 Post-Mortem Investigation**

Almost all wire fractures initiated from strand-to-duct fretting due to the high contact pressure between the two. The majority of wire fractures occurred at the drapage points, in the vicinity of concrete cracks, where the stress concentrations were high and the contact pressure was maximum. Abrasion and corrosion of the duct (Fig. 4.23) and the strands (Fig. 4.24) were observed at the contact points. This damage was more severe for specimen D-M-2-40 which was tested at a higher stress range. One or two wire fractures could be attributed to strand-to-strand or wire-to-wire fretting. Almost no signs of abrasion or corrosion could be found in either case. Ultimate-strength fractures caused by the high static load during the static flexural strength tests were found next to pre-existing fretting fractures. Cracks in the metal ducts (Fig. 4.25) were also found in the vicinity of concrete cracks.

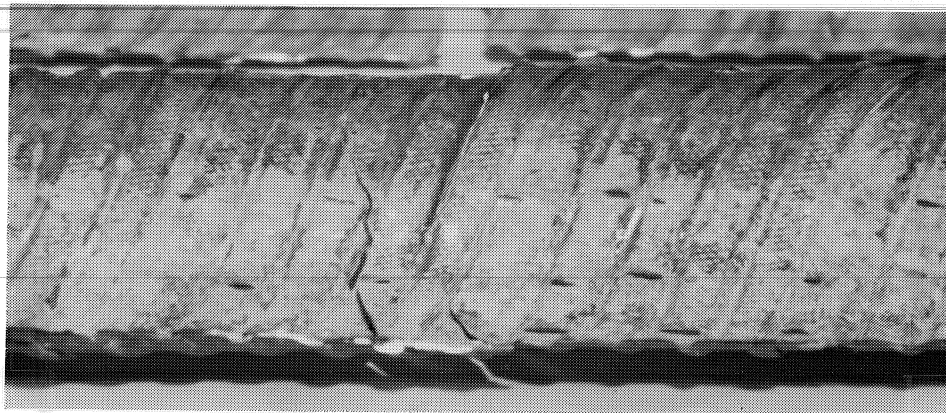


Figure 4.23 Fretting Signs on Metal Duct of a Group DM Specimen

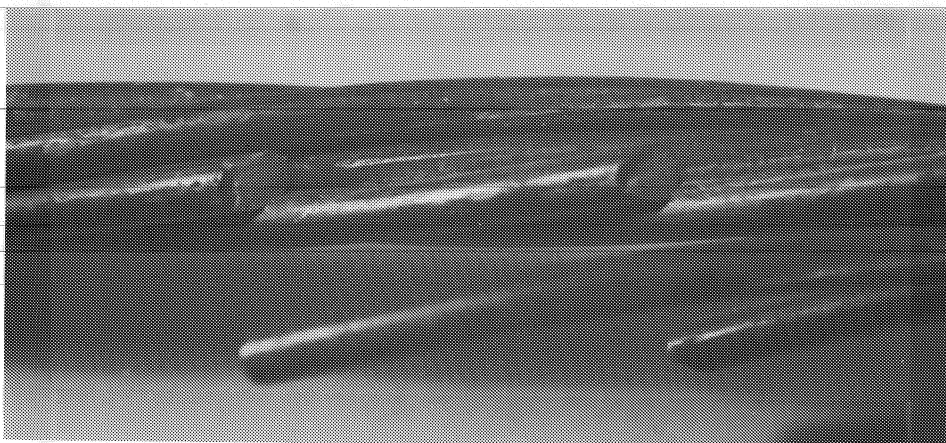


Figure 4.24 Fretting Fractures of Wires of a Group DM Specimen

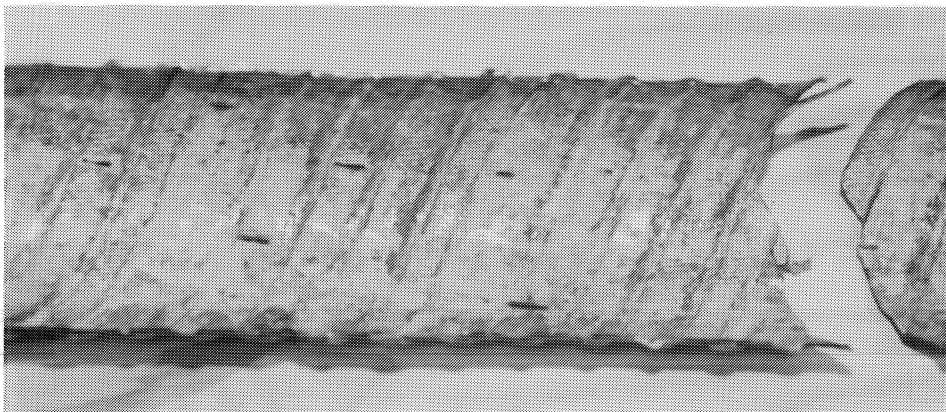


Figure 4.25 Fractured Metal Duct of a Group DM Specimen

#### **4.10 Specimens of Group DP**

##### **4.10.1 General**

Two specimens (D-P-4-30 and D-P-5-30) with draped tendon and plastic duct were tested in fatigue at a stress range of 30 ksi.

The initial stiffness and decompression load for each specimen was determined during the initial static load cycles. The decompression load was found to be 37 kips for the first specimen and 31 kips for the second. The difference in decompression loads is attributed to differences in time-dependent losses and different initial effective prestress forces for the two specimens.

The fatigue lives of the two specimens were different too. The fatigue life for the first specimen was 1,300,000 cycles, while for the second was only 700,000 cycles. This is attributed to the fact that although the stress range was the same for both specimens, the contact pressure was lower for the first specimen. The first specimen was tested at a upper tendon stress of 195.7 ksi and a mean tendon stress of 181 ksi while the corresponding stresses for the second specimen were 217.7 ksi and 203 ksi.

All other aspects of the fatigue behavior of both

specimens were normal. Stiffness history plots (Figures 4.26 and 4.27) followed a typical pattern. The first wire fracture was critical for the specimens of this group as well. After the first wire fracture, additional wire fractures followed at a fast rate causing significant reductions in the stiffness of each specimen.

#### **4.10.2 Post-Mortem Investigation**

Only six wire fractures were found in both specimens. Four of them initiated from wire-to-wire fretting. The other two were ultimate-strength fractures. All fractures were located at the draped points due to reasons that were explained in Section 4.9.2. Since the duct was plastic, there were no wire fractures due strand-to-duct fretting. However, in some cases the rubbing action between strand and duct caused penetration of the strand through the duct (Fig. 4.28) making the strand come in contact with the surrounding concrete. However, no fractures resulted because of strand-to-concrete contact.

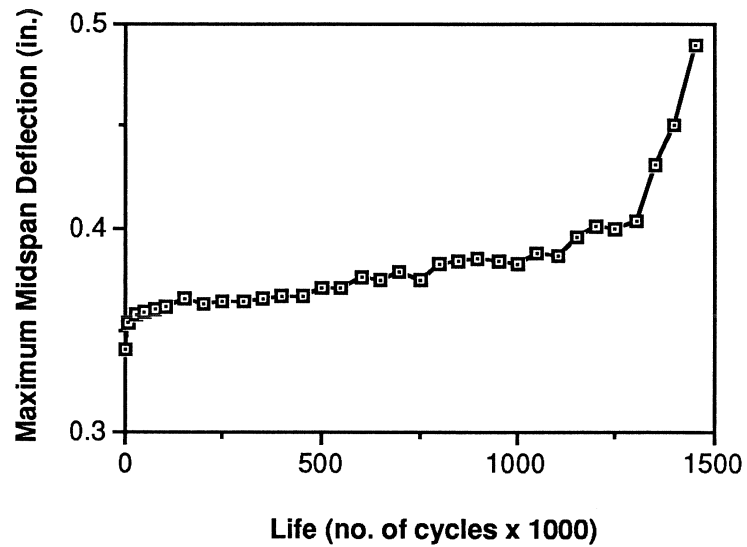


Figure 4.26 Stiffness History of Specimen D-P-4-30

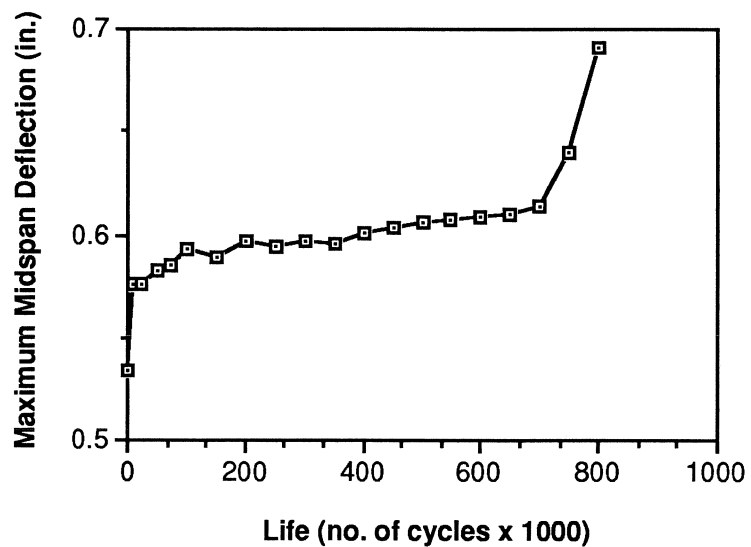


Figure 4.27 Stiffness History of Specimen D-P-5-30

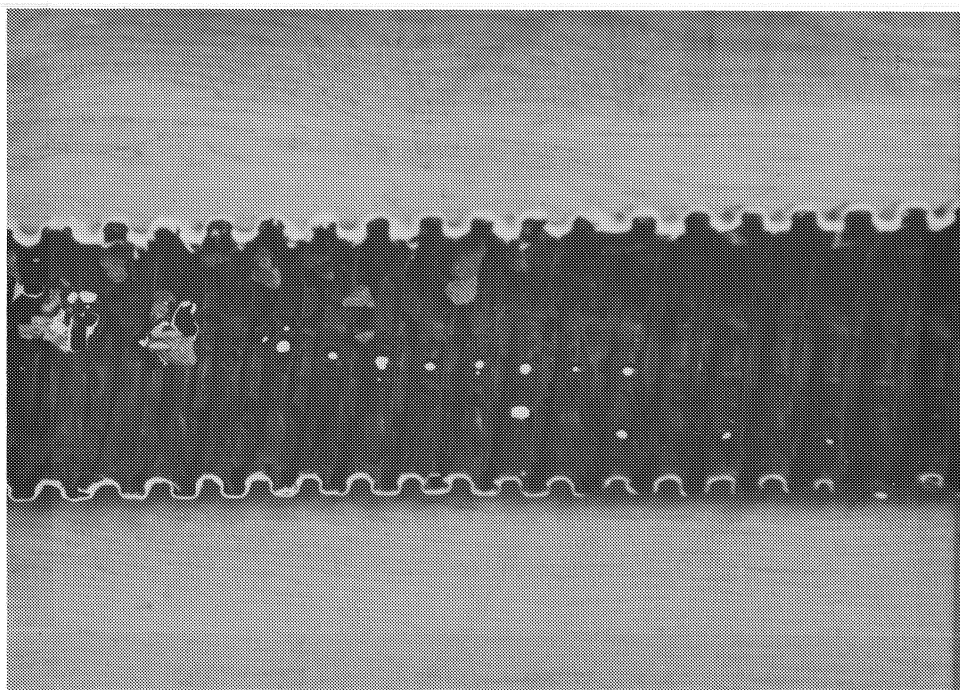


Figure 4.28 Condition of Plastic Duct of a Group DP Specimen



## CHAPTER 5

### EVALUATION AND COMPARISON OF TEST RESULTS

#### 5.1 Introduction

This chapter contains an evaluation of the test results and comparisons of this data with data from previous studies. The test results of this study are reported in Chapter 4. Background information for data from other testing programs was presented in Chapter 2. Test data used in this chapter were obtained from the following studies:

1. University of Texas strand in air fatigue tests by Yates [27].
2. University of Texas strand in air fatigue tests by Wollmann [26].
3. University of Texas single-strand reduced-beam tests by Yates [27].
4. University of Texas multiple-strand reduced-beam tests by Wollmann [26].
5. Reduced-beam tests by Oertle, Thurlimann, and Esslinger [14].
6. Girder tests by Rigon and Thurlimann [20].

7. Girder tests by Oertle, Thurlimann, and Esslinger [14].
8. Girder test by Muller [12].
9. University of Texas large-scale girder tests by Diab [6].
10. University of Texas large-scale girder tests described in this thesis.
11. Fretting simulation tests by Cordes and Lapp-Emden [4].

Data from the above studies are reported in Table 5.1. In the case of tests by Rigon and Thurlimann [20], and Oertle, Thurliamann and Esslinger [14], some manipulation of the data was necessary. Rigon and Thurlimann, and Oertle et al. did not maintain constant tendon stress ranges during some of their tests. They often increased the tendon stress range after a few million cycles if no fractures had occurred. They then continued testing at the new, higher stress range. Since it is nearly impossible to evaluate the effect each stress range had on the fatigue life, these data points were interpreted as runouts at the lower stress range. This procedure was recommended by Yates [27], was used by Wollmann [26], and is also adopted for this study.

Table 5.1 Summary of Fretting Fatigue Tests of Post-Tensioning Tendons

Researcher	Type of Tendon	Stress Range (ksi)	Fatigue Life (x 1000)
Yates (strand in air fatigue tests)	Strand A 0.5 in. dia. 7 wire strand	40.5	110 #
		40.5	109 #
		40.5	1401
		40.5	239
		40.5	127 #
		40.5	238 #
		40.5	124 #
		40.5	156 #
		40.5	99 #
		40.5	212
	Strand B 0.5 in. dia. 7 wire strand	30.0	1521 #
		30.0	701
		30.0	1946 #
		30.0	1792
		30.0	815
		40.5	306
		40.5	468
		40.5	1746 #
		40.5	684
		40.5	265 #
Wollmann (strand in air fatigue tests)	Strand C 0.5 in. dia. 7 wire strand	30.0	925
		30.0	406 #
		30.0	1298
		30.0	1797 #
Cordes (fretting simulation tests)	1-0.6 in. dia. 7 wire strand	30.0	2175 #
		40.0	289
		40.0	782
		30.0	3057
		30.0	9000 *
		24.7	2027 *
		30.5	1127
		37.7	752
		63.8	107
		36.3	816

# Failure occurred in the grip region

\* Runout

Table 5.1 Summary of Fretting Fatigue Tests of Post-Tensioning Tendons (continued)

Researcher	Type of Tendon	Stress Range (ksi)	Fatigue Life (x 1000)
Cordes (fretting simulation tests)	1-0.6 in. dia. 7 wire strand	50.8	310
		24.7	2002 *
		31.9	2238 *
		30.5	2211
		36.3	1237
	1-7.0 mm dia. single wire	18.9	2044 *
		21.8	1946
		23.2	2151 *
		27.6	1692
		60.9	175
		39.2	1051
		27.6	2002 *
		23.2	2002 *
		42.1	679
		29.0	1077
	1-12.2 mm dia. single wire	23.2	2355 *
		26.1	1327
		36.3	1245
		23.2	2172 *
		34.8	694
		31.9	803
		29.0	1326
		34.8	588
		29.0	985
		30.5	941
		29.0	935
		33.4	674
47.9	289		
36.3	750		
Rigon and Thurlimann (girder tests)	16-7.0 mm dia. parallel wires	43.7	765
		11.0	1580
		12.0	2000 *
		25.1	911
		11.3	4000 *

\* Runout

Table 5.1 Summary of Fretting Fatigue Tests of Post-Tensioning Tendons (continued)

Researcher	Type of Tendon	Stress Range (ksi)	Fatigue Life (x 1000)
Rigon and Thurlimann (girder tests)	16-7.0 mm dia. parallel wires	22.5	1159
		24.1	4000 * +
		18.0	1245
	4-0.6 in. dia. 7 wire strands	34.4	223
		18.3	422
		7.7	2000 *
		13.6	1440
		9.0	626
		9.0	3430
		15.1	3830
Diab (girder tests)	6-0.5 in. dia. 7 wire strands	47.0	229
		32.5	300
		23.0	320
Present Study (girder tests)	6-0.5 in. dia. 7 wire strands	25.0	2100
		40.0	800
		30.0	490
		30.0	1300 +
		30.0	700 +
Oertle et al. (girder tests)	4-0.6 in. dia. 7 wire strands	14.5	2000 *
Oertle et al. (reduced-beam tests)	1-0.6 in. dia. 7 wire strand	29.0	1400
		29.0	1500
		29.0	1500
		29.0	1600
		29.0	1700
		29.0	2100
		21.8	2200
		21.8	2600
		21.8	4000
		18.1	2300
		18.1	4100
	14.5	4000 *	

\* Runout

+ Plastic Duct

Table 5.1 Summary of Fretting Fatigue Tests of Post-Tensioning Tendons (continued)

Researcher	Type of Tendon	Stress Range (ksi)	Fatigue Life (x 1000)	
Oertle et al. (reduced-beam tests)	1-0.6 in. dia. 7 wire strand	43.5	1900 +	
		43.5	2000 +	
		39.9	2300 +	
		39.9	2900 +	
		36.3	2700 +	
		36.3	8500 * +	
		29.0	4000 * +	
		29.0	2000 * x	
		29.0	2400 * x	
		29.0	2500 * x	
		29.0	2500 * x	
		5-7 mm dia. parallel wires	29.0	900
			29.0	1100
	29.0		1300	
	21.8		1500	
	21.8		1700	
	21.8		2300	
	18.1		2100	
	18.1		2600	
	14.5		4500 *	
	39.9		5700 +	
	36.3		5500 +	
	36.3		7400 +	
	29.0		8000 +	
	1-7 mm dia. single wire	36.3	1300	
		36.3	2050	
		29.0	1400	
		29.0	1650	
		29.0	1700	
		29.0	2150	
		29.0	2300	
		29.0	2500	
		29.0	4750	
	29.0	6400		

\* Runout                      x Not grouted  
+ Plastic Duct

Table 5.1 Summary of Fretting Fatigue Tests of Post-Tensioning Tendons (continued)

Researcher	Type of Tendon	Stress Range (ksi)	Fatigue Life (x 1000)
Oertle et al. (reduced-beam tests)	1-7 mm dia. single wire	25.4	2050
		25.4	2600
		25.4	3600
		21.8	4150
		21.8	4500
		29.0	4000 * x
		58.0	2000 * +
		58.0	3000 * +
		43.5	2000 * +
		43.5	3000 * +
		36.3	3000 * +
Muller (girder tests)	1-26.5 mm dia. threaded bar	36.2	80
		36.2	120
		36.2	220
		28.9	400
		28.9	2000 *
		21.7	2000 *
	3-12.2 mm dia. parallel wires	36.2	750
		28.9	2050
		28.9	4000 *
		25.3	1200
		21.7	2200 *
	3-0.6 in. dia. 7 wire strands	28.9	620
		21.7	1800
		21.7	2300
21.7		2800 *	
Yates (reduced-beam tests)	1-0.5 in. dia. 7 wire strand	40.0	293
		30.0	323
		30.0	467
		30.0	841
		25.0	804
		25.0	1008

\* Runout                      x Not grouted  
+ Plastic Duct

Table 5.1 Summary of Fretting Fatigue Tests of Post-Tensioning Tendons (continued)

Researcher	Type of Tendon	Stress Range (ksi)	Fatigue Life (x 1000)
Yates (reduced-beam tests)	1-0.5 in.dia. 7 wire strand	22.0	4515
		20.0	1270
		19.0	1500
		19.0	6500 *
		30.0	1843 +
		40.0	1112 +
		25.0	3537 +
Wollmann (reduced-beam tests)	6-0.5 in. dia. 7 wire strands	40.0	100
		30.0	490
		20.0	620
		20.0	1020
		30.0	260
		30.0	380
		30.0	370 +
		30.0	500 +

\* Runout

+ Plastic Duct



Upon further examination of the data, it was decided to exclude Rigon and Thurlimann's data from further consideration. One reason for doing so is cited in Oertle and Thurlimann's statement concerning Rigon and Thurlimann's tests which are included in Reference 24.

"Die durchgeführten Versuche waren nicht auf das Studium der überraschend aufgetretenen Reibermüdung ausgelegt. Im besonderen war es nachtraglich nicht mehr möglich, die Vielfalt der einwirkenden Parameter (Spannungsamplitude, Hullohrmaterial, Krümmungsradius, Querpressung, Gruppenwirkung, usw.) zu separieren. Folglich wäre es auch unverantwortlich gewesen, quantitative Angaben über den Abfall der Ermüdungs - festigkeit von Reib-Ermüdung zu machen".

(Fretting fatigue was not foreseen in the Rigon and Thurlimann study, and the tests were not designed specifically for the study of fretting fatigue. In particular, it was impossible to separate the many parameters affecting fretting fatigue (stress range, duct material, radius of curvature, lateral pressure, group effects, etc.) after conclusion of the tests. Consequently, it would have been irresponsible to come

up with a quantitative evaluation of the decrease of fatigue life due to fretting fatigue in post-tensioned concrete.)

Another reason for excluding Rigon and Thurlimann's data is the indirect determination of the tendon stresses via elongation measurements over a 200 mm length for a passive reinforcement bar. This procedure appeared to have led to a significant underestimation of the actual tendon stresses at crack locations [14].

## **5.2 Statistical Method**

A statistical method was used for analyzing the fatigue data. This method is known as a regression analysis by the least squares method. The result is the best fitting straight line for the data considered.

Two key variables, number of cycles to failure,  $N$ , and stress range,  $S_r$ , were used in the evaluation of the test data. They are related to each other through the equation:

$$\text{Log } (N) = a + b \text{ Log } (S_r)$$

---

In Section 5.6 the effect of another variable, contact pressure,  $q$ , will be included in the analysis of the

data. The variables will be assumed to be related according to the following equation:

$$\text{Log } (N) = a + b \text{ Log } (S_r) + c q$$

How well the assumed equations represent the relationships between variables will be indicated by the correlation coefficient,  $R$ , and the standard error,  $s'$ .  $R$  takes a value between  $+1.0$  and  $-1.0$ . If  $R$  equals  $+1.0$  or  $-1.0$ , there is a perfect linear correlation between the variables. If  $R$  equals zero, there is no relationship between the variables. The standard error,  $s'$ , is a measure of scatter of the data about the regression equation. A value of  $s'$  equal to zero indicates a perfect linear correlation of the variables. In general, as the absolute value of  $R$  increases, the value of  $s'$  decreases. As the absolute value of  $R$  approaches  $1.0$  the value of  $s'$  approaches zero.

### **5.3 Paulson's Strand In Air Failure Zone**

Paulson's Strand in Air Failure Zone [17] is used throughout the remainder of this chapter for comparison with strand fretting fatigue data. This failure zone is bounded top and bottom in the stress range domain

(at 25 and 90 ksi) and by upper and lower fatigue limits. The lower stress range is not an endurance limit, and the failure zone represents a confidence region such that there is a 97.5% probability that 95 out of 100 of the strand data evaluated by Paulson will fall in the failure zone. Paulson's lower fatigue limit model for strand in air, labelled A-1L, is given in Table 5.2 and shown in Fig. 2.4.

#### **5.4 Strand In Air Fatigue Tests**

A set of 10 strand samples, referred to as strand B, and a set of 4 strand samples, referred to as strand C, were fatigue tested in air by Yates [27] and Wollmann [26], respectively. Strand B and strand C were used in fabrication of the large-scale beams tested during the present study. Yates fatigue tested another set of 15 strand samples from another spool of strand, referred to as strand A. The purpose for all these tests was to determine if the in-air fatigue behavior of the strand used in this study was different from the data evaluated and reported by Paulson. The results of these tests are summarized in Table 5.3.

Table 5.2 Linear Regression Analysis Results

Model I.D.	Mean Fatigue Life Model	Correlation Coefficient, R	Standard Error, s'
A-1L	$\text{Log}(N)=10.97-3.50\text{Log}(Sr)$	N.A.	N.A.
STR-1	$\text{Log}(N)=11.211-3.462\text{Log}(Sr)$	-0.663	0.269
B-26.5	$\text{Log}(N)=12.978-5.049\text{Log}(Sr)$	-0.808	0.221
W-12.2	$\text{Log}(N)=9.328-2.241\text{Log}(Sr)$	-0.796	0.124
W-7.0	$\text{Log}(N)=8.817-1.774\text{Log}(Sr)$	-0.660	0.228
S-0.6	$\text{Log}(N)=9.648-2.411\text{Log}(Sr)$	-0.900	0.163
S-0.5	$\text{Log}(N)=8.970-2.210\text{Log}(Sr)$	-0.662	0.288
SM-1	$\text{Log}(N)=9.724-2.632\text{Log}(Sr)$	-0.674	0.304
SP-1	$\text{Log}(N)=4.387+1.155\text{Log}(Sr)$	0.296	0.314
WM-1	$\text{Log}(N)=7.624-0.923\text{Log}(Sr)$	-0.333	0.217
WP-1	$\text{Log}(N)=8.437-1.048\text{Log}(Sr)$	-0.760	0.064

N.A. Not Available

N = Fatigue Life (no. of cycles)

Sr = Stress Range (ksi)

Table 5.3 Summary of Strand In Air Test Results

Researcher	Type of Tendon	Stress Range (ksi)	Fatigue Life (x 1000)
Yates (strand in air fatigue tests)	Strand A 0.5 in. dia. 7 wire strand	40.5	110 #
		40.5	109 #
		40.5	1401
		40.5	239
		40.5	127 #
		40.5	238 #
		40.5	124 #
		40.5	156 #
		40.5	99 #
		40.5	212
	Strand B 0.5 in. dia. 7 wire strand	30.0	1521 #
		30.0	701
		30.0	1946 #
		30.0	1792
		30.0	815
		40.5	306
		40.5	468
		40.5	1746 #
		40.5	684
		40.5	265 #
Wollmann (strand in air fatigue tests)	Strand C 0.5 in. dia. 7 wire strand	30.0	925
		30.0	406 #
		30.0	1298
		30.0	1797 #
		30.0	2175 #
		40.0	289
		40.0	782
		30.0	3057
30.0	9000 *		

# Failure occurred in the grip region

\* Runout

#### **5.4.1 Statistical Analysis and Comparison of Results**

In the analysis of the strand in air test results, failures that occurred in the grip region were excluded. Runouts were also omitted from the statistical analysis. A mean fatigue model, labelled STR-1, was then developed for the remainder of the data using linear regression analysis. The model is listed in Table 5.2 and is shown along with its data in Fig. 5.1. For comparison purposes, Paulson's failure zone is also plotted in Fig. 5.1. All data points fall within Paulson's failure zone indicating no significant differences in the in-air characteristics between the strands used in this test program and those evaluated by Paulson.

### **5.5 Previous Studies**

#### **5.5.1 Introduction**

A summary of previous studies is given in Chapter 2. This section is devoted to analyzing and comparing test results of the present and previous studies.

Test data for particular tendon types are initially considered. Then all strand-type tendons with metal duct are evaluated, followed by strand-type tendons with plastic duct, and finally all parallel-wire tendons with

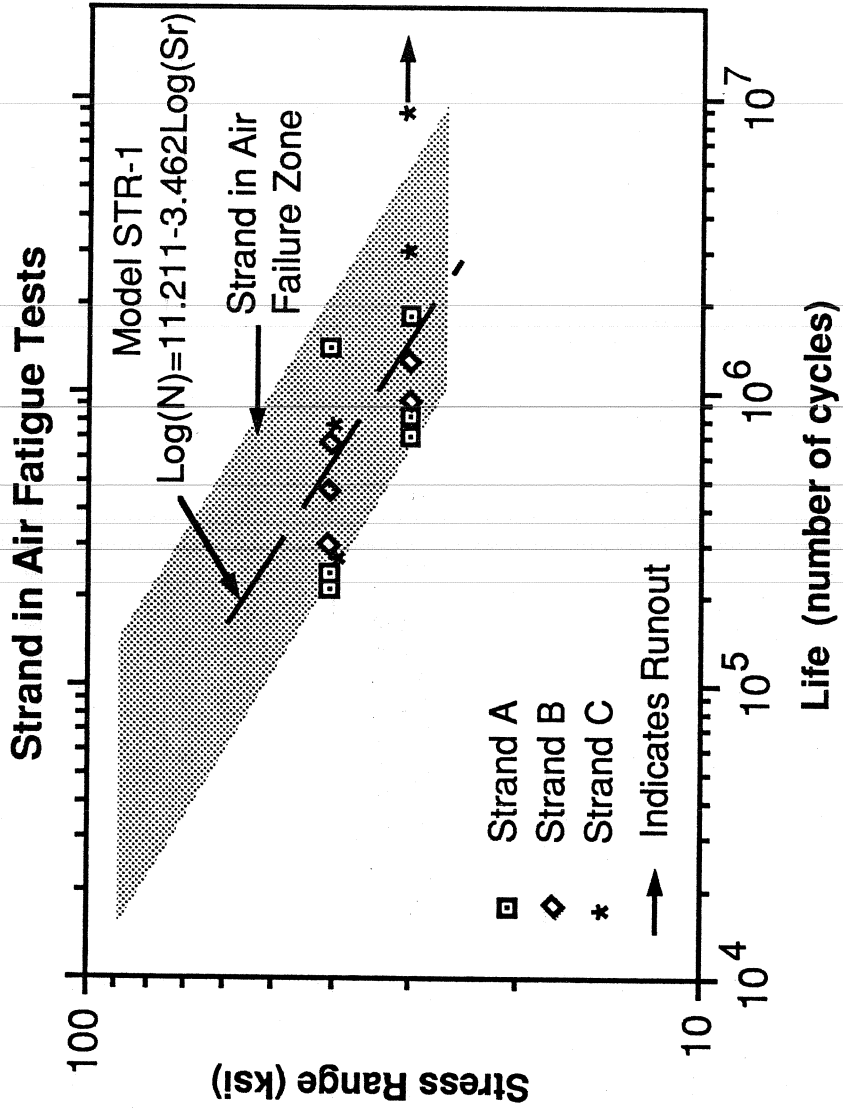


Figure 5.1 Comparison of Strand In Air Fatigue Data and Strand In Air Failure Zone



metal duct. When appropriate, fatigue data are compared with Paulson's failure zone, and the AASHTO Category B fatigue model. The AASHTO Category B fatigue model was chosen for comparison purposes because it is currently used for establishing the fatigue life of strands in cable stays [17,19] and in pretensioned beams [16].

#### **5.5.2 26.5 mm Diameter Threaded Bar Tests**

Muller [12] fatigue tested a series of post-tensioned beams with 1-26.5 mm diameter bar tendon. The results of these tests are summarized in Table 5.1. All data points (including runouts) are shown in Fig. 5.2 along with the calculated mean fatigue life and the AASHTO Category B fatigue model. The mean fatigue life is labelled B-26.5, and is listed in Table 5.2. Examining Fig. 5.2, it appears that the AASHTO Category B fatigue model, which is recommended for fatigue of continuous threaded bars [1], does not represent a safe lower bound for this type of tendon. Because the mean fatigue life is based on only four tests, it is likely that more data points are needed to develop a representative mean fatigue-life model for this type of tendon.

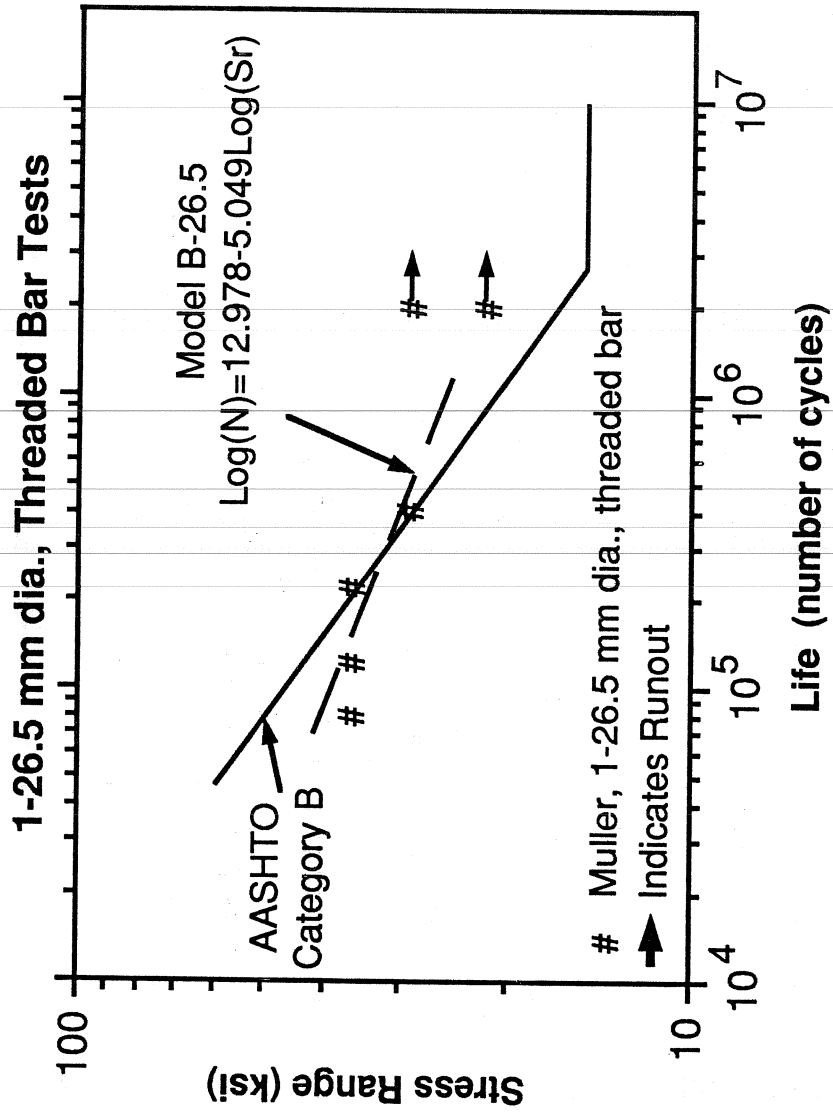


Figure 5.2 Comparison of 1-26.5 mm dia. Threaded Bar Tests with AASHTO Fatigue Model

### 5.5.3 12.2 mm Diameter Wire Tests

Muller [12] fatigue tested a series of post-tensioned beams with 3-12.2 mm diameter parallel wire tendons, and Cordes et al. [4] conducted fretting simulation tests on a series of 12.2 mm diameter single wires. The test results of both studies are shown in Fig. 5.3 along with a mean fatigue life model (labelled W-12.2) and the AASHTO Category B fatigue model. The scatter of the data is relatively small resulting in a good correlation coefficient ( $R=-0.796$ ) and a small standard error ( $s'=0.124$ ). The AASHTO fatigue model appears to provide a safe lower bound for not only the mean fatigue life, but also all tendon fatigue data.

### 5.5.4 7 mm Diameter Wire Tests

Oertle and Thurlimann [14], and Cordes et al. [4] conducted tests using 7 mm diameter wire tendons. Multiple-wire tendons tested by Oertle and Thurlimann contained parallel wires. The test results are shown in Fig. 5.4 along with their mean fatigue-life model (labelled W-7.0). In this case the scatter of the data is very large resulting in a lower correlation coefficient and higher standard error. For the particular case of tests with a 29 ksi stress range (12

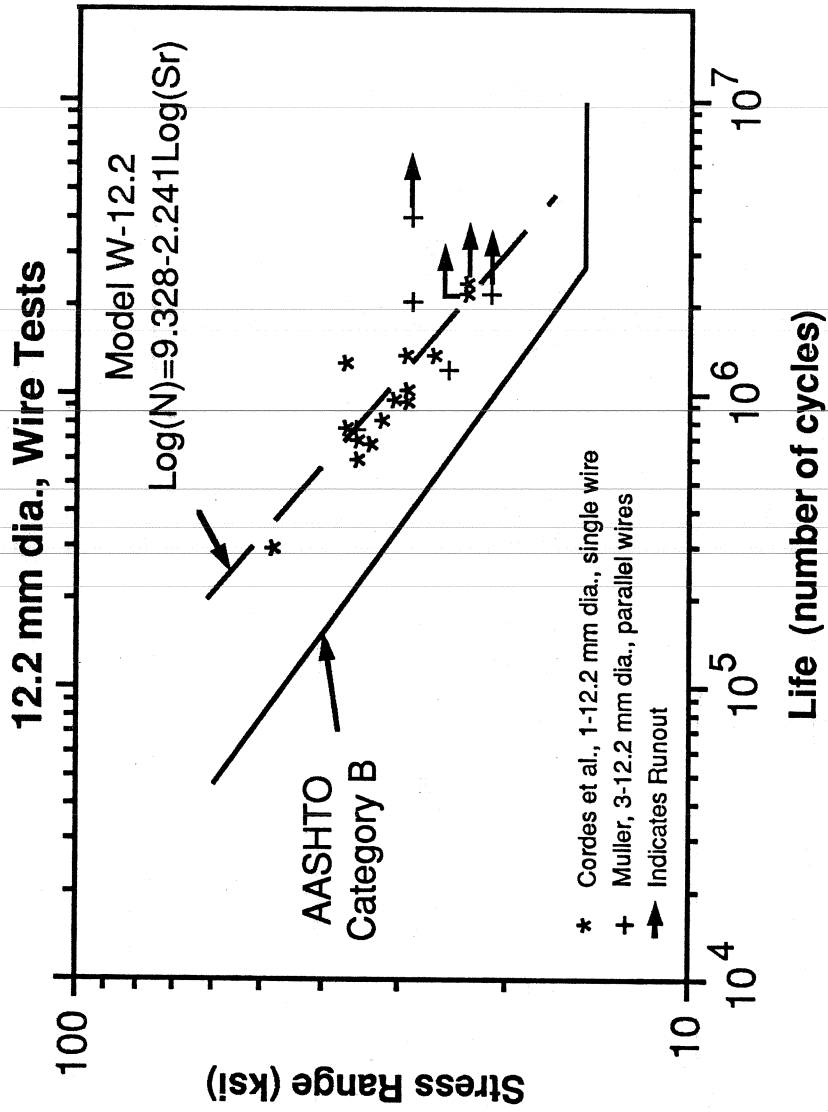


Figure 5.3 Comparison of 12.2 mm dia., Wire Tests with AASHTO Fatigue Model

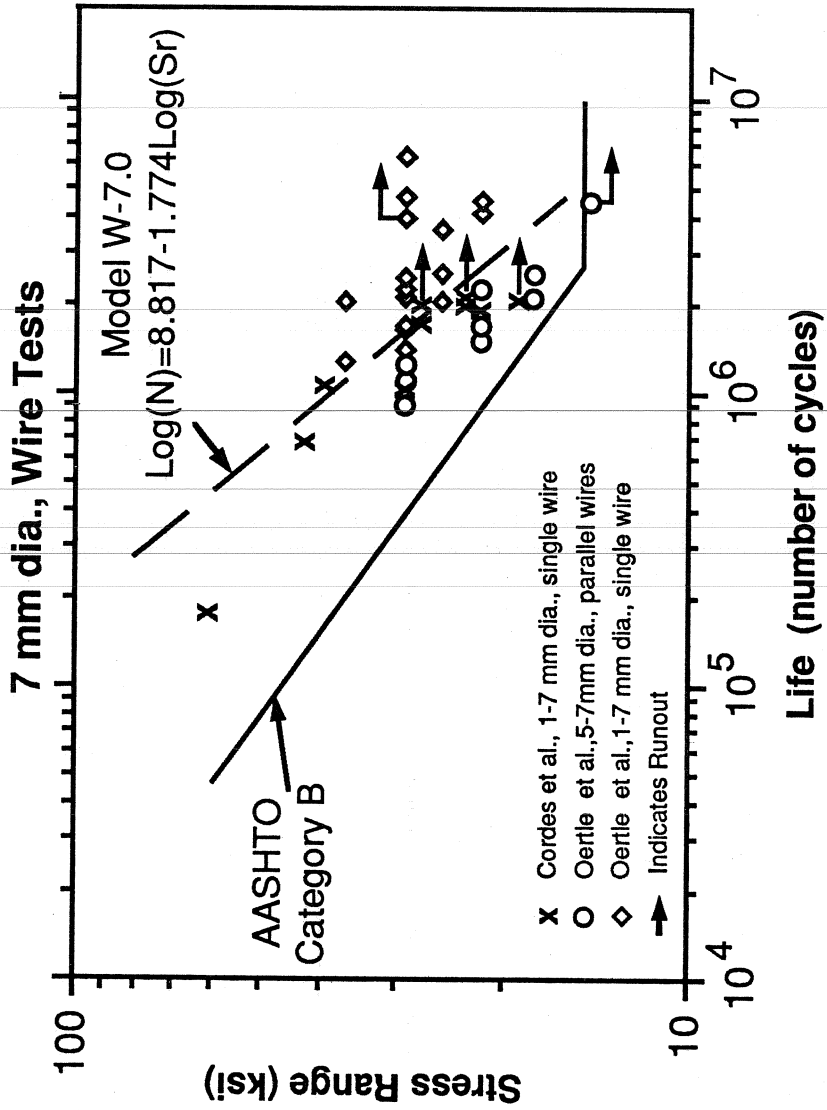


Figure 5.4 Comparison of 7 mm dia., Wire Tests with AASHTO Fatigue Model

data points, excluding one runout), fatigue lives varied from 900,000 cycles to 6,400,000 cycles. In addition, it is interesting to note that fatigue lives were generally longer for single-wire tendons than for multi-wire tendons.

The AASHTO Category B fatigue model appears to provide a lower bound for these data, although some data at low stress ranges lie very close to this limit. More data are needed for multiple-wire tendons at high stress ranges (above 30 ksi) in order to seriously test the validity of the AASHTO fatigue model.

#### **5.5.5 0.6 in. Diameter, 7 Wire Strand Tests**

Cordes et al. [4], Oertle et al. [14] and Muller [12] conducted fatigue tests using one or more 0.6 in. diameter, 7 wire strand tendons. The test results are shown in Fig. 5.5 along with the mean fatigue life model, labelled S-0.6. The scatter of the data points is relatively small ( $s'=0.163$ ) resulting in an acceptable correlation ( $R=-0.900$ ) between stress range and fatigue life. The AASHTO Category B fatigue model does not provide a lower bound for all the data; the single data point corresponding to Oertle's 4-0.6 in. diameter, 7 wire strand test lies below the AASHTO

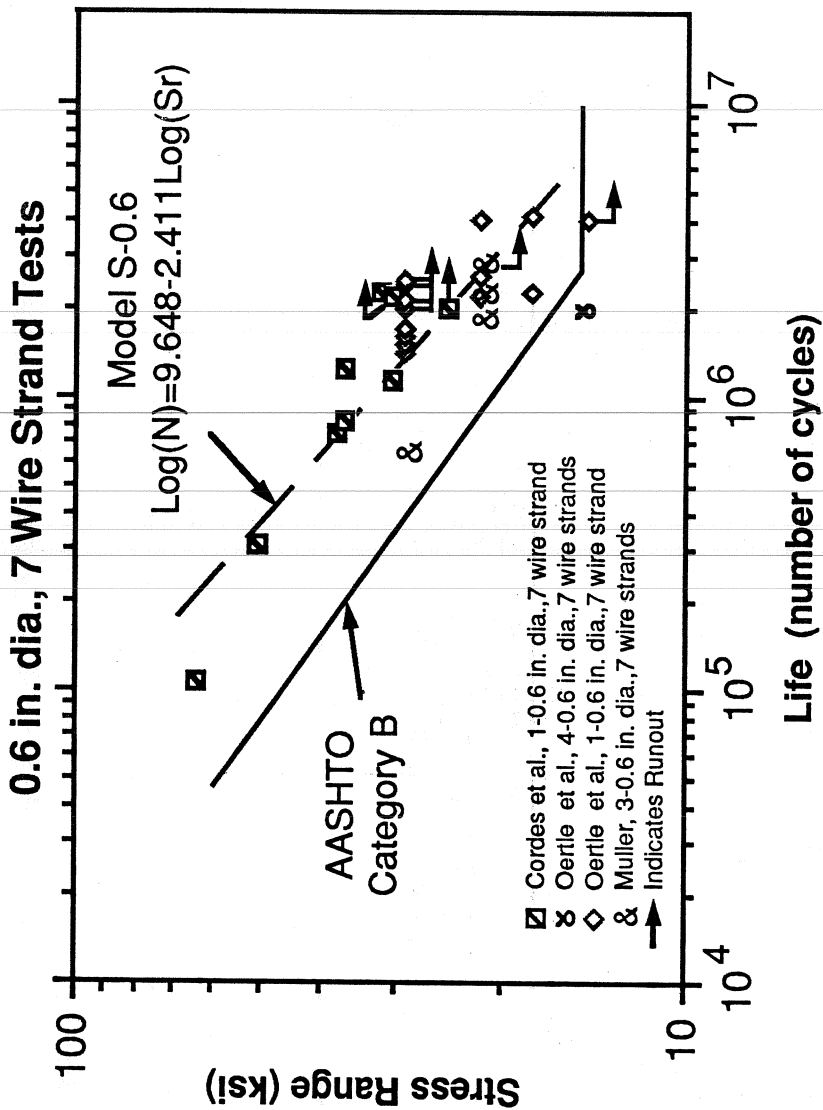


Figure 5.5 Comparison of 0.6 in. dia., 7 Wire Strand Tests with AASHTO Fatigue Model

fatigue model. However, this particular data point could be an outlier resulting from unaccounted circumstances which could have adverse effects on the fatigue performance of the beam. Once again, note that the multi-strand tendons generally have a lower fatigue life than the single-strand specimens. To establish the AASHTO fatigue model as a safe lower bound for this type of tendon, confidence intervals must be defined. We cannot be 100% sure that all data will fall above the AASHTO fatigue model. The data point under consideration could be one such instance. However, many more data points are needed for the establishment of the AASHTO Category B fatigue model as a design guide for this type of tendon.

#### **5.5.6 0.5 in. Diameter, 7 Wire Strand Tests**

All data for the 0.5 in. diameter, 7 wire strand tests come from the overall research project conducted at the Ferguson Structural Engineering Laboratory of The University of Texas at Austin. The data are plotted in Fig. 5.6 along with their mean fatigue model, labelled S-0.5. The dispersion of the data points is relatively large resulting in a low correlation coefficient ( $R=-0.662$ ) and a relatively high standard error



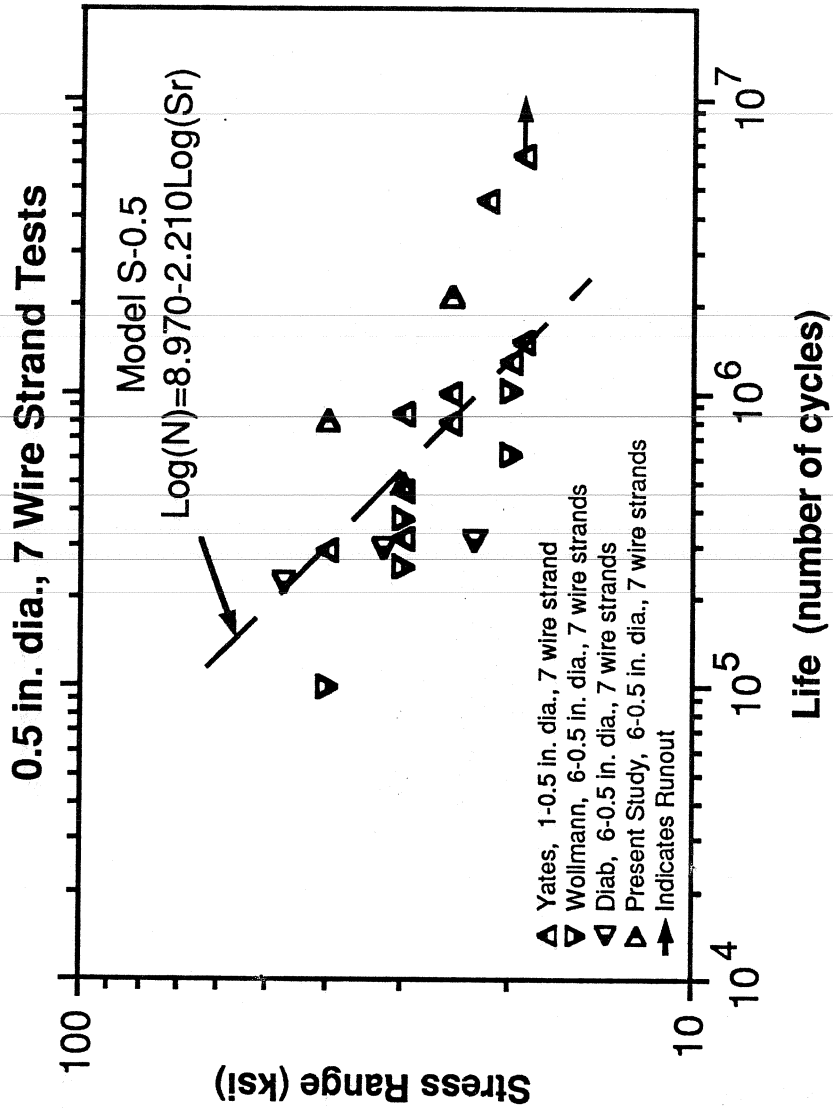


Figure 5.6 Results of 0.5in. dia., 7 Wire Strand Tests

( $s'=0.288$ ).

Wollmann's [26] and Yates' [27] data came from tests of similar reduced-beam specimens. One notable difference between the specimens was the number of prestressing strands. Wollmann used 6-0.5 in. diameter, 7 wire strands, while Yates used 1-0.5 in. diameter, 7 wire strand. Yates' specimens experienced higher fatigue lives than those of Wollmann. This can be seen in Fig. 5.6. This will be explained later by the fact that in Yates' tests strand-to-strand fretting was avoided because there was only one strand present, while in Wollmann's tests, strand-to-strand fretting was present reducing the fatigue lives of the specimens. On the other hand, as it is discussed later in Section 5.6, beams with one strand are subjected to higher local contact loads than beams with multiple strands, making fretting more severe. The influence each of the above effects (strand-to-strand fretting and local contact load) has on the fatigue life of a specimen is not clear.

For comparison purposes, Paulson's strand in air failure zone and the AASHTO Category B fatigue model are also plotted in Fig. 5.7. Most of the data fall outside Paulson's failure zone, indicating the adverse effect

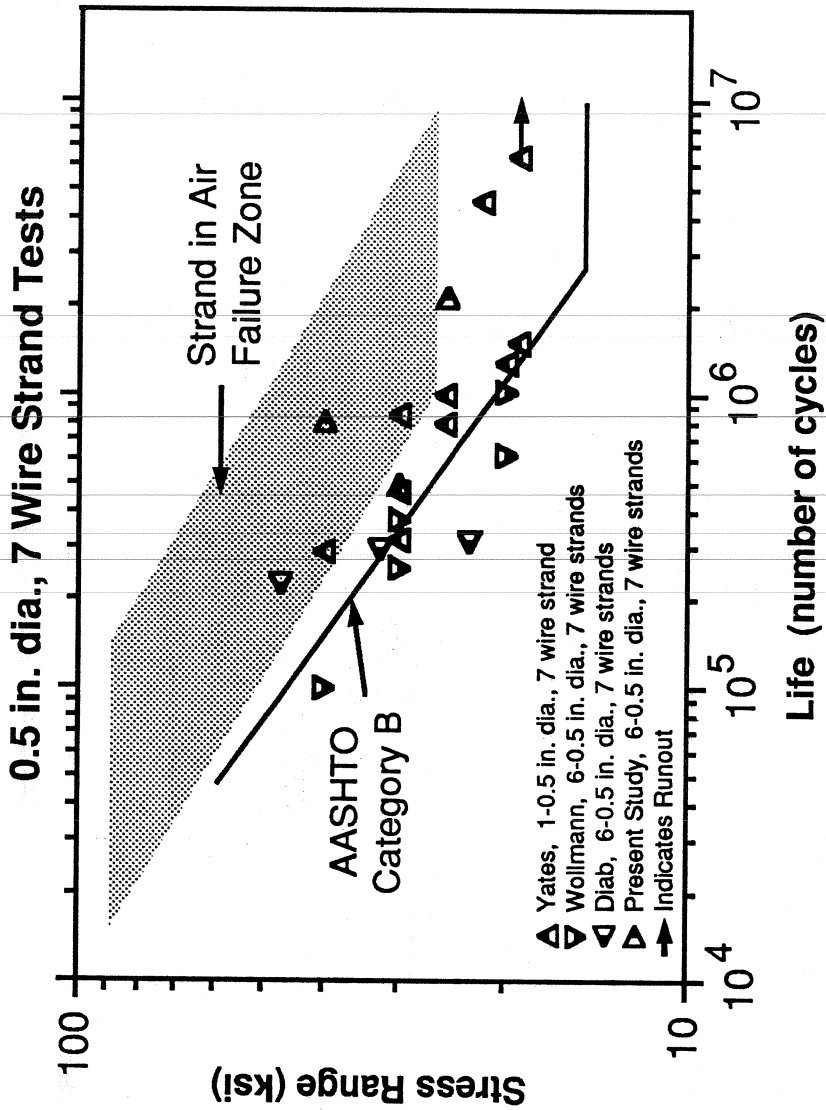


Figure 5.7 Comparison of 0.5in. dia., 7 Wire Strand Tests with Strand In Air Failure Zone and AASHTO Fatigue Model

of fretting on the fatigue life of post-tensioned members. Many data fall below the AASHTO fatigue model, indicating that it does not provide a reasonable lower bound for design of post-tensioned members with 0.5 in. diameter seven-wire strand tendons.

#### **5.5.7 Tests of Strand-Type Tendon with Metal Duct**

Many investigators have studied the fatigue behavior of beams with strand-type tendons and metal duct [6,12,14,26,27]. Data from these tests are listed in Table 5.4 and are plotted in Fig. 5.8 along with their mean fatigue life model, labelled SM-1, Paulson's strand in air failure zone, and the AASHTO Category B fatigue model. The scatter of the data is very large ( $R=-0.674$ ,  $s'=0.304$ ) and is most likely attributed to tendon size (number of strands) and geometry (arrangement of strands), and different procedures for determination of effective prestress.

Most data lie outside Paulson's failure zone, which indicates once again the adverse effects of fretting in the post-tensioned members. A significant number of data also lie below the AASHTO Category B fatigue model.

Table 5.4 Data for Strand-Type Tendons

Researcher	Type of Tendon	Stress Range (ksi)	Fatigue Life (x 1000)	K Factor	Contact Load, q (kips/ft)
Diab (girder tests)	6-0.5 in. dia. 7 wire strands	47.0	229	0.51	7.30
		32.5	300	0.51	7.91
		23.0	320	0.51	7.63
Present Study (girder tests)	6-0.5 in. dia. 7 wire strands	25.0	2100	0.51	.70
		40.0	800	0.51	5.96
		30.0	490	0.51	7.13
Oertle et al. (reduced-beam tests)	1-0.6 in. dia. 7 wire strand	29.0	1400	1.00	5.43
		29.0	1500	1.00	5.91
		29.0	1500	1.00	5.91
		29.0	1600	1.00	5.91
		29.0	1700	1.00	5.91
		29.0	2100	1.00	5.43
		21.8	2200	1.00	5.55
		21.8	2600	1.00	5.55
		21.8	4000	1.00	5.55
		18.1	2300	1.00	5.55
Muller (girder tests)	3-0.6 in. dia. 7 wire strands	28.9	620	0.65	4.35
		21.7	1800	0.65	4.26
		21.7	2300	0.65	4.26
		21.7	2800	0.65	4.26
		14.5	4000 *	1.00	5.67
Yates (reduced-beam tests)	1-0.5 in. dia. 7 wire strand	40.0	293	1.00	4.20
		30.0	323	1.00	4.06
		30.0	467	1.00	4.66
		30.0	841	1.00	4.28
		25.0	804	1.00	4.06
		25.0	1008	1.00	4.06
		22.0	4515	1.00	4.06
		20.0	1270	1.00	4.15
		19.0	1500	1.00	4.22
		19.0	6500	1.00	4.72
Wollmann (reduced-beam tests)	6-0.5 in. dia. 7 wire strands	40.0	100	0.51	7.50
		30.0	490	0.51	7.60
		20.0	620	0.51	8.10
		20.0	1020	0.51	8.10
		30.0	260	0.51	4.00 #
		30.0	380	0.51	4.10

\* Runout # Twisted Strand

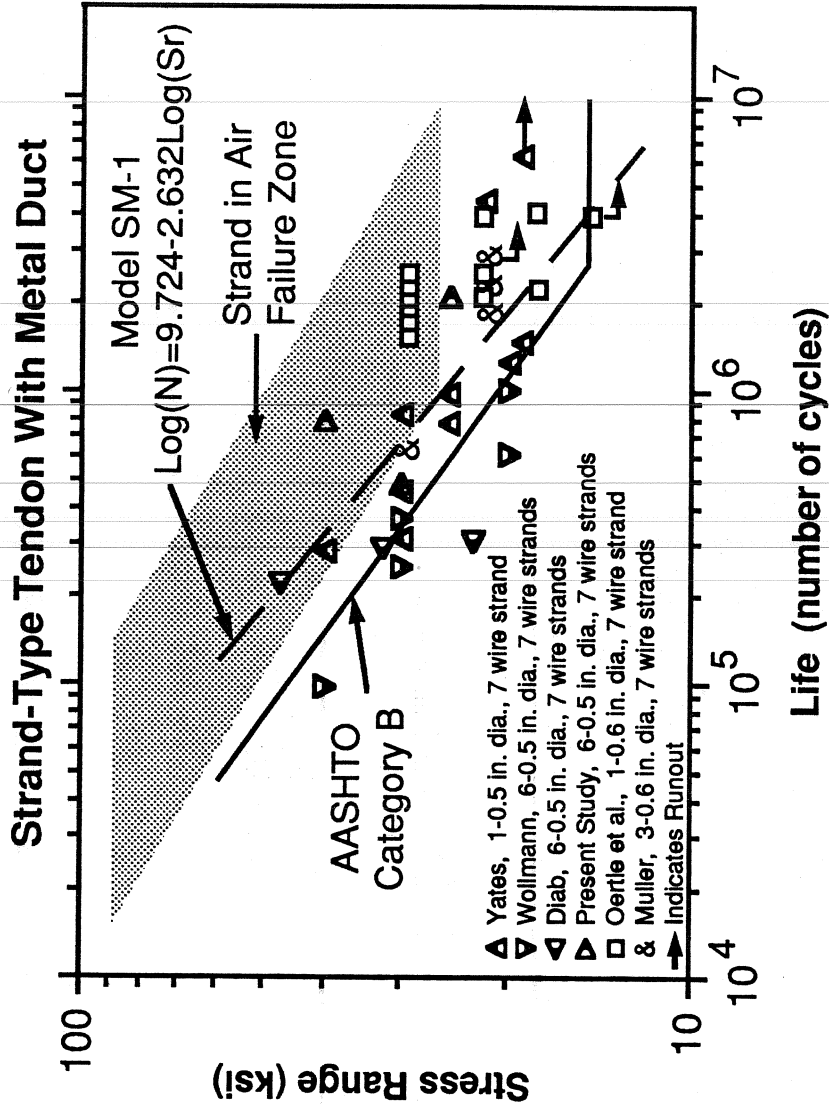


Figure 5.8 Comparison of Tests of Strand-Type Tendon With Metal Duct with Strand In Air Failure Zone and AASHTO Fatigue Model

### 5.5.8 Tests of Strand-Type Tendon with Plastic Duct

Tests of beams with a strand-type tendon and plastic duct were part of the studies by Oertle [14], Yates [27], Wollmann [26], and the present study as well. The data from the above tests are listed in Table 5.5 and are shown in Fig. 5.9 along with their mean fatigue life. The large scatter of the data and the positive slope of the mean fatigue life model can be attributed to the limited amount of data, differences in behavior between single and multi-strand tendons, and the fact that many tests were conducted at the same stress range. The data compare much more favorably with Paulson's strand in air failure zone and the AASHTO Category B fatigue model than do data for tendons with metal ducts.

Direct comparison between compatible sets of data is made in Fig. 5.10a and Fig. 5.10b. Open symbols are used in these figures to represent data from tests with metal duct, while similar shaded symbols are used for data from tests with plastic duct. It is clear that plastic duct dramatically improves the fatigue behavior of single-strand tendons. However, the behavior of multi-strand tendons is not so clearly benefitted, perhaps because plastic duct does not affect the strand-to-strand fretting that occurs in multi-strand tendons.

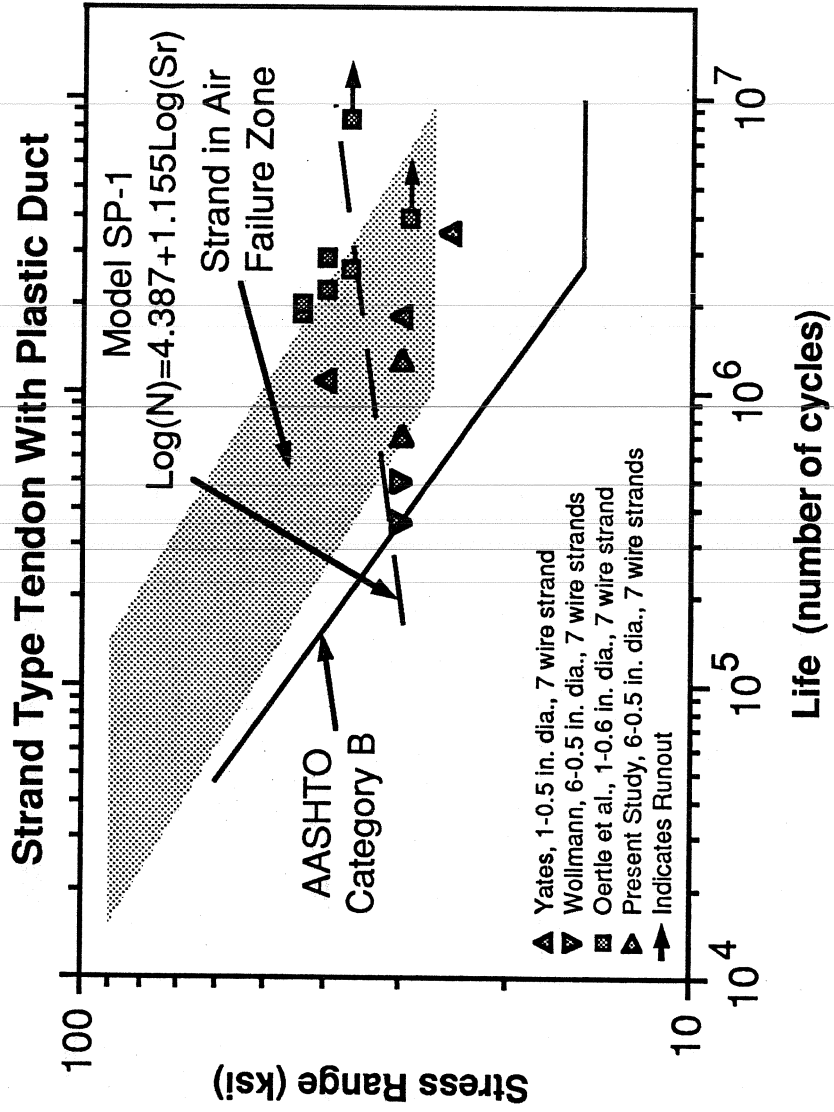


Figure 5.9 Comparison of Tests of Strand-Type Tendon With Plastic Duct with Strand In Air Failure Zone and AASHTO Fatigue Model



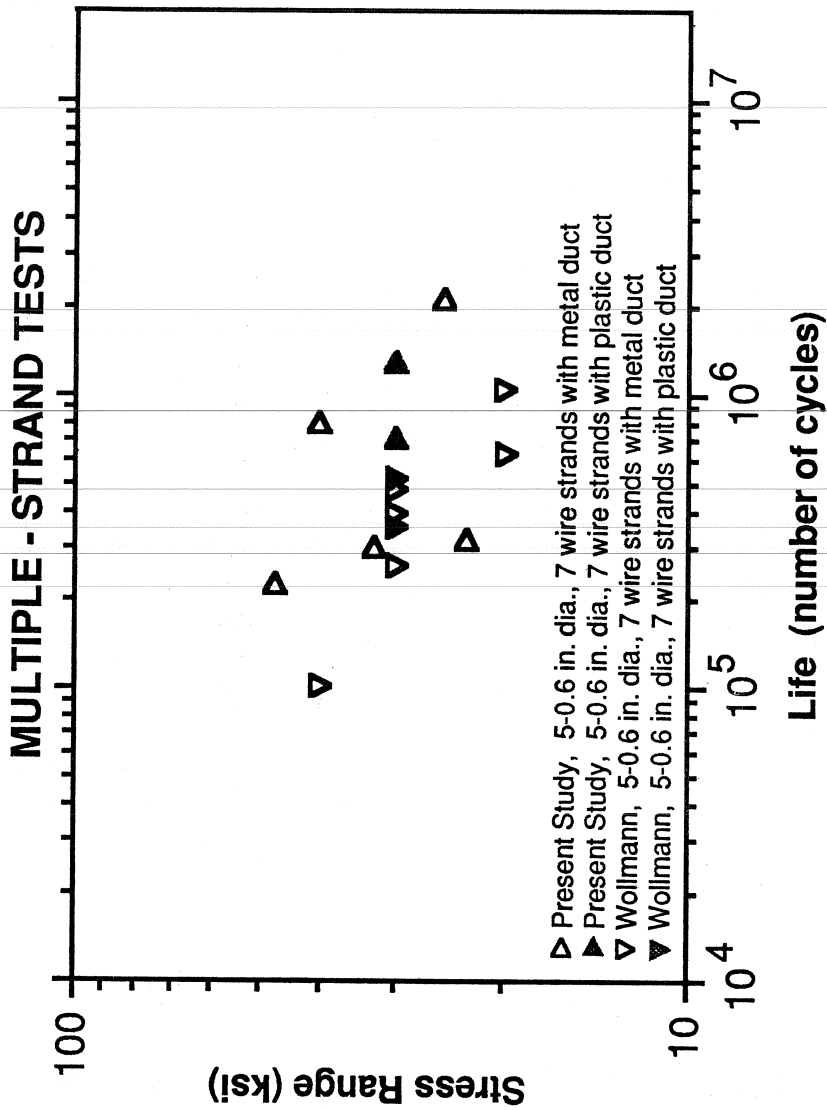


Figure 5.10a Comparison Between Multiple-Strand Tendon Tests for Metal Duct and Plastic Duct

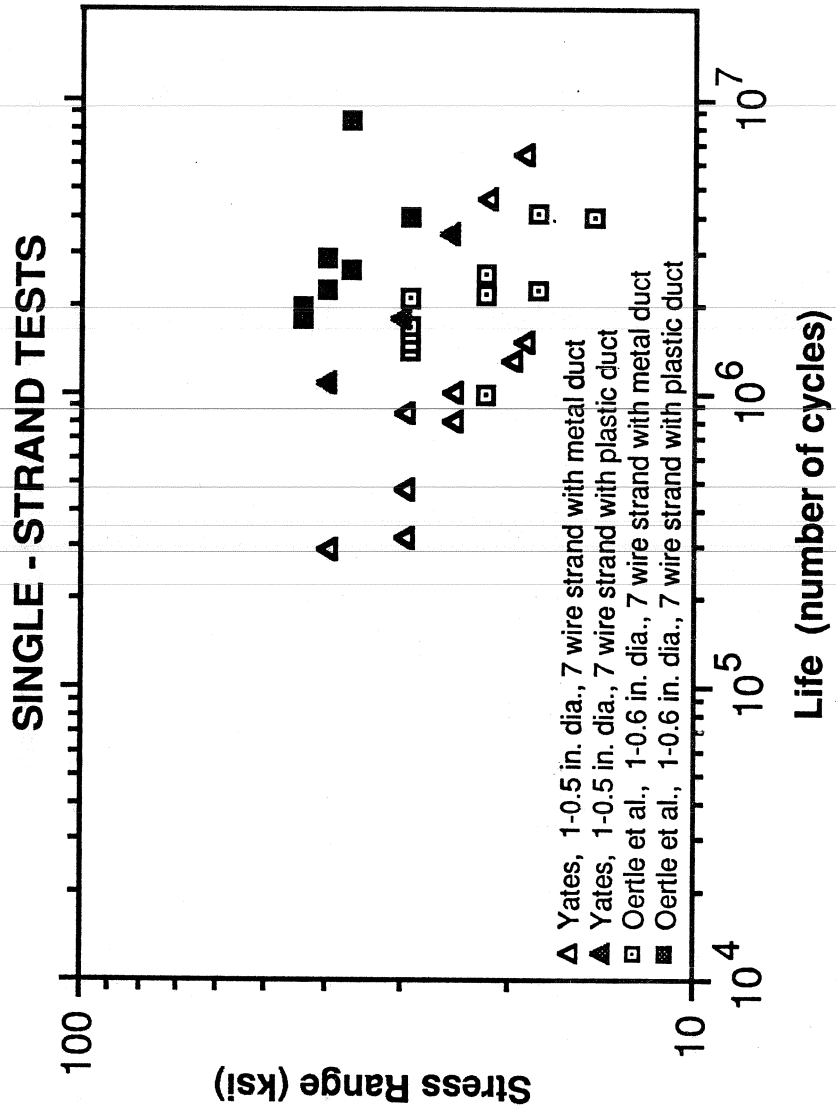


Figure 5.10b Comparison Between Single-Strand Tendon Tests for Metal Duct and Plastic Duct

### 5.5.9 Tests of Beams with Parallel-Wire Tendons

Oertle et al. [14] and Muller [12] fatigue tested a series of beams with wire tendons and metal or plastic duct. The test results for the beams with metal and plastic duct are shown in Figures 5.11 and 5.12 respectively, along with their corresponding mean fatigue life models (WM-1 and WP-1).

In the case of beams with metal duct, the data are so dispersed in both the X and Y directions that, statistically speaking, the model is "fragile". A small variation in the data or additional data could dramatically change the model. A similar situation exists in the case of the beams with plastic duct (Fig. 5.12).

Comparing the data in Fig. 5.11 with the data in Fig. 5.12 indicates that the beams with plastic duct performed better than those with metal duct. However, it is difficult to make direct comparisons between the data for metal and plastic duct because specimens with plastic duct were generally tested at stress ranges significantly higher than those used in tests of beams with metal duct.

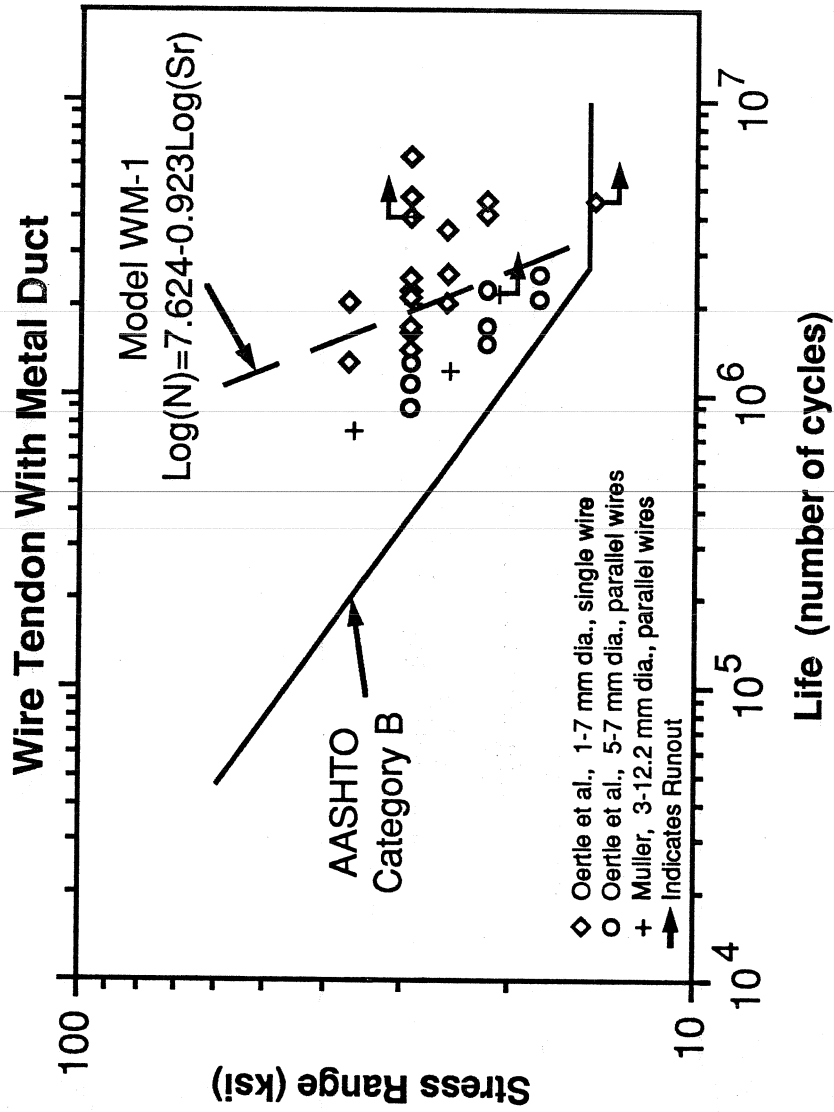


Figure 5.11 Comparison of Test Results from Beams with Wire Tendons and Metal Duct with AASHTO Fatigue Model

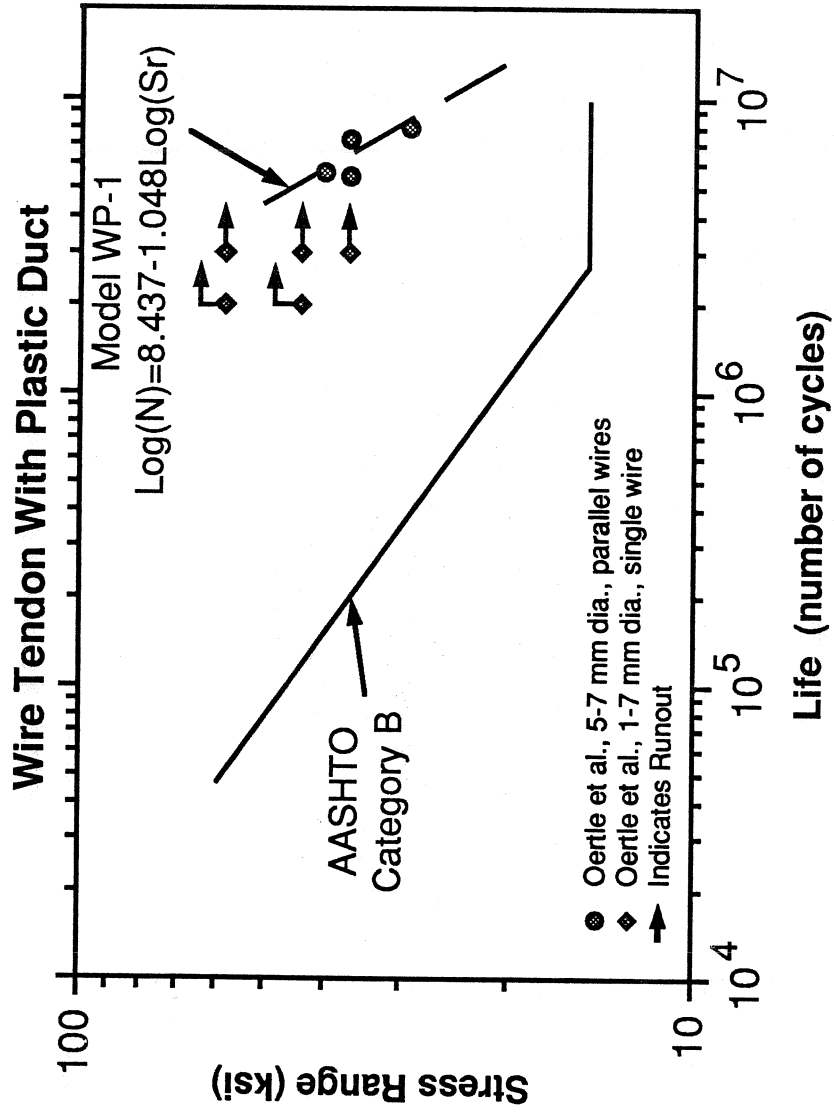


Figure 5.12 Comparison of Test Results from Beams with Wire Tendons and Plastic Duct with AASHTO Fatigue Model

## **5.6 Two-Variable Fretting Fatigue Model**

### **5.6.1 Introduction**

In the previous section it was assumed that fatigue life could be represented accurately as a function of the tendon stress range only. The large scatter and low correlation of some of the data presented in the previous section contradicts the above assumption. Other variables, the most important being the duct material, tendon arrangement, number of strands, slip amplitude, and contact pressure have significant effects on fretting fatigue of post-tensioned beams. The duct material variable can be taken care of by discriminating between plastic and metal duct. The tendon arrangement and number of strands can be integrated into a contact-pressure variable. Slip amplitude is highly dependent on the stress range and contact pressure. Therefore, as Yates suggested [27], fatigue life can be more accurately represented as a function of both stress range and contact pressure, discriminating at the same time between plastic and metal duct.

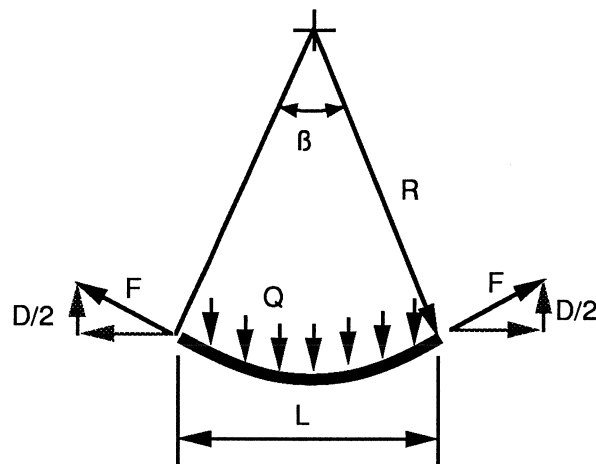
---

### **5.6.2 Estimation of Contact Load**

The estimation of the actual contact pressure in a

given tendon is virtually impossible because the area of contact between strands and duct is not known. Instead, the local contact load with units of force per unit length of tendon can be estimated using a method developed by Yates [27], which is a variation of the method described by Oertle [14]. Yates' method is illustrated in Fig. 5.13. In this method, the total lateral load,  $Q$ , exerted by all strands on the duct can be approximated with the tendon mean prestress force divided by the tendon radius of curvature (using small angle theory) as shown in Fig. 5.13a. The local contact load between the duct and an individual strand,  $q$ , can be expressed as a fraction of  $Q$  ( $q=K*Q$ , where  $K$  is less than or equal to unity). The value of  $k$  varies with duct and tendon geometry which includes the number and arrangement of strands within the duct, and the ratio of strand to duct size.

All strands are assumed to be tensioned equally, thus exerting equal vertical force,  $f$ . The value of  $f$  is equal to the total lateral load,  $Q$ , divided by the number of strands. Assuming no tangential friction between strands or between strands and duct, and that strands can be idealized having a circular cross section, the procedure described in Fig 5.13b can be



$$D = F \times \sin \beta$$

$$D \approx F \times L/R \text{ (small angles)}$$

$$Q = D/L \approx F/R$$

where:

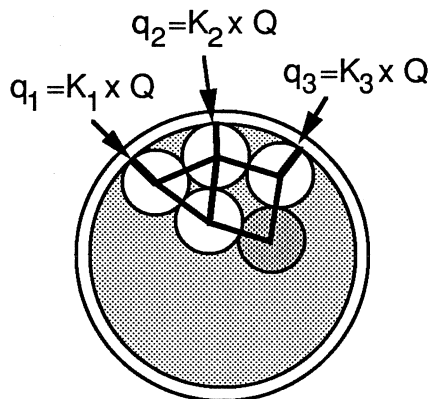
F = Tendon Force

R = Radius of Curvature

D = Total Vertical Force

Q = Distributed Vertical Load

a) Estimation of Lateral Load, Q



Assumptions:

- \* Each strand generates equal vertical load, f
- \* No tangential friction exists between strands or strands and duct
- \* Strands can be idealized having circular cross section

— Dark lines indicate direction of forces

#### Procedure

- 1) Assume stable geometry
- 2) Determine inclination of all forces (indicated by dark lines above)
- 3) Calculate statically determinant forces starting with outermost strand (shaded strand above)

b) Estimation of K Factors

Figure 5.13 Estimation of Lateral Load and K Factors (from Yates [27])



followed to estimate the values of K and local contact loads.

#### **5.6.2.1 General Characteristics of K Factors**

As mentioned in the previous section, K factors vary with tendon arrangement, number of strands, and ratio of strand to duct size. All these factors are interrelated, making each case unique and the calculation of K factors for each individual case necessary. However, there are some general characteristics of the K factors:

- 1) **Tendon Arrangement:** The greater the number of strands in contact with the duct, the greater the value of the highest K factor and the sum of all K factors is. An example is shown in Fig. 5.14.
- 2) **Number of Strands:** The greater the number of strands in the duct, the smaller the individual K factors are and the larger the sum of all K factors is. An example is given in Fig. 5.15.
- 3) **Ratio of Strand to Duct Size:** The larger the ratio of strand to inside duct size, the greater the individual strand K factors are and the larger the sum of all K factors is. An example is given in Fig. 5.16.

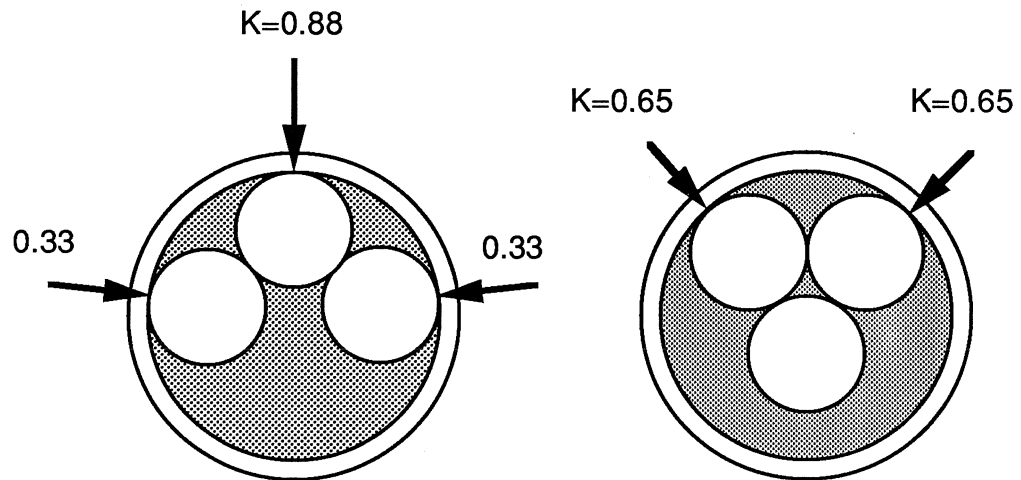


Figure 5.14 Variation of K Factors With Strand Arrangement

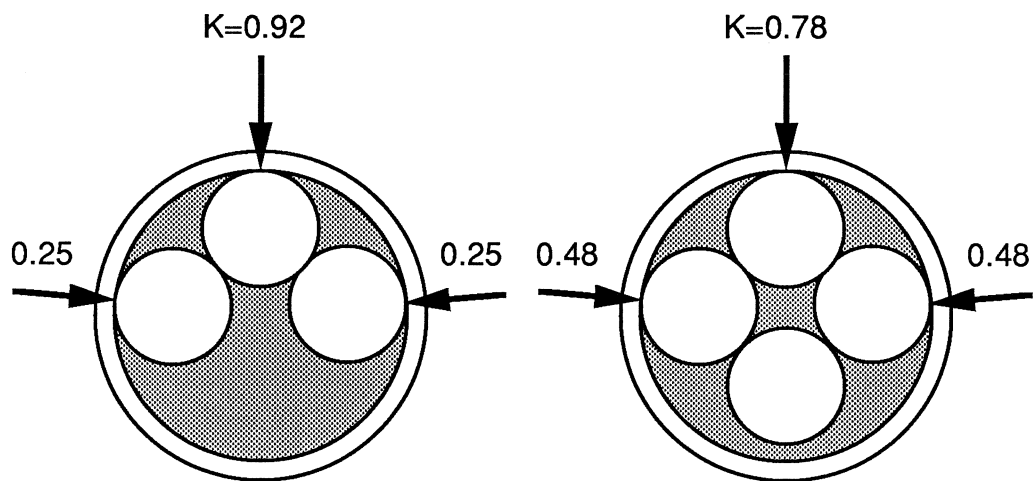


Figure 5.15 Variation of K Factors With Number of Strands

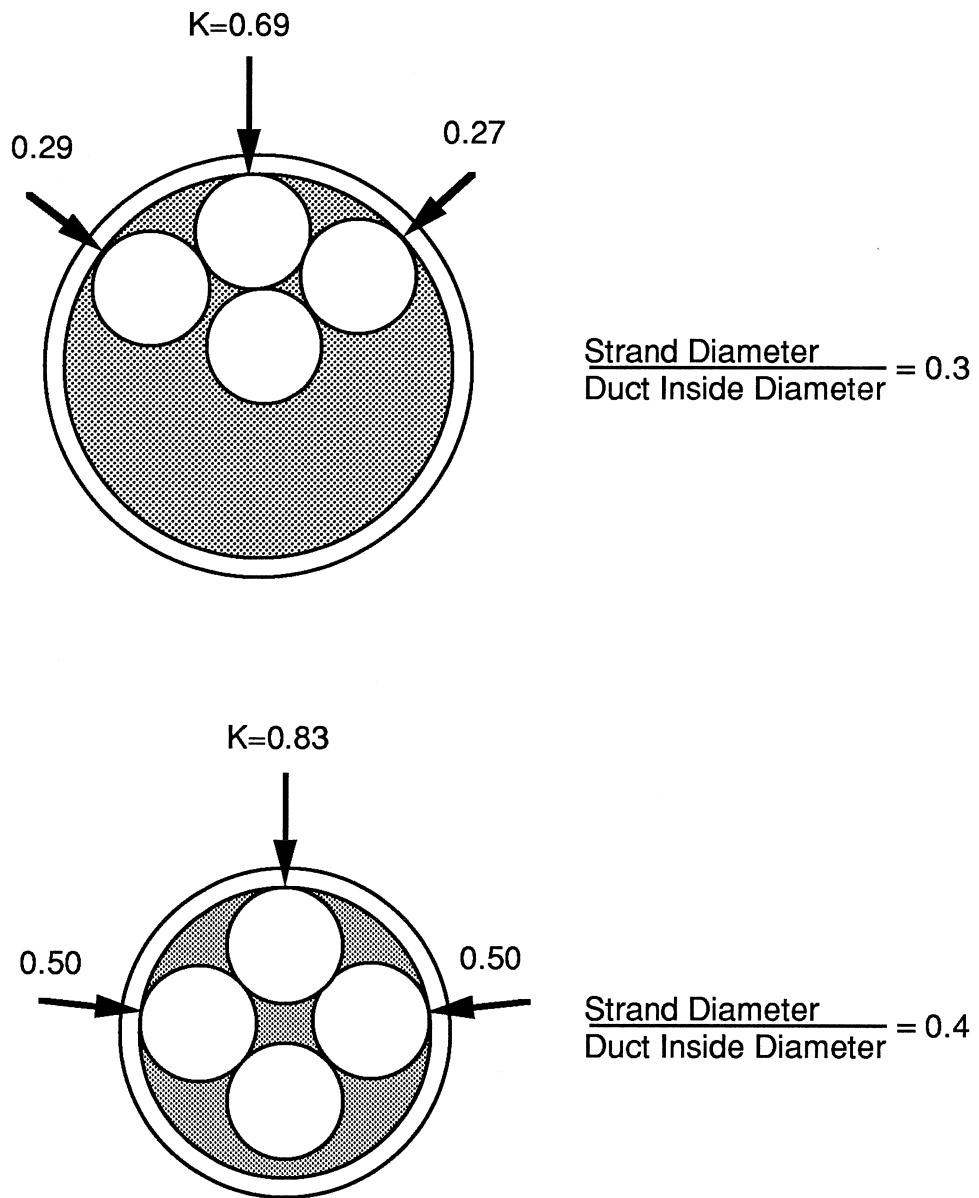


Figure 5.16 Variation of K Factors With Ratio of Strand to Duct Size

Following the first wire fracture, the total effective area of the tendon is reduced and the remaining wires are stressed more for the same stress range and tendon mean stress. Since we are interested in the first wire fracture within the tendon, only the largest K factor is needed. For a tendon with positive curvature, this corresponds to the strand with the highest elevation.

### **5.6.3 Evaluation of the Beam Test Data Using Multiple Linear Regression Analysis**

Having estimated the K factors and the local contact loads for the beam tests with tendon composed of strand or wires (Figures 5.17 and 5.18 respectively), the data were evaluated using a multiple linear regression analysis of the form:

$$\text{Log}(N) = a + b \text{Log}(S_r) + c q$$

All data used in this analysis are summarized in Table 5.4 for the case of strand-type tendons and Table 5.6 for the case of wire tendons. Muller's [12] test data from beams with 1-26.5 mm threaded bar tendon and all test data from beams with plastic duct were

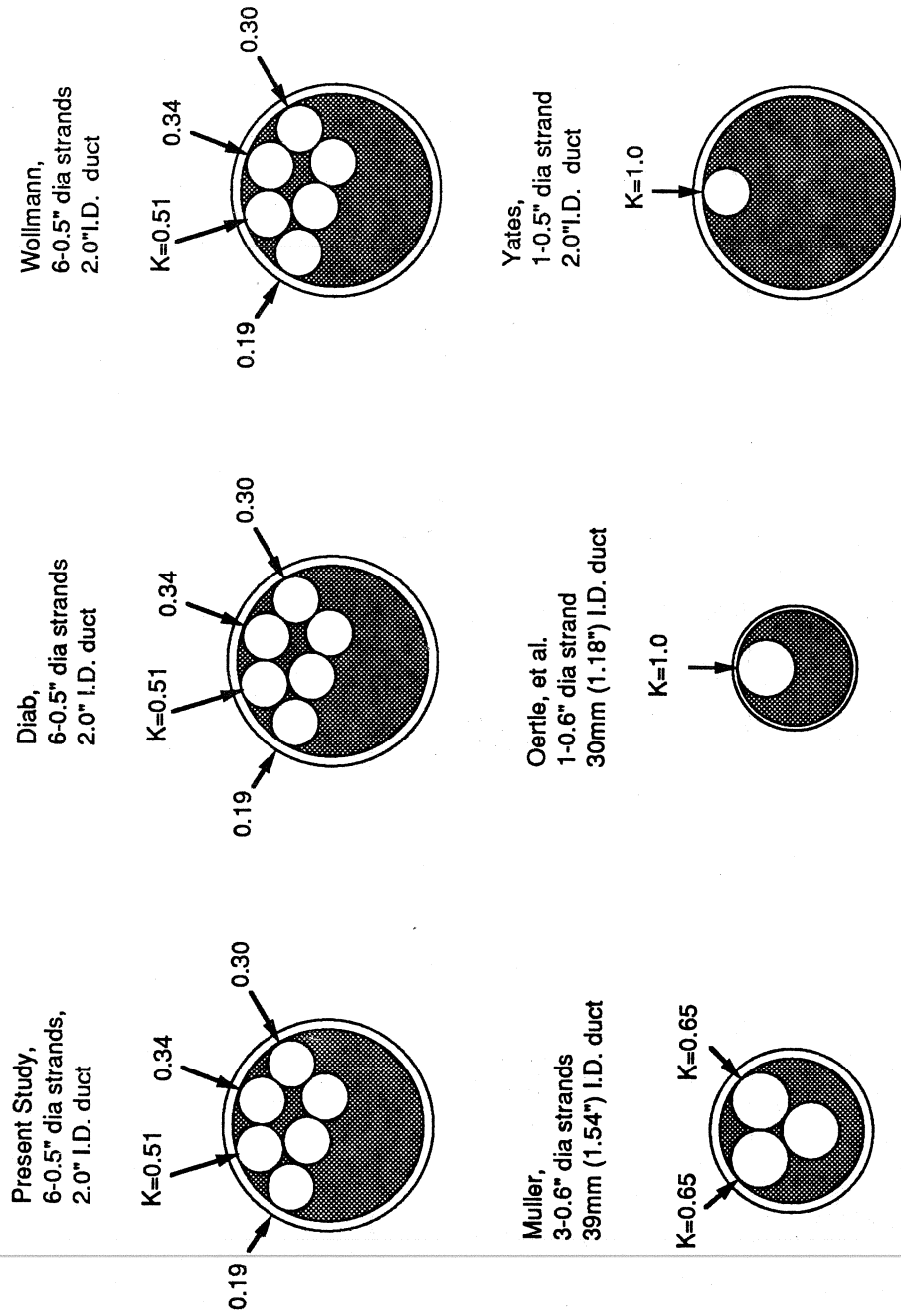
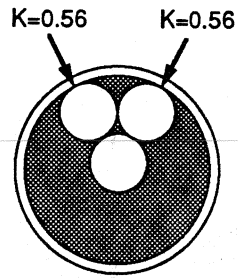
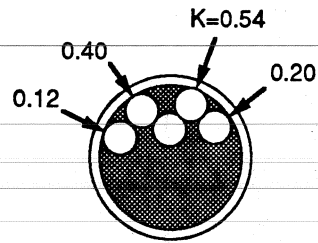


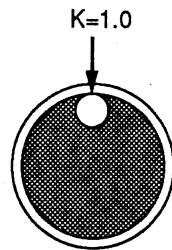
Figure 5.17 K Factors Used for Beams with Strand-Type Tendons



Muller  
 3-12.2mm dia wires  
 39mm I.D. duct



Oertle, et al.  
 5-7mm dia wires  
 30mm I.D. duct



Oertle, et al.  
 1-7mm dia wire  
 30mm I.D. duct

Figure 5.18 K Factors Used for Beams with Wire Tendons

Table 5.5 Data for Strand-Type Tendons with Plastic Duct

Researcher	Type of Tendon	Stress Range (ksi)	Fatigue Life (x 1000)
Yates (reduced-beam tests)	1-0.5 in. dia. 7 wire strand	30.0	1843
		40.0	1112
		25.0	3537
Wollmann (reduced-beam tests)	6-0.5 in. dia. 7 wire strand	30.0	370
		30.0	500
Oertle et al. (reduced-beam tests)	1-0.6 in. dia. 7 wire strand	43.5	1900
		43.5	2000
		39.9	2300
		39.9	2900
		36.3	2700
		36.3	8500 +
Present Study	6-0.5 in. dia. 7 wire strand	29.0	4000 +
		30.0	1300
		30.0	700

+ Runout

Table 5.6 Data for Parallel Wire Tendons

Researcher	Type of Tendon	Stress Range (ksi)	Fatigue Life (x 1000)	K Factor	Contact Load, q (kips/ft)
Oertle et al. (reduced-beam tests)	5-7 mm dia. parallel wires	29.0	900	0.54	3.85
		29.0	1100	0.54	3.85
		29.0	1300	0.54	3.85
		21.8	1500	0.54	3.93
		21.8	1700	0.54	3.93
		21.8	2300	0.54	3.93
		18.1	2100	0.54	4.00
		18.1	2600	0.54	4.00
	14.5	4500 *	0.54	4.00	
	1-7 mm dia. single wire	36.3	1300	1.00	1.47
		36.3	2050	1.00	1.47
		29.0	1400	1.00	1.56
		29.0	1650	1.00	1.49
		29.0	1700	1.00	1.49
		29.0	2150	1.00	1.49
		29.0	2300	1.00	1.49
		29.0	2500	1.00	1.17
29.0		4750	1.00	1.30	
29.0		6400	1.00	1.04	
25.4		2050	1.00	1.52	
25.4		2600	1.00	1.58	
25.4		3600	1.00	1.52	
21.8		4150	1.00	1.60	
21.8	4500	1.00	1.60		
Muller (girder tests)	3-12.2 mm dia. parallel wires	36.2	750	0.56	4.00
		28.9	2050	0.56	3.92
		28.9	4000 *	0.56	3.92
		25.3	1200	0.56	3.87
		21.7	2200 *	0.56	3.82

\* Runout



excluded from this analysis due to their limited number. The fretting simulation tests by Cordes et al. [4] were also omitted because they do not directly model the interaction of stress range, slip amplitude, and contact pressure which make up the fretting conditions found in a typical post-tensioned beam. All runouts were also omitted from the analysis.

#### **5.6.4 Results of the Regression Analysis**

Fatigue models were developed for different data sets using multiple linear regression analysis. All fatigue models are listed in Table 5.6 along with their corresponding fatigue models determined from a linear regression analysis excluding the contact load for comparison. The data sets are listed below with their corresponding fatigue model labels in parentheses :

- 1) Tests of beams with strand-type tendon.
  - a. All beams, (S-ALL).
  - b. Beams for which  $0 < q < 3$  kips/ft, (no model).
  - c. Beams for which  $3 \text{ kips/ft} < q < 6 \text{ kips/ft}$ , (S-3-6).
  - d. Beams for which  $6 \text{ kips/ft} < q < 9 \text{ kips/ft}$ , (S-6-9).

- 2) Tests of beams with wire tendon.
  - a. All beams, (W-ALL).
  - b. Beams for which  $0 < q < 3$  kips/ft, (W-0-3).
  - c. Beams for which  $3 \text{ kips/ft} < q < 6 \text{ kips/ft}$ , (W-3-6).
- 3) Tests of beams with single-strand tendon.
  - a. All beams, (SS-4-6). In this case the local contact load for beams with a single-strand tendon was between 4 kips/ft and 6 kips/ft.
- 4) Tests of beams with multiple-strand tendon.
  - a. All beams, (MS-ALL).
  - b. Beams for which  $4 \text{ kips/ft} < q < 6 \text{ kips/ft}$ , (MS-4-6).
  - c. Beams for which  $6 \text{ kips/ft} < q < 9 \text{ kips/ft}$ , (MS-6-9).

#### 5.6.4.1 Tests of Beams with Strand-Type Tendon

Mean fatigue life models were developed for the data corresponding to tests of beams with strands. These models, labelled S-ALL, S-3-6, and S-6-9 are shown in Fig. 5.19 and are listed in Table 5.7. In general, the correlation coefficients are larger in absolute value and the standard errors are smaller for these models than the corresponding values for the models in

**TESTS OF BEAMS WITH STRANDS AND METAL DUCT**

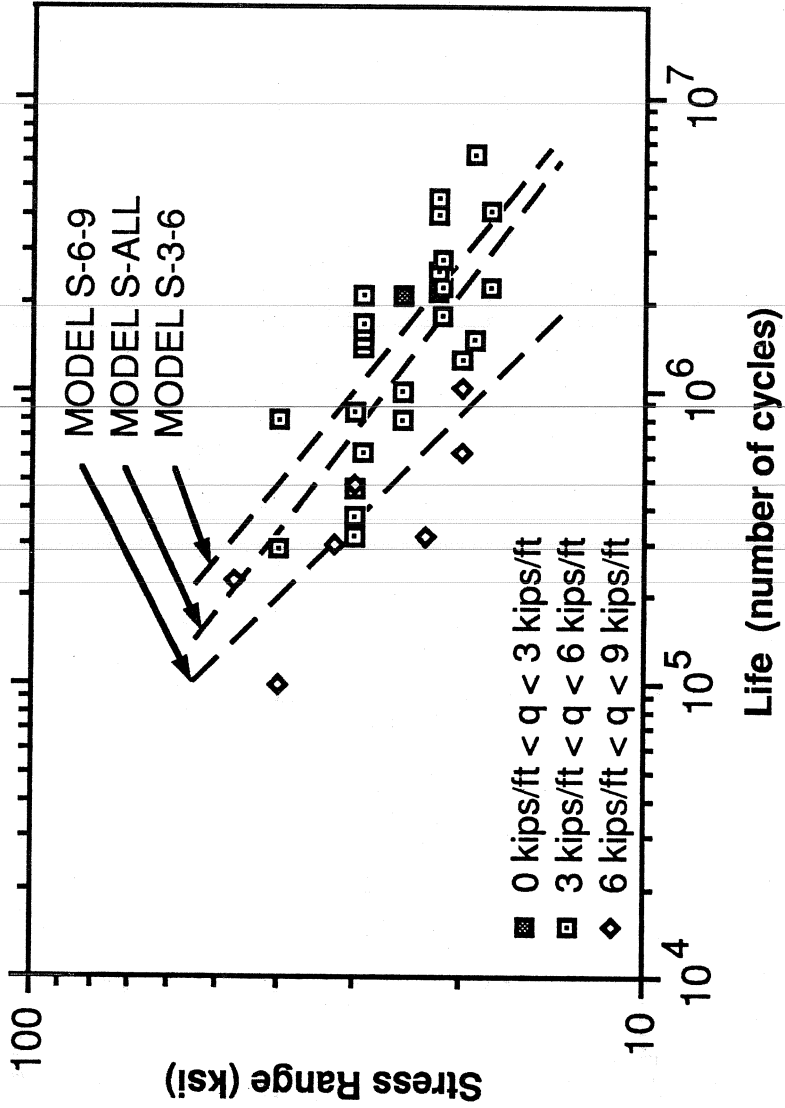


Figure 5.19 Fatigue Life as a Function of Stress Range and Contact Load for Beams with Strand-Type Tendon and Metal Duct

Table 5.7 Initial Multivariable Linear Regression Analysis Results

Model I.D.	Mean Fatigue Life Model	Correlation Coefficient, IRI	Standard Error, s'
S-ALL	Log(N)=9.941-2.526Log(Sr)-0.0641q Log(N)=9.724-2.632Log(Sr)	0.741 0.674	0.283 0.304
S-3-6	Log(N)=8.830-2.721Log(Sr)+0.2296q Log(N)=9.738-2.564Log(Sr)	0.881 0.724	0.170 0.242
S-6-9	Log(N)=9.056-1.913Log(Sr)-0.0903q Log(N)=8.124-1.749Log(Sr)	0.780 0.776	0.226 0.208
W-ALL	Log(N)=9.032-1.670Log(Sr)-0.1379q Log(N)=7.624-0.923Log(Sr)	0.778 0.333	0.145 0.217
W-0-3	Log(N)=11.178-2.451Log(Sr)-0.8402q Log(N)= 8.916-1.731Log(Sr)	0.806 0.528	0.133 0.184
W-3-6	Log(N)=7.320-1.416Log(Sr)+0.2107q Log(N)=8.227-1.474Log(Sr)	0.813 0.810	0.114 0.108
SS-4-6	Log(N)=8.937-2.680Log(Sr)+0.1982q Log(N)=9.962-2.706Log(Sr)	0.829 0.715	0.209 0.255
MS-ALL	Log(N)=9.238-1.967Log(Sr)-0.0986q Log(N)=9.183-2.335Log(Sr)	0.843 0.670	0.239 0.316
MS-4-6	Log(N)=10.787-4.919Log(Sr)+0.503q Log(N)=9.462-2.390Log(Sr)	0.985 0.745	0.078 0.260
MS-6-9	Log(N)=9.056-1.916Log(Sr)-0.0903q Log(N)=8.124-1.749Log(Sr)	0.780 0.780	0.226 0.208

N = Fatigue Life (no. of cycles)

Sr = Stress Range (ksi)

q = Contact Load (kips/ft)

which the contact load was not taken into account. This indicates that the contact load has a significant effect on the fatigue life of post-tensioned beams.

Model S-3-6 requires special consideration due to the unexpected coefficient on the contact load. As shown in Table 5.7 the coefficient of the contact load is positive which means that the effect of the contact load is to increase the fatigue life. In other words, this suggests that the more severe the fretting action is between strands and metal duct, the longer is the fatigue life of the tendon. The data for this model come primarily from reduced-beam tests by Yates [27], Oertle et al. [14] and Muller [12]. In an attempt to determine which data produced the positive contact load coefficient, separate multivariable linear regression analyses were performed for each set of data.

Table 5.8 shows the results of the different analyses. Muller's data show that the contact load has no significant effect on the fatigue life. The contact load coefficient was found to be very close to zero. Oertle's data show a negative effect of the contact load on the fatigue life. The contact load coefficient was found to be -0.1098. On the other hand, Yates' data show a positive effect of the contact load on the

Table 5.8 Multivariable Linear Regression Analysis Results for Tests  
with Strand and  $3 \text{ kips/ft} < q < 6 \text{ kips/ft}$

Researcher	Mean Fatigue Life Model	Correlation Coefficient, IRI	Standard Error, s'
Yates (10 data points)	$\text{Log}(N)=9.424-3.347\text{Log}(Sr)+0.305q$	0.832	0.279
Oertle et al. (11 data points)	$\text{Log}(N)=8.887-1.334\text{Log}(Sr)-0.110q$	0.808	0.108
Muller (4 data points)	$\text{Log}(N)=12.394-4.519\text{Log}(Sr)-3 \times 10^{-15} q$	0.963	0.096

N = Fatigue Life (no. of cycles)

Sr = Stress Range (ksi)

q = Contact Load (kips/ft)

fatigue life. The contact load coefficient was found to be +0.3048. Since the number of data points for both Oertle's and Yates' tests was about the same (10 vs. 11), and since Yates' positive coefficient is almost three times larger than Oertle's negative coefficient, the contact load coefficient for the overall model was influenced more by Yates' data. The question then shifts to why Yates' data indicate a positive correlation between the local contact load and the fatigue life. The most plausible explanation for the positive contact load coefficient is that Yates' tests were conducted with a very narrow range for the contact load. The contact load varied from 4.06 kips/ft to 4.72 kips/ft. The range of contact load (which is only 0.66 kips/ft) is considered too narrow to give meaningful results about the effect of the contact load on the fatigue life because of the uncertainty involved in estimating the contact load. Additional data with a much wider range of contact load are needed to develop a valid model.

#### **5.6.4.2 Tests of Beams with Wire Tendons**

Mean fatigue life models were developed for the data corresponding to tests of beams with wire tendons.

These models, labelled W-ALL, W-0-3 and W-3-6, are shown in Fig. 5.20 and are listed in Table 5.7. For the first two models the correlation coefficients are much larger and the standard errors are much smaller than the corresponding models in which the contact load is not included as an independent variable in the regression analysis. Once again this demonstrates the significant negative effect of the contact load on the fatigue life of a post-tensioned member. Model W-3-6 requires additional attention due to the positive contact load coefficient. The data points for this model correspond to tests by Oertle et al. [14] and Muller [12]. Separate multivariable linear regression analyses were conducted for Oertle's and Muller's data to see which data were responsible for the positive contact load coefficient in model W-3-6. The results are shown in Table 5.9. Oertle's mean fatigue life model which was computed for eight pieces of data had a negative contact load coefficient. On the other hand, Muller's model was determined for only three data. The coefficient of the contact load was positive, and all coefficients were very large. Therefore, Muller's data are responsible for the positive contact load coefficient in model W-3-6. In addition, for certain combinations of stress



# TESTS OF BEAMS WITH PARALLEL WIRES AND METAL DUCT

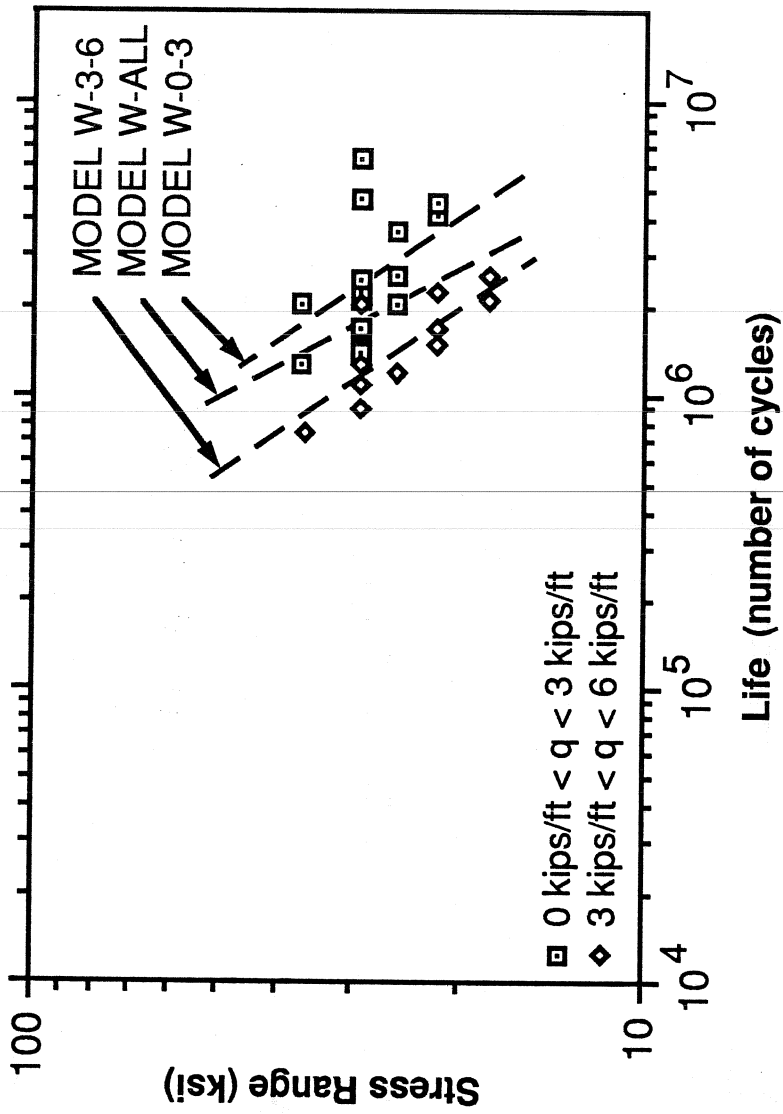


Figure 5.20 Fatigue Life as a Function of Stress Range and Contact Load for Beams with Wire Tendons and Metal Duct

Table 5.9 Multivariable Linear Regression Analysis Results for Tests with Parallel Wires and  $3 \text{ kips/ft} < q < 6 \text{ kips/ft}$

Researcher	Mean Fatigue Life Model	Correlation Coefficient, IRI	Standard Error, s'
Oertle et al. (8 data points)	$\text{Log}(N)=16.838-2.877\text{Log}(Sr)-1.713q$	0.806	0.084
Muller (3 data points)	$\text{Log}(N)=474.2-150.6\text{Log}(Sr)+178.7q$	1.0	0.006

N = Fatigue Life (no. of cycles)

Sr = Stress Range (ksi)

q = Contact Load (kips/ft)

range and contact load, the mean fatigue life model for Muller's data yields a negative fatigue life. For this reason, Muller's data in the range of  $3 < q < 6$  kips/ft are excluded in the final model W-3-6. The final models are shown in Table 5.10.

#### **5.6.4.3 Tests of Beams with Single or Multiple-Strand Tendon**

Different mean fatigue life models were developed for the data corresponding to tests of beams with either a single or multiple-strand tendon. The models, labelled SS-4-6, MS-ALL, MS-4-6 and M-S-6-9, are listed in Table 5.10. Model SS-4-6 is shown in Fig. 5.21 and the remaining models are shown in Fig. 5.22. In most of the cases, the correlation coefficients are larger and the standard errors are smaller for these models than the corresponding values for models for which the contact load was not considered.

Models SS-4-6 and MS-4-6 have positive load coefficients. The explanation for the positive contact load coefficient for model S-3-6 given in Section 5.6.4.1 holds true for model SS-4-6 too since both models were derived from primarily the same data. The additional data did not differ dramatically from the

Table 5.10 Final Multivariable Linear Regression Analysis Results

Model I.D.	Mean Fatigue Life Model	Correlation Coefficient, IRI	Standard Error, s'
S-ALL	Log(N)=9.941-2.526Log(Sr)-0.0641q Log(N)=9.724-2.632Log(Sr)	0.741 0.674	0.283 0.304
S-3-6	Log(N)=8.830-2.721Log(Sr)+0.2296q Log(N)=9.738-2.564Log(Sr)	0.881 0.724	0.170 0.242
S-6-9	Log(N)=9.056-1.913Log(Sr)-0.0903q Log(N)=8.124-1.749Log(Sr)	0.780 0.776	0.226 0.208
W-ALL	Log(N)=9.032-1.670Log(Sr)-0.1379q Log(N)=7.624-0.923Log(Sr)	0.778 0.333	0.145 0.217
W-0-3	Log(N)=11.178-2.451Log(Sr)-0.8402q Log(N)=8.916-1.731Log(Sr)	0.806 0.528	0.133 0.184
W-3-6	Log(N)=16.838-2.877Log(Sr)-1.7130q Log(N)=8.453-1.649Log(Sr)	0.813 0.810	0.114 0.108
SS-4-6	Log(N)=8.937-2.680Log(Sr)+0.1982q Log(N)=9.962-2.706Log(Sr)	0.829 0.715	0.209 0.255
MS-ALL	Log(N)=9.238-1.967Log(Sr)-0.0986q Log(N)=9.183-2.335Log(Sr)	0.843 0.670	0.239 0.316
MS-4-6	Log(N)=10.787-4.919Log(Sr)+0.503q Log(N)=9.462-2.390Log(Sr)	0.985 0.745	0.078 0.260
MS-6-9	Log(N)=9.056-1.916Log(Sr)-0.0903q Log(N)=8.124-1.749Log(Sr)	0.780 0.780	0.226 0.208

N = Fatigue Life (no. of cycles)

Sr = Stress Range (ksi)

q = Contact Load (kips/ft)

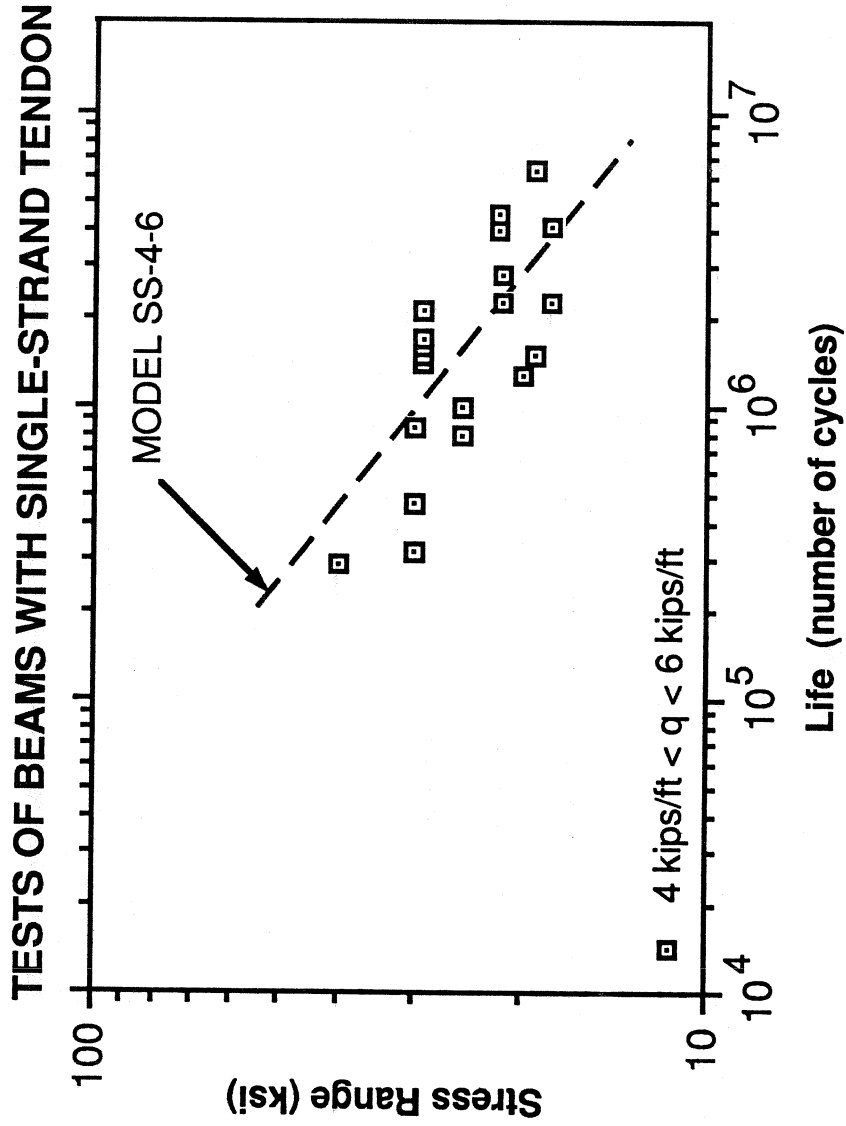


Figure 5.21 Fatigue Life as a Function of Stress Range and Contact Load for Beams with Single-Strand Tendon and Metal Duct

**TESTS OF BEAMS WITH MULTIPLE-STRAND TENDON**

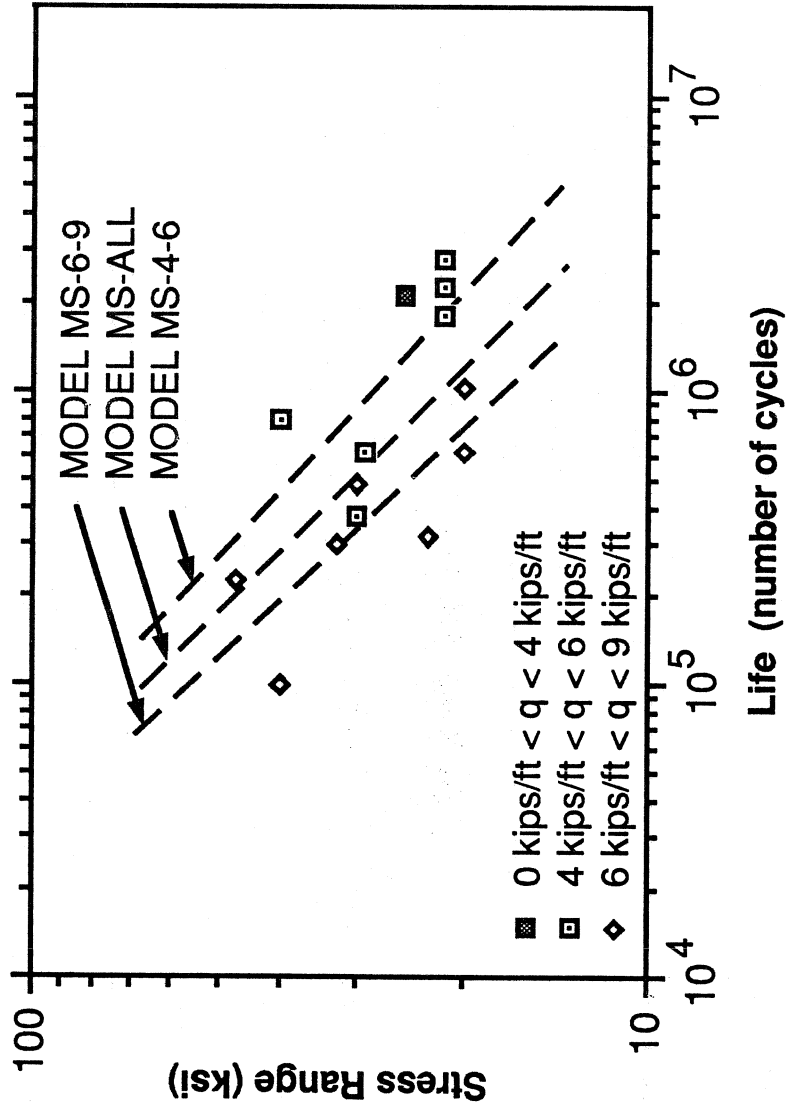


Figure 5.22 Fatigue Life as a Function of Stress Range and Contact Load for Beams with Multiple-Strand Tendon and Metal Duct

main body of data. The situation for model MS-4-6 is different. This model is derived from Muller's [12] data plus two additional data points. Muller's data yield a model with a contact load coefficient that is very close to zero (Table 5.8). Therefore, the positive contact load coefficient is attributed to only two data points. Additional data are needed for the development of a mean fatigue life model in the  $q$  equals 4 to 6 kips/ft range.

## CHAPTER 6

### SUMMARY, CONCLUSIONS AND RECOMMENDATIONS

#### 6.1 Summary

The present study is part of a comprehensive study initiated at The University of Texas at Austin to investigate the effects of fretting fatigue in post-tensioned concrete members. The study is divided into four series of tests: strand-in-air fatigue tests, single-strand reduced-beam fatigue tests, multiple-strand reduced-beam fatigue tests, and large-scale beam fatigue tests. This report is focused on the large-scale beam fatigue tests.

Five specimens were tested in fatigue having as variables the tendon stress range, duct material, and duct layout. The fabrication and testing procedures are discussed in detail in this report. A discussion on fretting fatigue and a literature review of related investigations is also included in this report. A presentation of the test results followed by an evaluation and comparison of these test results and results of previous studies is provided to better understand the adverse effects of fretting fatigue in



post-tensioned concrete.

## **6.2 Conclusions**

The conclusions presented in this section are drawn from the results of the large-scale post-tensioned beam tests and from a comparison of these tests with related investigations. The conclusions are associated with some important limitations and characteristics related to the large-scale beam fatigue tests which are the following:

1. The number of tests was relatively small making it difficult to draw definite conclusions and develop valid mean fatigue life models in some of the cases.
2. All tests were conducted under laboratory conditions excluding any environmental effects on fretting fatigue and on the fatigue lives of the specimens.
3. A completely accurate estimate of the tendon stress range was not possible.
4. The load frequency was not constant depending on the stiffness of the particular specimen and the condition of the pumps.

Keeping in mind the above limitations, the following conclusions were drawn:

1. Fretting fatigue reduces the fatigue life of post-

tensioned tendons if the post-tensioned beams in which the tendons are integrated are cracked. If not, fretting fatigue is not a problem in post-tensioned concrete. The fatigue life of a cracked, post-tensioned beam is usually lower than that of an equivalent pretensioned beam in which fretting fatigue is absent.

2. The severity of fretting fatigue and the fatigue life of a post-tensioned beam is influenced by many factors, the most important being: the tendon stress range, local contact pressure between an individual strand or wire and its duct, slip amplitude, duct material and type of tendon. The larger the tendon stress range or local contact pressure is, the lower the fatigue life is. No conclusive test results are now available on how much slip amplitude affects fatigue life. The type of duct material used is very important. Post-tensioned beams with plastic ducts usually have higher fatigue lives than equivalent post-tensioned beams with metal duct. However, this behavior is more pronounced for single-strand tendons than multi-strand tendons.
3. In post-tensioned beams with metal ducts, wire fractures are mainly caused by fretting between

strands and duct. In post-tensioned beams with plastic duct, the predominant cause for wire fractures is fretting between strands themselves or between individual wires of a strand.

4. It is clear that plastic duct dramatically improves the fatigue behavior of single-strand tendons. However, the behavior of multi-strand tendons is not so clearly benefitted, perhaps because plastic duct does not affect the strand-to-strand fretting that occurs in multi-strand tendons.
5. The local contact pressure is sensitive to the tendon radius of curvature, strand arrangement, number of strands, and duct-to-strand size ratio. Drap points are areas of high local contact pressure.
6. The current AASHTO Category B fatigue model does not provide a safe lower bound for post-tensioned beams with strand-type tendons and metal duct. It appears to be a safe lower limit for post-tensioned beams with parallel-wire tendons and metal duct.

### **6.3 Recommendations**

#### **6.3.1 Design Recommendations**

1. The tendon stress range should be based on a cracked-section analysis if there is any possibility that the

beam may be cracked during its design lifetime.

2. The tendon stress range and local contact load should be estimated as accurately as possible since a small variation in either may cause significant changes in the fatigue performance of the beam.
3. The local contact load should be kept as low as possible for minimizing fretting fatigue in a post-tensioned beam. The local contact load can be reduced by increasing the tendon radius of curvature, increasing the number of strands in the duct, or decreasing the strand-to-duct size ratio.
4. Plastic duct should be used, if possible, in single-strand tendons as a means for minimizing fretting fatigue.
5. For post-tensioned beams with strand-type tendons, metal duct, and local contact loads less than nine kips/ft, the AASHTO Category C fatigue model may be used as a lower limit for the fatigue life of girders (Figures 6.1 and 6.2). For post-tensioned beams with parallel-wire tendons, metal duct, and local contact loads less than six kips/ft, the AASHTO Category B fatigue model can be used as a lower limit for fatigue life (Fig. 6.3).

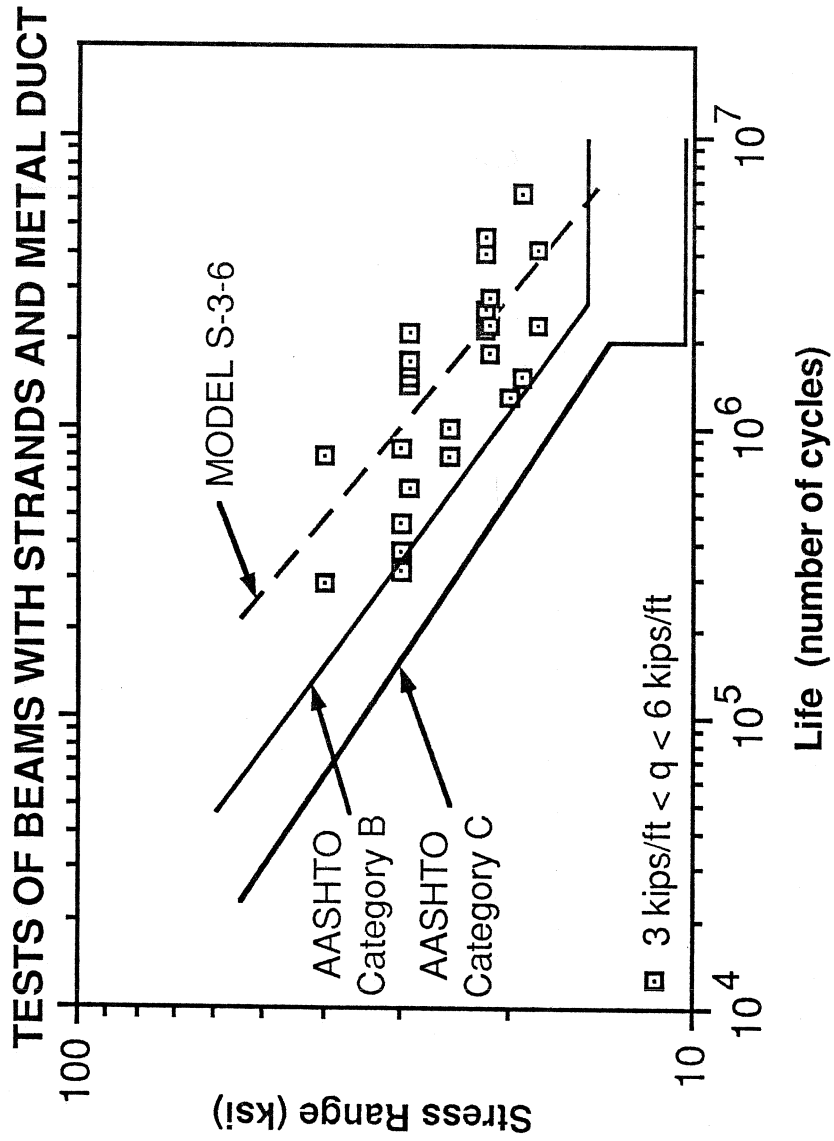


Figure 6.1 Comparison of Model S-3-6 with AASHTO Category B and AASHTO Category C Fatigue Models

**TESTS OF BEAMS WITH STRANDS AND METAL DUCT**

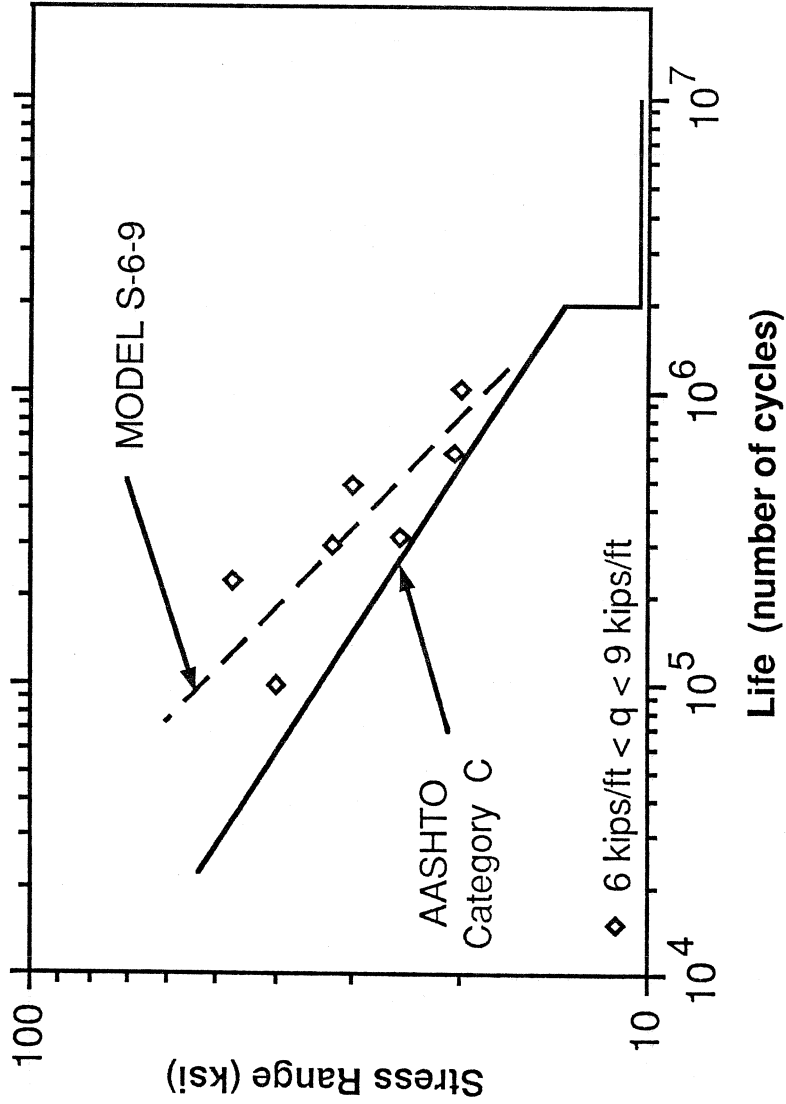


Figure 6.2 Comparison of Model S-6-9 with AASHTO Category C Fatigue Model

**TESTS OF BEAMS WITH PARALLEL WIRES AND METAL DUCT**

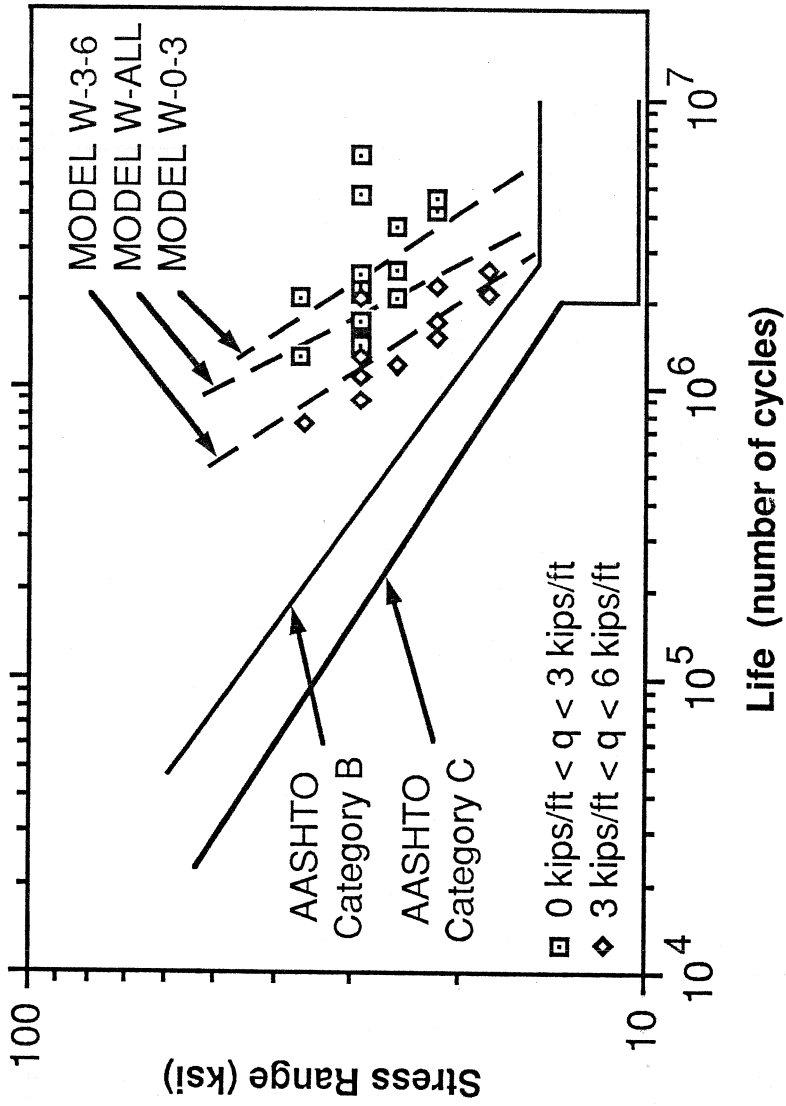


Figure 6.3 Comparison of Models W-0-3, W-3-6 and W-ALL with AASHTO Category B and AASHTO Category C Fatigue Models

### 6.3.2 Research Recommendations

1. More fatigue tests of post-tensioned beams with plastic and metal duct, and with a wide range of local contact loads and tendon stress ranges are necessary in order to better determine the effect of each of the variables on fretting fatigue and fatigue life of post-tensioned members.
2. The effects of important parameters on fretting fatigue, such as slip amplitude, environmental conditions, and grout strength should also be examined in future investigations.
3. A more accurate method to determine the tendon stress range should be developed.
4. More low stress-range tests are necessary to determine endurance limits for beams subjected to fretting fatigue.
5. Methods for minimizing fretting fatigue should be investigated further. Such methods may include reducing the tendon stress range, reducing local contact load or slip amplitude, using different duct geometry, and using various tendon coatings.



## R E F E R E N C E S

1. AASHTO, Standard Specification for Highway Bridges, 13th Edition, American Association of State Highway and Transportation Officials, 1983.
2. Bill, R.C., "Review of Factors that Influence Fretting Wear," Materials Evaluation Under Fretting Conditions, ASTM STP 780, American Society for Testing and Materials, 1982, pp. 165-182.
3. Brondum-Nielson, T., "Effect of Grouting on the Fatigue Strength of Post-Tensioned Concrete Beams," IABSE Final Report, Vol. 14, 1973.
4. Cordes, H., and Lapp-Emden, M., "Untersuchung zur Dauhaftigkeit von Spanngleidern fur die Besonderen Bedingungen der Teilweisen Vonspannung" Report 18/84, Institut fur Massivbari, Technical University Aachen, June 1984.
5. Cordes, H., and Trost, H., "Investigation of the Fatigue Strength of Prestressing Tendons Under the Special Conditions of Partial Prestressing," Presented at the NATO-Advanced Research Workshop, Paris, France, June 18-22, 1984.
6. Diab, J.G., Kreger, M.E., and Breen, J.E., "Fatigue

- Tests of Post-Tensioned Concrete Beams," Unpublished M.S. Thesis, The University of Texas at Austin, May 1989.
7. Foo, M.H., and Warner, R.T., "Fatigue Tests on Partially Prestressed Concrete Beams," Presented at the NATO-Advanced Research Workshop, Paris, France, June 18-22, 1984.
  8. Krueger, F.E., "Fretting Failures," Metals Handbook, Vol. 10, American Society for Metals, 8th Edition, pp. 154-160.
  9. Kusner, D., Poon, C., and Hoepfner, D.W., "A New Machine for Studing Surface Damage Due to Wear and Fretting," Materials Evaluation Under Fretting Conditions, ASTM STP 780, American Society for Testing and Materials, 1982, pp. 17-29.
  10. Magura, D.D., and Hognestad, E., "Tests on Partially Prestressed Concrete Girders," ASCE Proceedings, Vol. 92, St. 1, February 1966, pp. 327-350.
  11. Matsumoto, N., Kreger, M.E., Frank, K.H., and Breen, J.E., "A Fatigue Study of Deformed Reinforcing Bars," M.S. Thesis, The University of Texas at Austin, May 1985.
  12. Muller, H.H., "Fatigue Strength of Prestressing Tendons," Betonwerk and Fertigteil-Technik, December

- 1986, pp. 804-808.
13. Oertle, J., "Fretting Fatigue in Post-Tensioned Concrete," Lecture Presented at The University of Texas at Austin, September 1986.
  14. Oertle, J., Thurlimann, B., and Esslinger, V., "Versuch zur Reibermudung einbetonierter Spannkable," Institut fur Baustatic und Konstruktion, Zurich, Report No. 8101-2, October 1987.
  15. Oertle, J., and Thurlimann, B., "Reib-Ermudung einbetonierter Spannkable," Festschrift Christian Menn zum 60, Geburtstag, 1986, pp.33-38.
  16. Overman, T.R., Breen, J.E., and Frank, K.H., "Fatigue Behavior of Pretensioned Concrete Girders," Research Report 300-2F, Center for Transportation Research, The University of Texas at Austin, November 1984.
  17. Paulson, C., Frank, K.H., and Breen, J.E., "A Fatigue Study of Prestressing Strand," Research Report 300-1, Center for Transportation Research, The University of Texas at Austin, April 1983.
  18. Post-Tensioning Institute, Post-Tensioning Manual, Fourth Edition, Second Printing, 1987, 406 pp.
  19. PTI Ad Hoc Committee on Cable-Stayed Bridges, "Recommendations for Stay Cable Design and Testing," Post-Tensioning Institute publication, January 1986.

20. Rigon, C., and Thurlimann, B., "Fatigue Tests on Post-Tensioned Concrete Beams," Report 8101-1, Insitut fur Baustatik and Konstruktion, Zurich, May 1985.
21. Shahawi, M.E., and Batchelor, B., "Fatigue of Partially Prestressed Concrete," ASCE Journal of Structural Engineering, Vol. 122, No. 3, March 1986.
22. Stone, W.C., and Breen, J.E., "Analyses of Post-Tensioned Girder Anchorage Zones," Research Report 208-2, Center for Transportation Research, Bereau for Engineering Research, The University of Texas at Austin, April 1981.
23. Waterhouse, R.B., Fretting Corrosion, Pergamon Press Ltd., 1972, 244pp.
24. Waterhouse, R.B., Fretting Fatigue, Applied Science Publishers Ltd., London, 1981, 240 pp.
25. Waterhouse, R.B., "Occurance of Fretting in Practice and Its Simulation in the Laboratory," Materials Evaluation Under Fretting Conditions, ASTM STP 780 American Society for Testing and Materials, 1982, pp.3-16.
26. Wollmann, G.P., Breen, J.E., and Kreger, M.E., "Fretting Fatigue of Multiple-Strand Tendons in Post-Tensioned Concrete Beams", M.S. Thesis, The

University of Texas at Austin, December 1988.

27. Yates, D.L., Breen, J.E., and Kreger, M.E., "A Study of Fretting Fatigue in Post-Tensioned Concrete Beams," M.S. Thesis, The University of Texas at Austin, December 1987.

## VITA

Tasos Panteli Georgiou was born on March 29, 1962 in Nicosia, Cyprus, the son of Pantelis Georgiou and Kalliroi Georgiou. After graduating from the Pancyprian Gymnasium in 1979, he entered the Higher Technical Institute, in Nicosia, Cyprus, from which he graduated in May, 1982. Then, he served a two-year compulsory service as an officer in the Corps of Engineers section of the Cyprus National Guard. In September, 1984, he entered The University of Texas at Austin on an AMIDEAST scholarship. He received a Bachelors of Science degree in Civil Engineering in May of 1986 with High Honors. In September, 1986, he entered the Graduate School of The University of Texas at Austin.

Permanent Address :      12A Grivas Street  
   Nicosia  
   Cyprus

---

This thesis was typed by Maria Panayidou and the author.

